

**Mapping and Modeling the Urban Landscape in Bangkok, Thailand:
Physical-Spectral-Spatial Relations of Population – Environmental
Interactions**

Yang Shao

A dissertation submitted to the faculty of the University of North Carolina at Chapel Hill in
partial fulfillment of the requirements for the degree of Doctor of Philosophy in the
Department of Geography

Chapel Hill
2007

Approved by:

Advisor: Stephen J. Walsh

Reader: Aaron Moody

Reader: Ronald R. Rindfuss

Reader: Conghe Song

Reader: James C. Fraser

ABSTRACT

**YANG SHAO: Mapping and Modeling the Urban Landscape in Bangkok, Thailand:
Physical-Spectral-Spatial Relations of Population – Environmental Interactions
(Under the Direction of Stephen J. Walsh)**

This research focuses on the application of remote sensing, geographic information systems, statistical modeling, and spatial analysis to examine the dynamics of urban land cover, urban structure, and population-environment interactions in Bangkok, Thailand, with an emphasis on rural-to-urban migration from rural Nang Rong District, Northeast Thailand to the primate city of Bangkok. The dissertation consists of four main sections: (1) development of remote sensing image classification and change-detection methods for characterizing imperviousness for Bangkok, Thailand from 1993-2002; (2) development of 3-D urban mapping methods, using high spatial resolution IKONOS satellite images, to assess high-rises and other urban structures; (3) assessment of urban spatial structure from 2-D and 3-D perspectives; and (4) an analysis of the spatial clustering of migrants from Nang Rong District in Bangkok and the neighborhood environments of migrants' locations.

Techniques are developed to improve the accuracy of the neural network classification approach for the analysis of remote sensing data, with an emphasis on the spectral unmixing problem. The 3-D building heights are derived using the shadow information on the high-resolution IKONOS image. The results from the 2-D and 3-D mapping are further examined to assess urban structure and urban feature identification. This research contributes to image processing of remotely-sensed images and urban studies. The rural-urban migration process and migrants' settlement patterns are examined using spatial

statistics, GIS, and remote sensing perspectives. The results show that migrants' spatial clustering in urban space is associated with the source village and a number of socio-demographic variables. In addition, the migrants' neighborhood environments in urban setting are modeled using a set of geographic and socio-demographic variables, and the results are scale-dependent.

ACKNOWLEDGEMENTS

I would like to gratefully and sincerely thank my professor, dissertation advisor, and mentor, Dr. Stephen J. Walsh. Throughout the six years of my Ph.D study, he has been a tremendous help, and offered excellent guidance in both my research and personal life. He helped me plan my dissertation research, provided financial support throughout my doctoral work, assisted in funding my field work, offered incomparable advice on publications, and aided my preparation for job interviews. He continues to amaze me with his patience and quick response in reading my paper, proposal and dissertation chapters. He has been a great mentor and a role model to me. I hope that one day I can become a good and caring professor like him.

I would like to thank my doctoral committee for their advice and comments: Dr. Ronald R. Rindfuss, Dr. Conghe Song, Dr. Aaron Moody, and Dr. James C. Fraser. Thank you all for supporting me, and providing comments and suggestions. I would also like to thank Dr. Thomas Whitmore and Dr. Larry Band for their help and recommendations.

I would like to thank the following colleagues for their support and kindness: Philip McDaniel, Brian Frizzelle, Dr. Jun Liang, Evan S. Hammer, Sean McKnight, and Randy Pullen. Additionally, I would like to thank my fellow graduate students in the Spatial Analysis Lab: Dr. Greg Taff, Dr. Kriengsak Rojnkuressatien, Chris Erlie, Carlos Mena, Dan Weiss, Amy McCleary, Julie Tuttle, Laura Brewington, and Pati Polo. It has been a pleasure working with all current and former “Labrats”. I would also like to

extend my gratitude to the Carolina Population Center, which offered me invaluable opportunities to work on various Thai projects, both in Nang Rong and in Bangkok.

I would like to thank all my family members in China for their love and support. There are no words to express my gratitude. Finally, I would like to thank my wife, Xiaozheng Yao, for her love, support and encouragement.

TABLES OF CONTENTS

LIST OF TABLES.....ix

LIST OF FIGURES.....x

Chapter

1. INTRODUCTION.....	1
1.1 Overview.....	1
1.2 Research Aims and Significance.....	7
1.3 Methods.....	12
1.3.1 Mixture Modeling and Urban Change Detection.....	13
1.3.2 Building Height Estimation.....	15
1.3.3 Urban Form Analysis.....	15
1.3.4 Migrants' Settlement Patterns in Bangkok.....	16
1.4 Dissertation Organization.....	17
1.5 References.....	19
2. Mixture Modeling and Urban Change Detection.....	23
2.1 Introduction.....	23
2.2 MLP Neural Network: Background.....	28
2.3 Data.....	31
2.4 Methods.....	34
2.4.1 Classification Approach.....	34
2.4.2 Regression Approach.....	37

2.4.3	Accuracy Assessment and Generalization.....	38
2.4.4	Image Change Detection.....	39
2.5	Results.....	40
2.6	Conclusions.....	51
2.7	References.....	53
3.	Building Height Estimation.....	57
3.1	Introduction.....	57
3.2	Data.....	60
3.3	Methods.....	62
3.3.1	Image Segmentation.....	62
3.3.2	Shadow Detection.....	64
3.3.3	Shadow Length and Building Height Estimation.....	66
3.4	Results.....	67
3.5	Conclusions.....	82
3.6	References.....	84
4.	Urban Form Analysis.....	87
4.1	Introduction.....	87
4.2	Study Area.....	92
4.3	Data.....	93
4.4	Methods.....	94
4.4.1	Sampling Transect-Based Urban-Rural Gradients.....	94
4.4.2	Overall Urban-Rural Gradients and Urban Features.....	95
4.4.3	Urban Change and Urban Form.....	97

4.5	Results.....	98
4.6	Conclusions.....	114
4.7	References.....	116
5.	Spatial Clustering and Urban Settings of Rural Migrants in Bangkok.....	119
5.1	Introduction.....	119
5.2	Geographic Setting.....	122
5.3	Spatial Data.....	124
5.4	Background.....	125
	5.4.1 Migration and Urbanization.....	125
	5.4.2 Remote Sensing of Urban Places.....	127
5.5	Methods.....	128
	5.5.1 Point-Pattern Analysis of Migrants' Locations.....	128
	5.5.2 Neighborhood Environment of Migrants Locations.....	130
5.6	Results.....	132
5.7	Conclusions.....	141
5.8	References.....	143
6.	Conclusions.....	147
6.1	Technical Improvements in Remote Sensing.....	150
6.2	Implications on Urban and Human Settlement Analysis.....	153
6.3	References.....	157

LIST OF TABLES

Table

2.1	Landsat TM/ETM images for the study area.....	32
2.2	Number of training pixels (and percentages) for each class.....	36
3.1	IKONOS image acquisition data, sun azimuth angle, and sun elevation angle.....	62
3.2	Error matrix for image classification.....	68
3.3	Threshold values and the remaining image objects.....	74
4.1	Areal distribution of urban features for 1993 and 2002: Urban core, inner zone, urban fringe, and rural areas.....	107
5.1	Correlation coefficients of spatial clustering and socio-demographic variables....	135
5.2	Coefficients for the impervious cover percentage model.....	139
5.3	Coefficients for the spatial pattern model.....	140

LIST OF FIGURES

Figure

2.1	A typical three-layer MLP neural network.....	29
2.2	Landsat TM/ETM images for the study area.....	32
2.3	Selected training pixels from two training sets (small vs. large sample size).....	35
2.4	Spatial extents of IKONOS image and Landsat ETM image.....	39
2.5	Comparison of RMSE values from varying sample size and class likelihood.....	41
2.6	Comparison of RMSE values from varying prior probabilities.....	43
2.7	Accuracy assessment of neural network classification/regression approaches.....	44
2.8	Overall performance of neural network classification/regression approaches.....	45
2.9	Improved classification results from neural network regression approach.....	47
2.10	Imperviousness of Bangkok from 1993, 1999, and 2002.....	48
2.11	Fuzzy representation of image change detection for 1993-1999 and 1999-2002.....	49
2.12	Per-pixel change detection for 1993-1999 and 1999-2002.....	50
3.1	IKONOS images from 1999 and 2002.....	61
3.2	Examples of shadow objects for high- and low-rise buildings.....	65
3.3	Image classification results from OBIA.....	67
3.4	Water/shadow objects derived from OBIA.....	69
3.5	Derived large rives, streams, and ponds.....	70
3.6	Histogram plot of the Perimeter-Area ratio for water/shadow objects.....	71
3.7	Color ramp of the Perimeter-Area ratio for water/shadow objects.....	72
3.8	Comparison of shadow objects from high- and low-rise buildings.....	72
3.9	Spatial neighborhoods of small water ponds in urban-rural fringe areas.....	73

3.10	“Clean” shadow objects from high-rise buildings.....	74
3.11	Perimeter pixels from shadow objects.....	75
3.12	Accuracy evaluation of the shadow length estimation.....	76
3.13	Error sources of shadow length estimation.....	78
3.14	Accuracy evaluation of the building height estimation.....	79
3.15	3-D urban of Bangkok, Thailand.....	81
4.1	Transects for urban-rural gradient analysis.....	95
4.2	Density, mean patch size, and patch number of impervious cover along transects A and B.....	101
4.3	Urban-rural gradient analysis using moving window (3-km window size): Density, mean patch size, and patch number of impervious cover.....	103
4.4	Impervious density image of 1993 (150-m window size).....	105
4.5	Urban feature identification using density and mean patch size indices: Urban core, inner zone, urban fringe, and rural areas.....	106
4.6	Comparison of urban core areas derived from 2-D and 3-D inputs.....	109
4.7	Urban change pixels and their spatial neighborhoods: Measures of the density, mean patch size, and patch number of imperviousness.....	111
5.1	Nang Rong district, Northeastern Thailand.....	123
5.2	Bangkok, Thailand: a Landsat TM view.....	124
5.3	Intensity surfaces derived from migrants’ locations in Bangkok.....	132
5.4	Spatial clustering of migrants from origin villages (500-meters threshold).....	134
5.5	Spatial clustering of migrants from origin villages (1000-meters threshold).....	134
5.6	Impervious cover for Bangkok and surrounding areas.....	137

5.7 Box-plots of the percentage impervious cover from varying kernel sizes.....138

CHAPTER 1

INTRODUCTION

1.1 Overview

Rapid urban growth has received increasing attention from urban and regional planners, geographers, demographers, decision-makers, and researchers from the social, natural, and spatial sciences. Although recent statistics show that urban areas account for only a small fraction of the Earth's surface area, most agree that continuing urban expansion has far-reaching and disproportionate effects on mass, energy, and resource fluxes over large geographic extents (Small et al., 2005). One of the main concerns is related to the environmental consequences of urban development. The land transformations from agriculture and other natural lands to urban land uses are typically irreversible and may lead to possible environmental degradation, primarily associated with the deterioration of air and water quality (Kalnay and Cai, 2003). Moreover, researchers argue that urban development may reduce the number of native species and generate substantial local extinction rates of local flora and fauna (Luniak, 1994; Marzluff, 2001). Currently, the highest urban growth rates are in the developing countries. Many fast growing cities are located in China, Thailand, Malaysia, and other regions with rapid economic development and population growth. The dominant trend of land use/cover change is from cultivated land to urban and build-up and the rates of land transformations to such developed places are striking (Yeh and Li, 1997). The rates, from-to land use types, and the trajectories of land transformations from natural to built-

up land uses have become a central concern of groups and organizations involved in questions related to sustainable development and food security (Hong and Li, 2000). In addition to the areal expansion of urban places, the spatial structure of urban areas is also important, particularly the loss of green-space in built-up areas and the fate of land use at the urban-rural interface. For instance, the spread of low density settlement patterns through urban sprawl is often considered an inefficient and wasteful use of land resources, although it certainly has other ecological and socio-economic implications and benefits (Clapham, 2003).

The timely information about the condition and status of urban land use/cover is important for planning and management purposes. In most developing countries, however, the land use/cover maps are often limited and generally outdated, and the data sources and quality may also be questionable (Donnay et al., 2001). Therefore, it is generally difficult to estimate the rates and trajectories of urban growth based on the best available information, particularly for historical periods and for comparisons to other geographic areas and periods. Satellite remote sensing is one such data source that provides a consistent data source for the characterization of urban land use/cover types and their changes over space and through time (e.g., Forster, 1983; Mesev, 1998; Paola and Schowengerdt, 1995). Currently, medium spatial resolution imagery (e.g., Landsat TM/ETM) is considered an ideal data set for many urban applications, especially for urban growth analysis and modeling (Carlson, 2003), because of the rich time-series, depth of the historical coverage, large geographic extent of image scenes, broad geographic coverage for most of the developed and developing worlds, and their multi-spectral resolutions for landscape characterization. Challenges in the use of remotely

sensed data, particularly the intermediate spatial resolution satellite data, however, are substantial, extending from methodological and conceptual perspectives. First, the spectral mixture problem of the integrated pixel in which multiple land use/cover types contribute to a single “integrated” spectral response pattern at the pixel level is highly likely in urban areas, particularly when a 30 x 30 m pixel is used to characterize the landscape. What results is often relatively low image classification accuracy for complex and fragmented landscapes that are typical of urban settings (Small, 2003). Large numbers of pixels may have mixed spectral signals from two or more land use/cover types (i.e., impervious cover and vegetation), when medium spatial resolution data are used for urban mapping. Therefore, traditional per-pixel classifications may be less useful in representing the urban landscape. Second, most current urban mapping applications only consider land use/cover at the two-dimensional or 2-D level; the building height information has generally not received sufficient attention in remote sensing of urban places, particularly satellite-based remote sensing, and, as such, information on population densities, for instance, may be excluded from the typical information base of urban settings. The ability to characterize the three-dimensional or 3-D urban setting may provide very useful and even essential information for assessing urban structure and socio-demographic implications of urban areas and urban structures. Third, there is very limited information that describes the urban form or urban structure, especially for the urban areas in developing countries. Urban form considers the myriad of urban features in urban places, whereas urban structure considers the spatial organization of urban features, including land use/cover, arrayed across the landscape. Researchers have inferred social-demographic implications from urban form and their dynamics, although

most studies that link pattern to process are conducted for cities in North American and Europe. One of the main objectives of this research is to examine advanced remote sensing image analysis techniques to improve urban characterization. It is also important to assess the robustness and consistency of the remote sensing derived products for analyses through time and for other regions of the world. The level of accuracy and consistency is critical for the estimation of urban growth rates and patterns, and so approaches that are repeatable and generate high quality and informative data are of utmost concern.

Moving beyond urban mapping, many researchers are interested in developing models to understand the causes and consequences of land use/cover change. A considerable number of urban growth models have been developed, including simple statistical models and more complicated spatial simulation models, such as Cellular Automata and Neural Network models. Statistical models have been used to assess the associations between land use/cover changes and a variety of geographic, biophysical, and socio-demographic variables (e.g., Seto et al., 2003; Walsh et al., 1999). Spatial simulation models such as Cellular Automata or CA provide an improved capability to examine alternate scenarios of land use/cover change and to predict future growth forms in urban settings, although there are considerable uncertainties with regard to model calibration and validation (e.g., Clarke, 1998). Wilson et al. (2003) examined urban growth patterns and developed a set of spatial models to quantify urban development across the landscape. The urban processes of population and structure infilling, diffusive expansion, and isolated urban growth may provide very useful descriptions of urban form and function relations useful to local urban planners and decision-makers. The concepts

of linking form and function through remote sensing characterizations and pattern and process relations through statistical and spatial models, however, have not been rigorously employed for cities in developing countries, where urban growth or development may take different forms compared with those from developed countries. This research will examine the existing models and analytical approaches that have proved useful in characterizing urban growth patterns in Bangkok, a primate city in Thailand.

Urbanization and urban growth, more generally, is the consequence of three factors: rural–urban migration, differential natural increase, and re-classification of the urban administrative area as a consequence of planned and actual uses (Cohen et al., 2003; United Nations, 2004; White et al., 2003). In Thailand, over the past several decades, rural-urban migration has been a major contributor to urban growth (Phongpaichit, 1993), especially the growth of Bangkok. Bangkok is the destination for about 50-percent of rural-urban migrants in Thailand (NSO Thailand, 2000). The city has experienced an increase in population density from 3,001 people per square kilometer in 1980 to 4,051 people per square kilometer in 2000 (NSO Thailand, 2000). About 37-percent of the population in Bangkok was born outside of the province of residence (NSO Thailand, 2000). These large numbers of migrants relocating in Bangkok from rural source areas are of critical concern for urban planners, government officials, and social and spatial scientists. As such, uncontrolled rural-urban migration may cause rapid population growth in urban areas and quickly outstrip urban services and related infrastructure. This is largely due to the age-selection of the migration process in which people willing to relocate in urban settings from rural locations are often young and in

reproductive age. Increased total population and population density in urban setting may also cause a number of possible social/environmental problems such as urban poverty, homelessness, traffic congestion, infrastructure deficiencies, and a general reduction in the quality of life. Also, the living conditions of migrants, including housing and neighborhood conditions are often poor. Some researchers argue that the settlement patterns of rural-urban migrants can be directly related to informal housing and urban slums (Wu, 2002), and may also cause problems related to physical health and a variety of long-run, social outcomes for children (Jencks and Mayer, 1989).

Most previous rural-urban migration studies have focused on the push-pull factors of population relocation from source to destination areas. Studies regarding migrants' settlement patterns in urban settings have received much less attention in the geography literature. One possible reason is the general lack of good and available data to understanding the socio-economic and demographic characteristics of migrants and their relationship to other migrants from similar or nearby towns in rural places. It is generally difficult to track migrants' locations in urban areas. Migrants' settlements vary from informal housing to single-family homes. Some migrants are permanent, while others are temporary or seasonal (Guest, 1996; Korinek et al., 2005). Some migrants live close to other migrants, and others are areally dispersed. Currently, the lack of data and subsequent analyses severely limit our understanding of the settlement patterns of rural-urban migrants, the impact of rural-urban migration on cities, as well as the impact of cities on migrants themselves. This study will use a unique data set that describes the spatial pattern and demographic characteristics of rural-urban migrants from Nang Rong to Bangkok, Thailand. The data were collected in 2000 as part of the Nang Rong Projects

(see the web site at [http://www.cpc.edu/Nang Rong](http://www.cpc.edu/Nang_Rong)). Out-migrants from 22 of the original 51 survey villages in Nang Rong who temporarily or permanently relocated to Bangkok (as well as other locations not assessed here) were geo-coded and linked to their home addresses (and in some cases to the factories where they worked) using GPS technology. Spatial analyses were conducted that relate migrant patterns to urban characteristics, defined through remote sensing image processing and subsequent interpretations. The spatial organization of migrants in Bangkok and their neighborhood environments are of particular interest.

The interconnectedness of people, place, and environment is the central research context of this research. The focus of the research is the remote sensing image analysis and physical-spectral-spatial relationships of land use/cover patterns measured by remote sensing systems and GIS techniques in a major urban setting (i.e., the greater Bangkok area). The context of this research is framed within a set of broad questions including:

- What are the characteristic features of urban areas and urban form?
- Which remote sensing and GIS approaches can effectively be used to characterize urban features and their dynamics?
- To what extent can GIScience techniques be used to study land use/cover patterns and dynamics, as well as population characteristics in urban places?

1.2 Research Aims and Significance

The overall goal of this study is to examine the urban setting of Bangkok, Thailand through studies involving surface imperviousness; 3-D urban mapping from satellite data; urban morphology using a satellite image time-series and human settlement

patterns captured through land use/cover classifications; GIS coverages that describe the basic urban infrastructure of Bangkok; landscape pattern analysis metrics of rural, urban, and rural-urban transitions; and geo-coded migrant locations in Bangkok and their source areas in Nang Rong.

The first research aim is to map and monitor the biophysical characteristics of urban settings in Bangkok through digital image classification and pattern recognition approaches. A set of 2-D urban mapping and change-detection techniques are examined via three research objectives: (1) derive impervious cover using Neural Network-based sub-pixel classifications; (2) examine the rates of urban growth from 1993 to 1999 and 1999 to 2002; and (3) develop an urban growth model using the concepts of areal infilling, diffusive expansion, and isolated development (Wilson et al., 2003), and identify any other pattern-process relationships that might be unique to Bangkok, or primate cities more generally. As previously indicated, the use of traditional per-pixel classification techniques can be problematic for mapping urban environments, because large numbers of pixels may have mixed spectral signals from two or more land cover types. Recent advances in urban remote sensing focus on the development of sub-pixel classification techniques that describe fractions or proportions of land use/cover types in pixels as sub-resolution information. Linear Mixture Models are the most widely used approach for decomposing pixels into their component parts, although more complicated algorithms such as Decision Trees (e.g., DeFries et al., 1999; Xian et al., 2005) and Neural Networks (e.g., Atkinson et al., 1997; Carpenter et al., 1999; Fernandes et al., 2004) have been increasingly used. Many argue that these non-parametric models are superior to linear mixture models for solving spectral “unmixing” problems. A main

problem with the use of non-parametric models is that the results are often sensitive to the characteristics of training data and training protocols. Until now, few researchers have assessed their impacts on the classification results. Moreover, most current spectral mixture models focus on a single image classification; few have attempted to apply the spectral mixture model to time-series data and subsequent urban land cover change analysis. This research will develop a neural-network based, sub-pixel classifier to derive impervious cover from a time-series of Landsat TM/ETM imagery. The challenge is to consider its generalizability in the spatial and temporal domains. The main advantage of the sub-pixel approach is that it is typically considered to be a more accurate and realistic representation of urban landscapes. It should be noted that the sub-pixel land-cover proportions (e.g., percentage of impervious cover) and their dynamics can be easily converted to traditional per-pixel approaches, thus the unmixing approach provides greater flexibility for data representation and analysis.

The second research aim considers the 3-D urban characterization and mapping. Few previous studies on urban mapping and urban form consider the building height, or 3-D information in their characterization. This is largely due to the limitations imposed by the cost of the imagery, satellite images vs. aerial photography, and digital image analysis techniques vs. manual interpretation using traditional photogrammetric methods to discern building height. In fact, building height information may be critical for certain urban applications, especially for the delineation of urban core, urban fringe, and rural areas. The building height also has consideration implications for socio-demographic characterization of urban places. For instance, the function of a high-rise building can be very different from a single-story structure, although they may be simply grouped into the

same urban class (i.e., impervious cover) in conventional 2-D urban mapping applications. The use of aerial photogrammetry techniques are the most common approach to derive 3-D information using standard equations and devices such as stereoscopes and parallax wedges. Building height can be derived from a single or stereo-pairs of aerial photographs (Paine and Kiser, 2003). LIDAR (Light Detection and Ranging) data has also been used for estimating building heights (Gamba and Houshmand, 2000), but the cost and data availability severely limit its application in large urban areas in developing countries, for change-detection studies and in studies with a deep historical context as LIDAR is a recently developed technology for landscape mapping applications. Few researchers have used satellite remote sensing data to characterize the building height largely due to the limitation on spatial resolution (Shettigara and Sumerling, 1998). The newly available hyper-spatial, remote sensing data (e.g., IKONOS and QuickBird) have improved spatial resolutions, thus offering new opportunities for 3-D urban mapping using similar approaches to traditional photogrammetry. This study will examine the use of high spatial resolution satellite imagery to estimate building heights in a crowded and complex urban setting. The approach will use the shadow information represented in the spectral response patterns of IKONOS data and the ephemeris information of the image linked to the solar geometry at that location. The challenge is to identify and analyze shadow objects on the satellite image. Three research objectives are proposed: (1) examine object-oriented computer algorithms to identify shadow/water objects from high satellite resolution imagery; (2) examine the object shape, size, and spatial neighborhood characteristics to delineate shadow and water objects, areas of spectral similarity and traditional confusion in image

processing; (3) estimate building height using the relationship between building, shadow, and solar position (e.g., elevation angle and azimuth angle) for Bangkok.

The third research aim is to characterize urban form using image classification results and 3-D building heights. The definition of urban form may be subjective in the field of urban studies, but a common approach is to analyze the spatial pattern of the various land use/cover categories, especially the impervious cover (Donnay, 1994). The spatial pattern of impervious cover from a single image may provide direct information about urban structure or urban-rural gradients. The evolution of urban form, however, has not received much attention in the urban remote sensing literature. This research will employ landscape pattern analysis to study urban form from static and dynamic perspectives. In addition to the spatial organization of impervious cover, the building height information is also considered in the characterization of urban form. Two research objectives are further proposed: (1) examine alternative approaches to characterize urban-rural gradients and delineate patterns that are suggestive of the urban core, urban fringe, and rural areas; and (2) examine the temporal variability of urban-rural gradients from 1993 to 2002.

The fourth research aim is to study the rural-urban migrants' settlement pattern in Bangkok, Thailand. Three research objectives will be addressed: (1) analyze the migrants' settlement pattern with regard to the urban form and urban development; (2) assess the neighborhood environments of rural-urban migrants; and (3) examine the spatial clustering of rural-urban migrants in the urban setting. The studies on the interrelationships between migrants' locations, urban form, and urban development are generally absent from the urban and remote sensing literatures. Very few statistics are

available for a set of simple questions including: Are migrants choosing to settle in the urban center or urban fringes? Are migrants choosing to settle in newly urbanized areas in the cities, or in pre-existing urban places, possibly more familiar to earlier migrants from the same or spatially- and/or socially-connected villages? In addition, the literature on migrants' neighborhood environments (i.e., imperviousness, green/open spaces, and road accessibility) are considerably less represented than migrants' housing conditions (e.g., Wu, 2002). Finally, it is also important to study the influential factors for migrants' settlement pattern in an urban setting. These factors include job location, housing/rent price, duration of stay in the urban area (i.e., permanent/temporary), and the relevance of social networks in explaining the geographic distribution of migrants from the same or different rural villages. A common origin or source area can be viewed as one type of social ties, or social network, although not the only one (see Korinek et al., 2005). Spatially-explicit investigations of social ties are generally rare, at least in the geography literature (see Faust et al. 2000 as an example of a social network analysis that operated within a spatial context). This study will apply spatial analyses and GIS techniques to examine the residential clustering of migrants from Nang Rong to Bangkok. Patterns of residential clustering will be examined in relation to origin or source villages, asking whether migrants from the same village are more likely to live in close proximity to one another than those from different villages. The origin village represents a social context for migration and a set of social ties that travel with the migrant from the origin to the destination.

1.3 Method

The study of urban space and population-environment interactions relies on many data types and sources. Spatial and social data at multi-levels are combined to address specific research questions; the data types used in this research are described below.

A rich satellite image datasets have been assembled for Bangkok, Thailand. The time-series of Landsat Thematic Mapper (TM)/Enhanced Thematic Mapper (ETM) data includes multiple scenes acquired for the period of 1993-2002. In terms of high spatial resolution data, two IKONOS scenes (i.e., May 2000 and November 2002) were acquired for the Bangkok metropolitan area. Some GIS layers were acquired through a Nang Rong project trip held in Bangkok and Nang Rong district in 2004. In addition, a geo-located point file of migrant locations in Bangkok from the 22 survey villages was generated from the 2000 survey. Villagers who had out-migrated to Bangkok, the Eastern Seaboard, and other places were followed and surveyed. There are approximately 1,100 individual migrants who left 22 study villages in 2000 and settled in Bangkok at one of nearly 800 locations throughout the city. This survey was linked to the households and villages of their origin location in Nang Rong. Questions related to the pattern of rural-urban migrants are examined as a meaning of addressing the rural-urban connection.

1.3.1 Mixture Modeling and Urban Change Detection

A Multi-Layer Perceptron (MLP) neural network model was trained to estimate sub-pixel land use/cover proportions from Landsat TM/ETM imagery. Four land use/cover classes are considered: impervious cover, vegetation, bare soil, and water/shadow. The model is similar to Ridd's (1995) conceptual Vegetation-Impervious surface-Soil (V-I-S) model. The shadow class is included, because many urban pixels, especially in the urban center, may have considerable proportions of shadow. The

spectral signals of shadow, however, are very similar to the water class. Therefore, these two classes are combined into a single class in the spectral mixture model. Using high spatial resolution IKONOS imagery as the reference data set, large numbers of training pixels are identified from the 2002 Landsat ETM image. A number of network training protocols are examined, including the numbers of hidden nodes, learning rate, early stop criteria, and momentum. The sub-pixel classification results are cross-validated using the IKONOS data set as the reference image in the validation exercise. The training and validation procedures are conducted through a trial-and-error evaluation approach. The network with the best generalization ability is retained as the primary sub-pixel classifier.

Landsat TM imagery from 1993 and 1999 are radiometrically normalized to Landsat ETM 2002 imagery using an image regression approach. These two rectified images are directly classified using the same primary sub-pixel classifier. This approach is efficient, because there is no need to collect training samples from different images (i.e., 1993 and 1999) as the same classifier can be applied to different images. The image change detection was conducted by comparing the impervious cover proportions for each pixel from 1993 to 1999 and from 1999 to 2002. This approach provides urban land use/cover change maps at the sub-pixel level. It is also straightforward to convert the land use/cover change map from the sub-pixel level to the per-pixel level. A threshold value of 0.5 was found to identify urban change pixels in this analysis. The rate of urban growth is quantified for two time-periods, 1993 to 1999 and 1999 to 2002. Moreover, urban growth patterns are characterized as infilling growth, diffusive expansion growth, and isolated growth. Infilling growth is defined as an "urbanized pixel" surrounded by more than 40-

percent existing urban pixels, whereas diffusive expansion is defined as an “urbanized pixel” surrounded by less than 40-percent existing urban pixels (Wilson et al., 2003).

1.3.2 Building Height Estimation

The building height is derived using the shadow information on the high-resolution IKONOS imagery. The IKONOS image was first classified through an object-based algorithm instead of the more traditional pixel-based approaches. The land use/cover classes include impervious cover, soil, vegetation, and shadow/water. Three key image analysis procedures are designed to derive the building height information: (1) identify shadow objects from IKONOS image. Shadows typically have very similar spectral signals as the water class. A number of spatial indices are developed to separate shadow and water objects. These include the size, shape, and the spatial relationship of the target object to its neighboring objects. For instance, the adjacency of shadow objects and impervious objects can be an important index for the differentiation of shadow and water objects; (2) the shadow length is measured according to the direction of the solar azimuth angle. The building height is calculated using the relationship between building, shadow length, and sun elevation angle; (3) derived building heights are validated using field data from Bangkok, Thailand. The focus of building height estimation is on the high-rise buildings. Actual building height data are obtained for a sample of buildings. The correlation coefficient and RMSE (Root Mean Square Errors) value are generated for accuracy evaluation.

1.3.3 Urban Form Analysis

The urban form is characterized using three image analysis approaches: (1) the arbitrary distance measure to the urban center. The urban center is first defined as a single

point representing the historical urban center area. Spatial buffers around these points are constructed using a number of distance threshold values. Within each buffer zone (i.e., 10~20km), the density and spatial organization of impervious cover is analyzed. This provides an arbitrary urban-rural gradient based on the distance to the urban center; (2) the second approach to define urban form considers the “characteristic scale” of impervious cover. Semivariance analysis is conducted to find the characteristic scale of the impervious cover. At this characteristic scale, a moving spatial/statistical kernel is used to examine the abundance and spatial organization of imperviousness. Critical thresholds are derived from kernel statistics to aid the urban area differencing. For instance, the urban fringe area may exhibit a relatively low density of imperviousness as compared to the urban center. The spatial pattern of impervious cover at the urban fringe area may show more fragmentation as compared to the urban center area; (3) the third approach examines the building height for the urban form characterization. The locations of high-rise buildings are used to differentiate the urban core and urban periphery, because most high-rise buildings are business centers, hotels, and offices that are located in urban centers. To assess the temporal variability of urban form, the first two image analysis approaches are applied to a time-series of Landsat TM/ETM imagery. However, due to the lack of available high-resolution image data, the temporal variability of urban form has not been characterized using the third image analysis approach.

1.3.4 Migrants’ Settlement Patterns in Bangkok

First, the migrants’ locations are linked to urban form. The objective is to identify the percentage of migrants that live in urban centers, urban fringe, and rural areas. This analysis provides an overall picture of migrants’ settlement patterns in urban

spaces, with an emphasis on Bangkok. Second, the migrants' locations are compared to urban development or growth patterns. The location of new urbanized areas is identified through image change detections. The relationship between migrants' location and new urbanized area is assessed through simple overlay analysis within a GIS. This approach provides useful information about whether rural-urban migrants' are directly linked to urban development. Third, the migrants' neighborhood environments are characterized and modeled. Two sets of models are developed. The dependent variables are the abundance of impervious cover and the spatial organization of impervious cover. Independent variables include a number of geographic variables (e.g., distance to roads) and socio-demographic variables (e.g., age, sex, education, etc). Finally, the spatial patterns of migrants' locations in Bangkok are examined using spatial clustering techniques to determine whether migrants live in spatial clusters organized by economic activity, demographic characteristics, or rural village residence patterns.

1.4 Dissertation Organization

The remainder of the dissertation is organized as follows: Chapter 2 examines in detail the Neural-Network based sub-pixel classification method for characterizing urban land use/cover and dynamics. The rates of urban growth are assessed for two time-periods from 1993 to 1999 and from 1999 to 2002. In addition, the patterns of urban growth are quantified using a set of urban models. Chapter 3 examines the 3-D urban mapping techniques using high spatial resolution IKONOS imagery. The height estimation is focused on high-rise buildings. Advanced image analysis techniques, particularly objective-oriented algorithms, are used to identify shadow objects. The subsequent building height estimation is based on the relationship between building,

shadow, and solar position at the day/time and location of image acquisition. Chapter 4 assesses the alternative approaches for the characterization of urban form. The input to the analysis is from the 2-D and 3-D urban mapping analyses. The evolution of urban form is assessed for the period 1993 to 2002. Chapter 5 describes the rural-urban migrants' settlement patterns in Bangkok, Thailand. The migrants' spatial clustering, neighborhood environments, and their linkages to the urban form and urban development are examined. Chapter 6 presents conclusions, synthesizes the findings among the chapters, and describes an agenda for future work.

References

- Atkinson, P.M., Cutler, M.E.J., Lewis, H. (1997). Mapping sub-pixel proportional land cover with AVHRR imagery. *International Journal of Remote Sensing*, 18(4), 917-935.
- Batty, M., Longley, P. (1994). *Fractal cities: a geometry of form and function*. London and San Diego: Academic Press.
- Carlson, T. (2003). Applications of remote sensing to urban problems. *Remote Sensing of Environment* 86, 273-274.
- Carpenter, G.A., Gopal, S., Macomber, S., Martens, S., Woodcock, C.E. (1999). A neural network method for mixture estimation for vegetation mapping. *Remote sensing of environment* 70, 138-152.
- Clarke, K.C., Gaydos, L. (1998). Loose-coupling a cellular automaton model and GIS: Long-term urban growth prediction for San Francisco and Washington/Baltimore. *International Journal of Geographic Information Science* 12:699-714.
- Clapham, W.B. (2003). Continuum-based classification of remotely sensed imagery to describe urban sprawl on a watershed scale. *Remote Sensing of Environment* 86, 322-340.
- Cohen, B, White, M, Montgomery, M.R., McGee, T., Yeung, Yue-Man. (2003). Urban Population Change. National Research Council, *Cities Transformed: Demographic Change and Its Implications in the Developing World*. Panel on Urban Population Dynamics, Mark R. Montgomery, Richard Stren, Barney Cohen, and Holly E. Reed (editors). Washington, DC: The National Academies Press, 75-107.
- DeFries, R., Townshend, J., Hansen, M. (1999). Continuous fields of vegetation characteristics at the global scale at 1-km resolution. *Journal of Geophysical Research*, 104, 16911-16923.
- Donnay, J.P., Barnsley, M.J. Longley, P.A. (2001). *Remote Sensing and Urban Analysis*. Taylor & Francis.
- Faust, K., Entwisle, B., Rindfuss, R.R., Walsh, S.J., Sawangdee, Y. (2000). *Spatial Arrangement of Social and Economic Networks Among Villages in Nang Rong District, Thailand*. *Social Networks*, 21: 311-337.
- Fernandes, R., Fraser, R., Latifovic, R., Cihlar, J., Beaubien, J., Du, Y. (2004). Approaches to fractional land cover and continuous field mapping: a comparative assessment over the BOREAS study region. *Remote sensing of environment* 89, 234-251.

- Forster, B. (1983). Some urban measurements from Landsat data. *Photogrammetric Engineering and Remote Sensing*, 49, 1693–1707.
- Gamba, P., Houshmand, B. (2000). Digital surface models and building extraction: a comparison of IFSAR and LIDAR data. *Geoscience and Remote Sensing, IEEE Transactions* 38, 4:1959-1968.
- Guest, P. (1996). Assessing the consequences of internal migration: methodological issues and a case study on Thailand based on longitudinal household survey data. *Migration, Urbanization, and Development: New Directions and Issues*. United Nations Population Fund and Kluwer.
- Hong Y., Li, X. (2000). Cultivated land and food supply in China, *Land Policy*, 17: 73-88.
- Jencks, C., Mayer, S.E. (1989). The social consequences of growing up in a poor neighborhood. L. Lynn and M. McGeary (editors). *Inner City Poverty in the United States*. Washington, D.C.: National Academy Press.
- Kalnay, E. and Cai, M. (2003). Impact of urbanization and land-use change on climate. *Nature* 423:528-531.
- Korinek, K., Entwisle, B., Jamplakay, A. (2005). Through thick and thin: layers of social ties and urban settlement among Thai migrants. *American Sociological Review* 70: 779-800.
- Luniak, M. (1994). The development of bird communities in new housing estates in Warsaw. *Memorabilia Zoologica* 49: 257–267.
- Marzluff J.M. (2001). Worldwide urbanization and its effects on birds. Marzluff J.M, Bowman, R, Donnelly, R (editors). *Avian Ecology in an Urbanizing World*. Norwell (MA): Kluwer.
- Mesev, V. (1998). The use of census data in image classification. *Photogrammetric Engineering and Remote Sensing*, 64, 431–438.
- Paine, D.P., Kiser, J.D. (2003). *Aerial photography and image interpretation*. Second edition. John Wiley and Sons, Hoboken, New Jersey, USA.
- Paola, J.D., Schowengerdt, R.A. (1995). A review and analysis of back-propagation neural networks for classification of remotely sensed multi-spectral images. *International Journal of Remote Sensing*, 16, 3033–3058.
- Phongpaichit, P. (1993). The Labour Market Aspects of Female Migration to Bangkok. *Internal Migration of Women in Developing Countries*. New York: United Nations, 179-191.

- Ridd, M.K. (1995). Exploring a V-I-S (vegetation-impervious surface-soil) model for urban ecosystem analysis through remote sensing: Comparative anatomy for cities. *International Journal of Remote Sensing* 16, 2165–2185.
- Seto, K.C., Kaufmann, R. K. (2003). Modeling the drivers of urban land use change in the Pearl River Delta, China: Integrating remote sensing with socioeconomic data. *Land Economics* 79(1): 106-121.
- Shettigara, V.K., Sumerling, G.M. (1998). Height determination of extended objects using shadows in SPOT images. *Photogrammetric Engineering and Remote Sensing*, 64, 35± 44.
- Small, C., Pozzi, F, Elvidge, C.D. (2005). Spatial analysis of global urban extent from DMSP-OLS night lights. *Remote Sensing of Environment*, 96, 277-291.
- Small, C. (2003). High spatial resolution spectral mixture analysis of urban reflectance. *Remote Sensing of Environment* 88, 170–86.
- United Nations. (2004). Department of Economic and Social Affairs. *World Urbanization Prospects: The 2003 Revision*. New York: United Nations.
- Walsh, S.J., Evans, T.P., Welsh, W.F., Entwisle, B., Rindfuss, R.R. (1999). Scale dependent relationships between population and environment in northeast Thailand. *Photogrammetric Engineering and Remote Sensing* 65(1):97-105.
- White, M., Montgomery, M.R., Brennan-Galvin, E.M., Visaria, P. (2003). Urban Population Dynamics: Models, Measures and Forecasts. In National Research Council, *Cities Transformed: Demographic Change and Its Implications in the Developing World*. Panel on Urban Population Dynamics, Mark R. Montgomery, Richard Stren, Barney Cohen, and Holly E. Reed (editors). Washington, DC: The National Academies Press: 108-154.
- Wilson, J.S., Clay, M., Martin, E., Struckey, D., Vedder-Risch, K. (2003). Evaluating environmental influences of zoning in urban ecosystems with remote sensing. *Remote Sensing Environment* 86, pp. 303-321.
- Wu, W. (2002). Temporary migrants in Shanghai: Housing and settlement patterns. In *Globalization, market reform, and the new Chinese city*, edited by J. R. Logan, 212-226. New York: Blackwell.
- Xian, G., Crane, M. (2005). Assessments of urban growth in the Tampa Bay watershed using remote sensing data. *Remote Sensing of Environment* 97, 203-215.

Yeh, A.G.O., Li, X. (1997). An integrated remote sensing and GIS approach in the monitoring and evaluation of rapid urban growth for sustainable development in the Pearl Rive Delta, China. *International Planning Studies*, 2, 193-210.

CHAPTER 2

MIXTURE MODELING AND URBAN CHANGE DETECTION

2.1 Introduction

The spectral mixture problem, or unmixing, has been studied intensively in remote sensing. In urban environments, particularly, unmixing has often been applied, because of the typically heterogeneous land cover types that occur and their complex spatial organization. Many urban pixels have mixed spectral signals from two or more land cover types involving some proportion of vegetated and non-vegetated surfaces (Song, 2005). This is especially the case when images with low or medium spatial resolution are employed in urban environments, or other complex settings, for land cover classification. Therefore, traditional per-pixel classifications are often problematic in representing urban landscapes and estimating built-up or vegetated areas. Spectral Mixture Analysis (SMA), or “unmixing”, has long been used to solve the mixture problem in remote sensing applications (e.g., Adams et al., 1995; Smith et al., 1990). Ridd (1995) proposed a conceptual Vegetation - Impervious surface- Soil (V-I-S) model to unmix the pixels in urban settings. This type of linear mixture modeling has been employed by many researchers to derive one or more urban landscape elements (e.g., Phinn et al., 2002; Small, 2001; Ward et al., 2000; Wu and Murray, 2003; Song, 2005).

Impervious surfaces are of particular interest, because they indicate important urban and non-urban structures, suggest historical and contemporary social and

biophysical processes, and represent the probable quality of life of the associated population (Lo, 1997; Yang and Lo, 2002). In addition to linear spectral mixture analysis, numerous other models have been employed to derive land cover composition at the sub-pixel level. Using a Fuzzy C-Means algorithm, Fisher and Pahirana (1990) found significant, but varied, relationships between the fuzzy membership values and land cover proportions. Wang (1990) presented a fuzzy supervised classification in which the class membership function was defined using a modified maximum-likelihood algorithm, and Foody et al. (1992) also found high correlations between the land cover proportions and the class membership probabilities derived from the maximum-likelihood algorithm.

Over the last decade, considerable effort has been expended in the use of non-parametric models to derive sub-pixel proportions. Decision Trees (e.g., DeFries et al., 1999; Xian et al., 2005) and Neural Networks (e.g., Atkinson et al., 1997; Carpenter et al., 1999; Fernandes et al., 2004) have been of particular interest and applicability. Many have suggested that these types of models are superior to traditional spectral mixture analysis and fuzzy supervised classification approaches, because they do not make assumptions about the nature of the spectral mixing, and the function is simply learned from training samples. Several neural network models are common. For instance, ARTMAP models have been increasingly used due to their stable and fast performance (Carpenter et al., 1999; Liu et al., 2004). The Multi-Layer Perceptron (MLP) neural network model is probably one of the most widely used neural network models in sub-pixel classification (e.g., Atkinson, 1997; Fernandes et al., 2004; Foody, 1996; Liu, 2005). Depending on whether sub-pixel proportions are incorporated at the network training stage, Foody et al. (1997) defined the neural network approaches as full fuzzy or

partial fuzzy classification. In the full fuzzy approach, the sub-pixel proportions are known for the training pixels and the proportions are directly used as the network targets in training. These network targets are treated as continuous variables (e.g. 0-1). On the other-hand, the sub-pixel proportions are unknown for training pixels in the partial fuzzy approach. Training pixels are selected in the same manner as in traditional per-pixel neural network classification. The network targets are set as discrete variables (e.g. 1-of-M coding system such as 1,0,0). The network output signals, however, are retained in a “fuzzy” manner (i.e., between 0 and 1). Within the neural network literature, these two approaches are generally referred to as the Neural Network Regression and Neural Network Classification problems, based on the characteristics of the network targets (continuous or discrete). In the regression problem, the neural network approximates the regression function between the input patterns and the target values. In the classification problem, the network outputs approximate the probabilities of class membership for each class (Bishop, 1995).

A review of recent neural network applications in sub-pixel estimation shows that the neural network regression approach is used more often, and the results are promising as compared to linear spectral mixture analysis and fuzzy supervised classification (Atkinson et al., 1997; Zhang and Foody, 1998). One limitation of the regression approach is that sub-pixel proportions are required for training. The proportions are typically derived from aerial photography or satellite imagery with relatively higher spatial resolution. The high spatial resolution data, however, are often expensive to obtain, cover limited geographic areas, and requires a substantial amount of processing time and effort to co-register fine and medium spatial resolution imagery (e.g., QuickBird

and Landsat Thematic Mapper data, respectively). For instance, the high spatial resolution image may be available for urban core areas only. It is highly questionable to employ the trained neural network for larger spatial extents including urban fringes and surrounding rural areas, where the types and the spectral signals of land cover (i.e., agricultural field) can be very different from urban core areas. Fernandes et al. (2004) found that the neural network sub-pixel classification accuracy is substantially lower if the test sites are further away from the training sites (i.e., 100-km). The poor generalization ability can seriously impact the implementation of the neural network regression approach for mapping in large urban environments. The neural network classification approach, on the other-hand, is a straightforward supervised classification. Although the training pixels need to be identified by photointerpretation, typically using maps and air photographs as reference, it does not require that sub-pixel proportions be known in the network training stage. Therefore, training data can be selected in a more relaxed manner for all apparent classes in the image. The major limitation of the neural network classification approach is that it generally has a relatively lower accuracy in terms of overall performance (Schowengerdt, 1996; Zhang and Foody, 2001; Moody et al., 1996). For instance, Foody (1996) trained the network with pure pixels and found that the network outputs were close to the two extremes (0 or 1). These network outputs are not directly suitable for the estimation of sub-pixel proportions. A number of practical techniques were employed to improve the classification performance, including the re-scaling of network outputs (Foody, 1996) and the modification of the activation function (Warner and Shank, 1997).

One common problem of these neural network classification approaches is that they assume the network outputs approximate the probabilities of class membership, which are often interpreted as sub-pixel proportions in remote sensing applications (e.g. Foody et al., 1992; Ju et al., 2003; Lee et al., 2006). Richard and Lippmann (1991) indicate that MLP neural networks require a large number of training data points to model the posterior probabilities. They state that the training data also needs to be representative in both class likelihood distributions and class prior probabilities. In many remote sensing classification practices, however, these requirements are ignored. For instance, the training pixels are normally selected from spectrally homogeneous areas and the numbers of training pixels are often very limited. This type of sampling scheme may not reflect the spectral variability of cover types (Gong and Howarth, 1990; Huang et. al., 2002). In addition, the proportion of occurrences of each class in the training set or the prior probabilities of the training set can also affect the network training and classification results. Few researchers, however, have evaluated the impacts of prior probability on the classification results, especially for the sub-pixel classification problems. From an urban application perspective, it is also important to study the temporal variation of land cover. In most previous change detection studies, the pixels are labeled as discrete values (0 or 1) indicating change/no change or a specific type of land cover change. The sizes or shapes of land cover change patches, however, can vary greatly across the landscape. Some changes occur at sizes smaller than the imposed spatial resolution of the satellite sensor system. With sub-pixel classification results, it is possible to consider a fuzzy representation of land cover change.

This chapter is designed to examine and improve the neural network classification approach for an urban mapping application. The theory and empirical testing are discussed for the following two methodological improvements: (1) evaluation of the impacts of the class likelihood distribution on the sub-pixel classification results. In one training set, training pixels are identified from spectrally homogeneous areas and the number of training pixels is relatively small. In the other training set, large number of training pixels are identified from both spectrally homogeneous and heterogeneous (i.e., edge pixels) areas; (2) impacts of varying prior probabilities in the training set are also examined. Specifically, number of training pixels is arbitrarily reduced for one class in a given training dataset, while keeping the number of training pixels in the other classes constant. The results from the neural network classification approach are compared with those from the more widely used neural network regression approach. The classifier with the higher accuracy is used to derive the proportional impervious cover from a Landsat TM/ETM image time-series. The rates of urban growth from 1993 to 1999 and 1999 to 2002 are examined.

2.2 MLP Neural Network: Background

MLP is composed of multiple layers of processing nodes and links. Figure 2.1 illustrates a typical three-layer MLP.

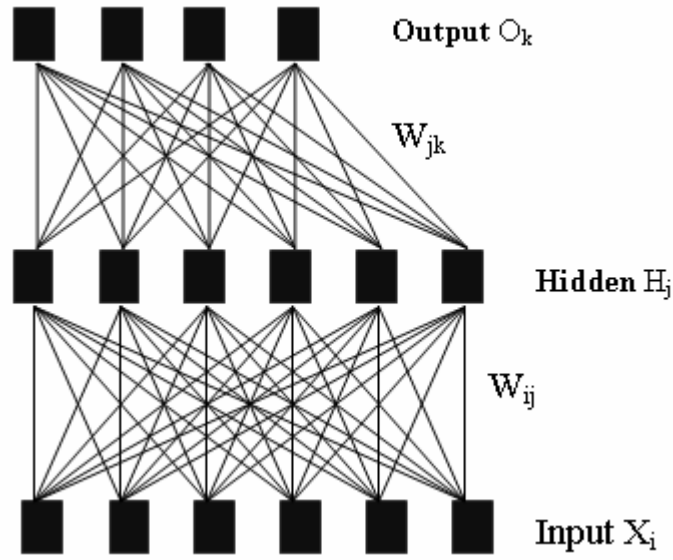


Figure 2.1. A typical three-layer MLP neural network

Input, hidden, and output units are denoted by X_i , H_j , and O_k respectively. W_{ij} denotes the links from input nodes to hidden nodes, and W_{jk} indicates the links from hidden nodes to output nodes. H_j is computed according to Equation 1, and O_k is computed according to Equation 2.

$$H_j = f\left(\sum_{i=1}^n X_i W_{ij}\right) \quad \text{Equation 1}$$

$$O_k = f\left(\sum_{j=1}^m H_j W_{jk}\right) \quad \text{Equation 2}$$

In Equations 1 and 2, f indicates an activation function: a sigmoid function is generally used. The function must be differentiable. The sigmoid function saturates at both extremes. M and n are the numbers of the nodes at the hidden layer and the input layer, respectively. To train neural networks, the weights are first initialized with random values; input patterns such as the spectral signals of training pixels are presented forward

through the network. The resultant values at output nodes are compared with the target values (T_k) using the sum of the squared error (Equation 3).

$$E = \frac{1}{2} \sum_{k=1}^c (T_k - O_k)^2 \quad \text{Equation 3}$$

A back-propagation algorithm is used to adjust the weights and minimize the overall error (Rumelhart et al., 1986). Using the 1-of-M target coding system (e.g. 1,0,0), the output of the MLP classifier can approximate the Bayesian a posterior probabilities if large numbers of training samples are available (Richard and Lippmann, 1991). The Bayesian posterior probability can be written as:

$$P(c_i | x) = \frac{p(x | c_i) \times P(c_i)}{P(x)} \quad \text{Equation 4}$$

In remote sensing applications, x can be seen as the DN (Digital Number) value from one spectral band or a DN vector from multispectral space. $P(c_i|x)$ is the posterior probability, indicating the probability that a pixel belongs to class c_i given the pixel's DN value(s), x . $p(x|c_i)$ is the likelihood -- the probability that a pixel has DN value/vector x , given it is in class c_i . $P(c_i)$ is the class prior probability. It is the probability that a randomly chosen pixel in the image is of class c_i , or simply, the fraction of pixels in the image belonging to class c_i . $P(x)$ is a normalization term, and is calculated as:

$$P(x) = \sum_{i=1}^k p(x | c_i) \times P(c_i) \quad \text{Equation 5}$$

For a given training set, the frequency distribution of classes can be seen as the prior probabilities of the training set. As McIver and Friedl (2002) suggest, the selection of training pixels is often subjective, depending on data availability and user preferences. Therefore, the prior probabilities of the training set can be very different from the prior

probabilities of the full image. In most previous research, however, the trained network is applied to the whole image and the network outputs are directly used as the estimation of sub-pixel proportions. This procedure assumes that the prior probabilities in the full image are equal to those from the training set. This assumption is not necessarily true and may lead to poor classification results. The network outputs may also be sensitive to a number of training protocols that include network architecture, learning rates, and the criteria used to stop training (Duda and Hart, 2001). Large amounts of time must be invested in the network training stage, especially to evaluate the impacts of training protocols on the performance of the classification (Gopal and Woodcock, 1996; Paola and Schowengerdt, 1995).

2.3 Data

Six Landsat TM/ETM images (see Table 2.1) are obtained for the land use/cover classification and change-detection analysis. A mosaic of the Landsat image is produced for each of the time periods, and a subset of 2370×2690 pixels is created to cover the Bangkok Metropolitan Area and its surrounding provinces (see Figure 2.1). A Landsat-7 image (1999) is treated as the master image, and the image to image registration is performed for the Landsat-5 image (1993) and the Landsat-7 image (2002) respectively. The geometric error of registration is less than 0.5 pixel.

Table 2.1:

Landsat TM/ETM Images for the Study Area.

Acquisition date	Path	Row
December 25, 1993	129	50
December 25, 1993	129	51
November 16, 1999	129	50
November 16, 1999	129	51
January 8, 2002	129	50
January 8, 2002	129	51

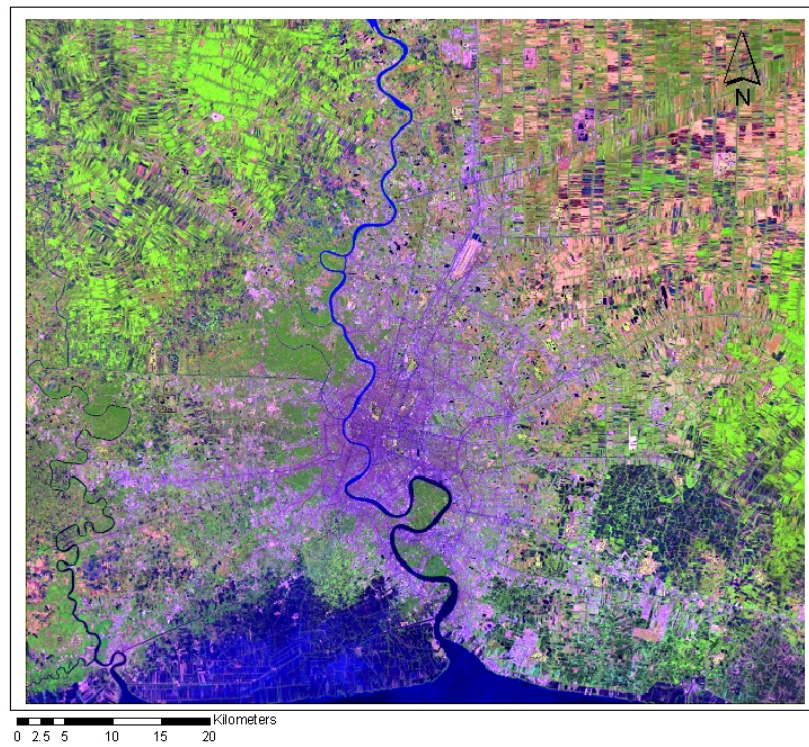


Figure2.2a. December 25, 1993 image.

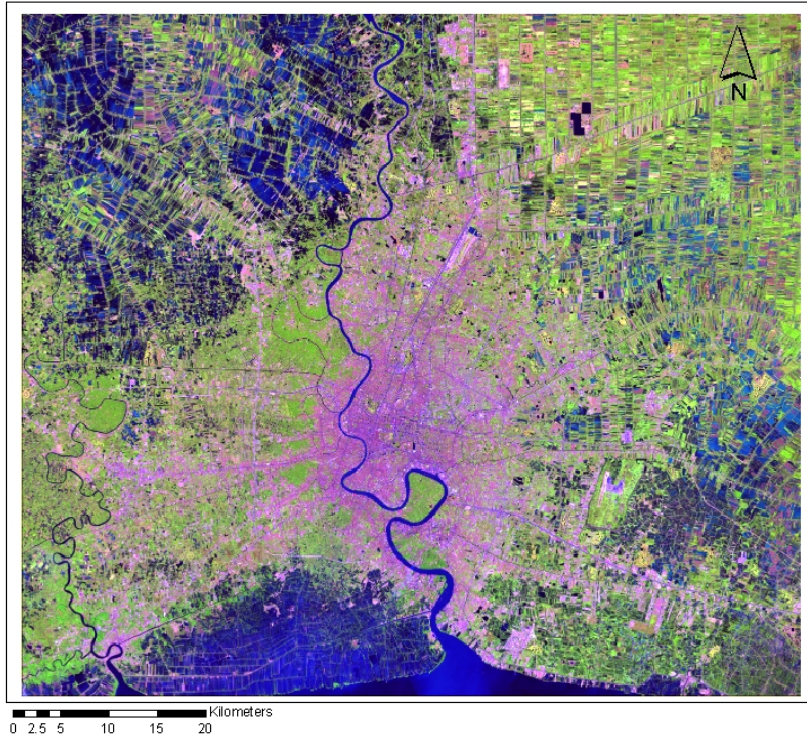


Figure2.2b. November 16, 1999 image.

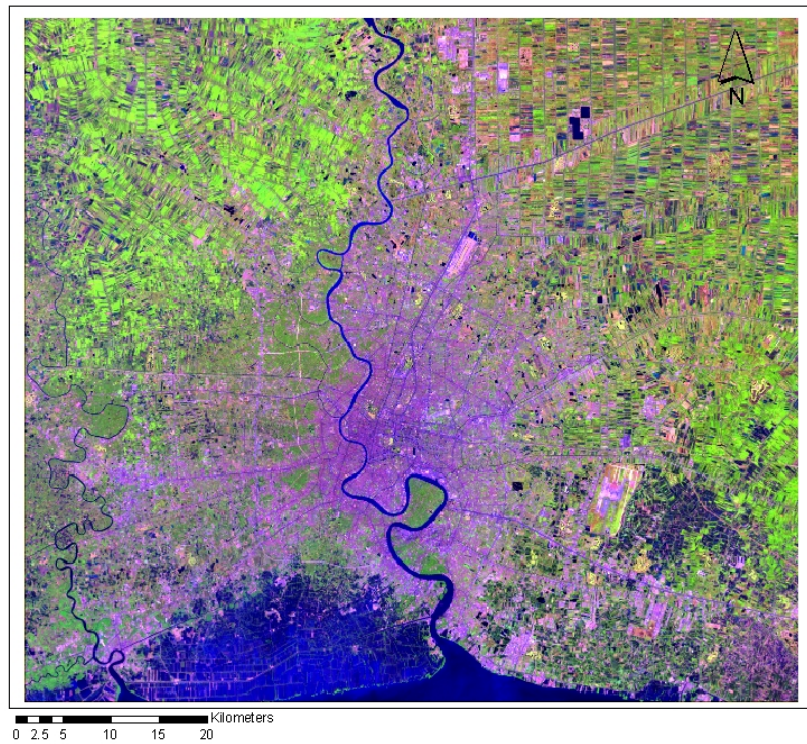


Figure2.2c. January 8, 2002 image.

High-spatial resolution IKONOS data from November 2002 and May 2000 were also obtained. Substantial numbers of shadow pixels can be observed from the November 2002 IKONOS image, and, as such, may cause difficulty in image classification and uncertainty in area estimation. Therefore, the May 2000 IKONOS image is treated as the primary ground truth data to evaluate the performance of sub-pixel classifications.

2.4 Method

2.4.1 Using the Classification Approach

The Landsat ETM (November 16, 1999) image is chosen as the primary dataset for testing the sub-pixel classification approach. A five-class classification scheme is designed for the neural network classification task: impervious cover, vegetation, bare soil, water/shadow, and agricultural fields. The scheme is an extended version of the Vegetation-Impervious cover-Soil (V-I-S) model. In this study, the agricultural fields indicate the cleared rice/cash crops that have different spectral signals from bare soil due to crop residue. Two methods are employed to identify training samples. The first approach follows a common practice and sampling scheme for a supervised classification. A total of 904 pixels (236, 225, 212, 231 and 215 for impervious, vegetation, water/shadow, soil, and agricultural fields respectively) are collected from spectrally-homogeneous areas on the Landsat ETM image. The high spatial resolution IKONOS image and Google Earth maps are employed as reference data for identify training sites. In the second sample selection approach, large numbers of training samples (4923, 2842, 1813, 2017, and 2453 for impervious, vegetation, water/shadow, soil, and agricultural field respectively) are manually selected. In addition to spectrally-homogeneous areas, pixels at the edges of impervious/vegetation patches are also

selected. Figure 2.3 shows the distributions for selected training pixels in Band3 and Band4 feature space for the two training datasets, respectively. Only one in every 20 vegetation and impervious cover pixels are plotted here to make it more readable.

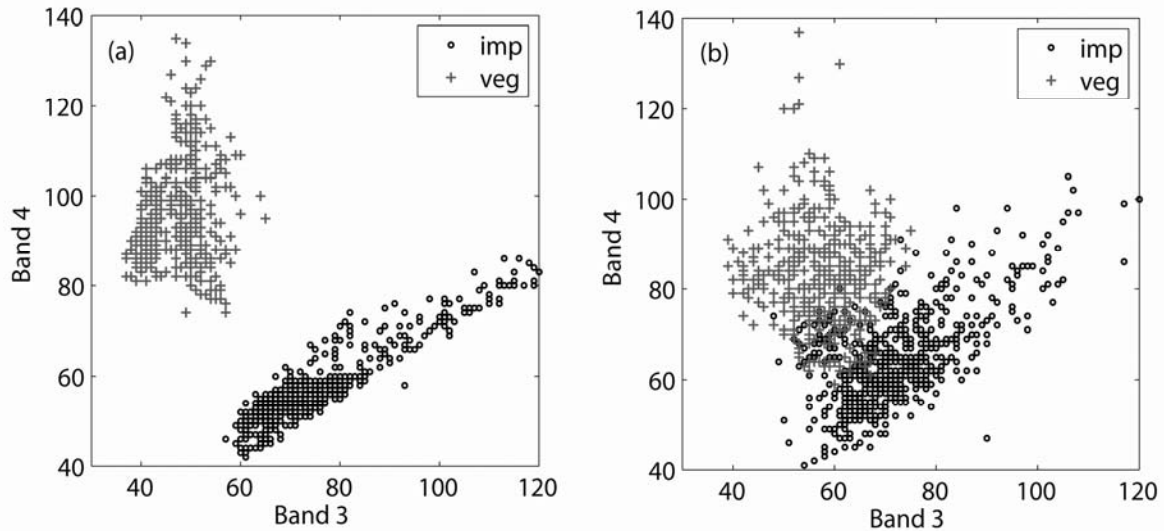


Figure 2.3. Select training pixels from two training sets (small vs. large sample size).

The software employed in this study is called Stuttgart Neural Network Simulator (<ftp.informatik.uni-tuebingen.de>). It is a powerful software package for neural network analysis on UNIX workstations. A three-layer neural network was employed in this study: six inputs nodes were used indicating six spectral bands from Landsat imagery. Five output nodes indicate five land-cover types: vegetation, impervious, water/shadow, soil, and agricultural field. Different numbers of nodes were tested for the hidden layer: 6, 12, and 18. The Landsat ETM spectral signals were scaled to values between 0 and 1 prior to their input into the MLP for training and classification. Three different learning rates were tested: 0.1, 0.2 and 0.3. The momentum was specified as 0.9. The network training was stopped as the learning curve began to converge.

The proportion of occurrences of each class in the training set, or the prior probabilities of the training set, can also affect the network training and classification results. To examine the impacts of prior probability on the classification results, the frequency distributions of classes in the second training set are modified arbitrarily. Specifically, the training pixels were reduced or increased for impervious cover, while the numbers of training pixels from other classes (e.g., vegetation, soil and water/shadow) remain the same. In this study, 75-percent and 125-percent of impervious pixels are randomly selected from the second training set. The randomly selected impervious pixels are combined with training pixels from other land cover classes to generate additional training datasets. It should be noted that the random selection of training pixel may cause variations in the class likelihood distributions. Therefore, the procedure of random selection and training dataset generation are repeated 5 times. The classification results are examined for each of the training dataset. Table 2.2 shows the number of training pixels for each class and their fractions in different training datasets.

Table 2.2:

The Number of Training Pixels (and Percentages) for Each Class

Training dataset	Impervious cover	Vegetation	Water	Soil	Agricultural fields	Total
2	4923 (35%)	2842 (20%)	1813 (13%)	2017(14%)	2453(17%)	14048
3	3692(29%)	2842(22%)	1813 (14%)	2017(16%)	2453(19%)	12817
4	6105(40%)	2842(19%)	1813(12%)	2017(13%)	2453(16%)	15230

2.4.2 Using the Regression Approach

To evaluate whether the neural network classification methods generate acceptable accuracy, the sub-pixel estimation was also implemented as with the more widely used regression approach. The sub-pixel proportions are required for network training for the neural network regression approach. The high resolution IKONOS image was first classified into 30 spectral clusters using an unsupervised classification procedure. The IKONOS image only covers limited areas in the urban core and some urban fringe areas, and the dominant land cover types are impervious cover, vegetation, soil, and shadow/water. Therefore, the spectral clusters were subsequently grouped into these four broad land cover types. The classified IKONOS image was degraded to 30×30 -m resolution to spatially correspond to the Landsat ETM data, providing a “fractional map” for each of the four land cover types.

The fraction maps derived from IKONOS data are directly incorporated in the network training. Specifically, six input nodes were used indicating six spectral bands from Landsat ETM imagery. The four output nodes indicate land cover fractions from the four land cover types. Different numbers of nodes were tested for the hidden layer -- 6, 12, and 18. A total of 3000 random pixels were selected from the Landsat ETM image. These Landsat pixels, together with their land cover fractions at the sub-pixel level, were combined to build the training samples and targets for the MLP. To avoid overfitting, the network training was stopped after every 100 epochs to determine the optimum stopping point for network training, and the entire fractional maps were used as testing data at each stopping point.

2.4.3 Accuracy Assessment and Generalization

To assess the accuracy of sub-pixel classification, the RMSE values between the IKONOS-generated fractional map and the neural network outputs were examined. The error of co-registration can seriously impact the results (Song 2005; Townshend et al., 1992), thus aggregated class proportions were generated using a 3x3 window (90m x 90m) for both the fractional map and the MLP classification results before calculating RMSE. RMSE is calculated using the following equation:

$$RMSE = \sqrt{\frac{\sum_{i=1}^n (E_i - A_i)^2}{n}}$$

Equation 7

where E_i is the estimated fraction cover from Landsat ETM pixels, A_i is the actual fraction cover derived from high-resolution IKONOS data, and n is the total number of windows used in testing.

For both neural network classification and regression approaches, the networks with the best classification performance (i.e., smallest RMSE) are retained for the classification of the entire image. It should be noted that the high resolution IKONOS data only covers limited areas of the urban core and some urban fringe areas (see Figure 2.4). The high classification accuracy achieved at the urban core and fringe areas does not guarantee its generalizability to rural-dominated landscapes. As described earlier, some agricultural fields may have very similar spectral signals to those from impervious cover. Overestimation of impervious cover is a common problem for many remote sensing applications. Therefore, it is important to examine the generalizability of network classifiers over large spatial extents. The visual interpretation of Landsat ETM image and

Google Earth maps is the most feasible approach for the validation of image classification over large spatial extents.

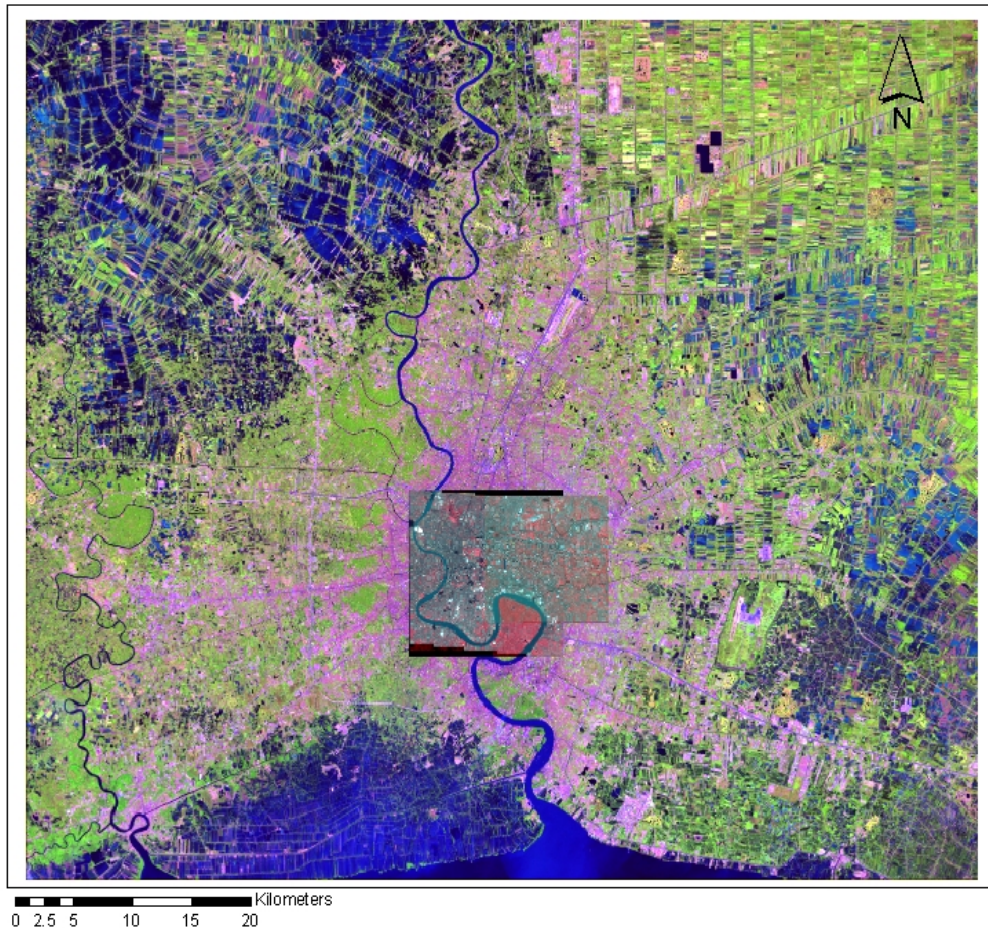


Figure 2.4. The Spatial Extents of IKONOS Image and Landsat ETM Image.

2.4.4 Image Change Detection

The Neural network classification approach is employed to derive proportional impervious cover for Landsat-5 TM (1993) and Landsat-7 ETM (2002) images. The reason to choose the neural network classification approach over the regression approach is largely due to data availability. For the Landsat-5 TM (1993) image, there is no high resolution data available for generating fractional maps, which is necessary for the neural network regression approach. Therefore, large numbers of training samples representing

impervious, vegetation, water/shadow, soil, and agricultural fields are manually selected from Landsat-5 TM image (1993) and Landsat-7 ETM (2002) image. Again, different network learning protocols are assessed for sub-pixel classification. To evaluate the classification performance or consistency over time, 100 3x3 windows (90m x 90m) are selected as testing sites. The sample windows are typically located at commercial areas in the urban core, primary roads, and some old residential areas at the urban fringe. The land covers in these testing windows are considered stable through time. Cross-plots of impervious cover percentages are generated for these testing windows (i.e., 1993 vs.1999 and 1999 vs. 2002). The classification results with the highest consistency (i.e., low scattering for the cross-plots) are employed for image change detection analysis.

The urban land cover change information is presented at both sub-pixel and per-pixel levels. At the sub-pixel level, the change of proportional impervious cover is calculated for each pixel from 1993 to 1999 and from 1999 to 2002, respectively. The fuzzy representation of land cover change map can be easily converted to per-pixel based change maps using a threshold of 0.5. The annual rates of urban growth are calculated for two time periods: 1993 to 1999 and 1999 to 2002.

2.5 Results

The RMSE values are used to assess the classification performances. For each training set, a variety of numbers of network trainings are conducted using different combinations of learning rates (0.1, 0.2, and 0.3) and hidden nodes (6, 12, and 18). For any given network architecture and learning rate, the network training is repeated 5 times. Figure 2.5 shows a boxplot of RMSE values for the first two training sets. Training set 1 has 904 training pixels, while training set 2 has 14048 training pixels. Figure 5 indicates

that the sub-pixel classification results improve with an increasing training sample size. The RMSE values for training set 1 show a wide scattering (i.e., from 0.11 to 0.184), while the RMSE values from training set 2 are consistently lower, in the range of 0.106 to 0.125. This is important from both an estimation-accuracy and a time-efficiency perspective. For instance, it is possible to achieve high accuracy of sub-pixel classification using a limited number of training samples. However, the classification results vary substantially with learning rate, network architecture, and network initialization. It requires more time for trial-error testing to achieve acceptable accuracy. On the other-hand, the classification results are less sensitive to these network training protocols. In fact, the classification results are always acceptable, if large numbers of training pixels are available.

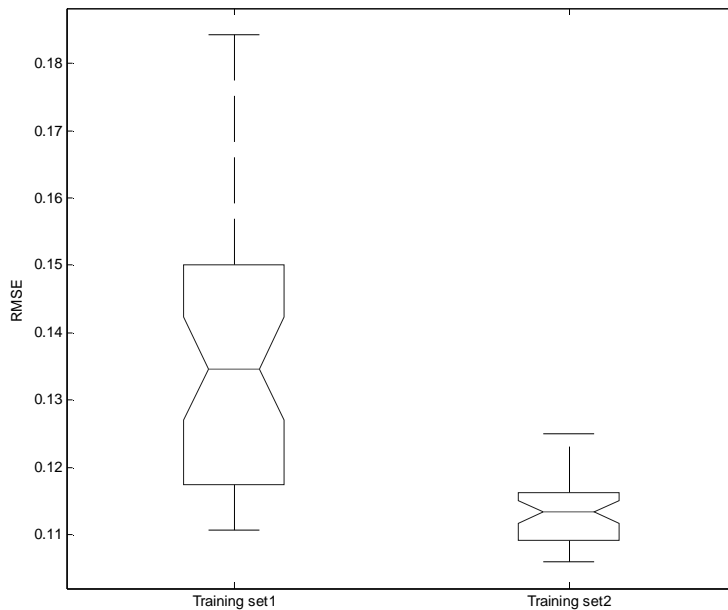


Figure 2.5. Comparison of RMSE values from varying training sample sizes: training set 1 (small sample size), training set 2 (large sample size).

The results reported here are supported by Richard and Lippmann's (1990) simulation work. They demonstrated that the estimation of posterior probabilities deteriorates dramatically when the size of the training set decreases from 3000 samples per class to 1000 samples per class. More importantly, if the training pixels are solely selected in spectrally homogeneous areas, the within-class variance may be underestimated (Gong and Howarth, 1990; Huang et. al., 2002). Previous research also suggests that network outputs can be uncertain if input patterns are novel to the trained network (Bishop, 1994). This implies that neural networks may produce erroneous outputs for pixels with mixed signals, if the network is trained using pure pixels only.

The impacts of the prior probabilities on the sub-pixel classification are also evaluated. The ranges of RMSE values are slightly different using training sets with varying prior probabilities: training set 2 (0.106-0.125), training set 3 (0.105-0.1318), and training set 4 (0.104-0.1307). Figure 2.6 shows the boxplot of the RMSE values for a variety of numbers of network trainings using different combinations of training sets, learning rates, and network architectures. Although the boxplot shows different ranges or scattering of RMSE values from three training datasets, a simple t-test shows that there is no significant difference between the average classification performances. For each training dataset, RMSE values are very similar using different learning rates (0.1, 0.2 and 0.3). The results are slightly better when 12 or 18 hidden nodes are used.

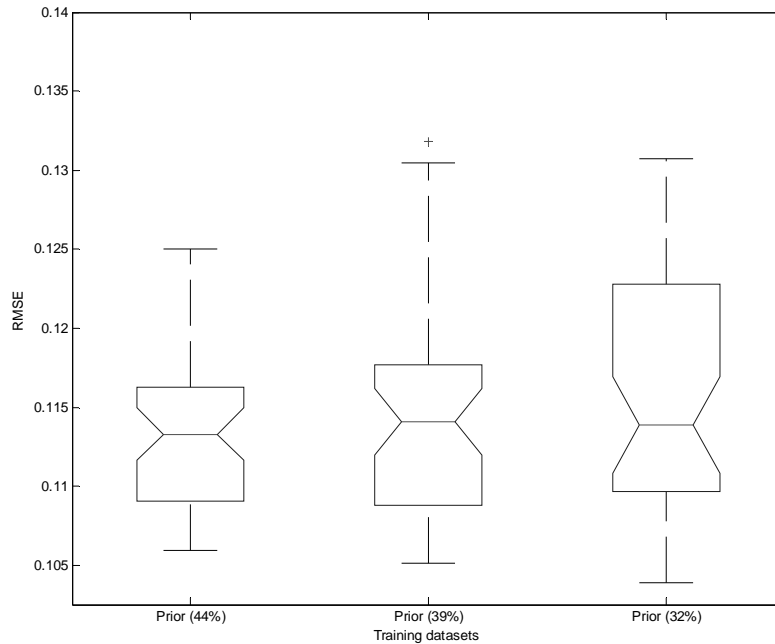


Figure 2.6. Comparison of RMSE values from varying prior probabilities.

In the regression approach, the high-resolution data are incorporated in both network training and testing stages. The range of RMSE for the regression approach is from 0.097 to 0.105. Figure 2.7a and 2.7b show the scatter-plots of estimated sub-pixel proportions plotted against the actual proportions. The actual proportions of impervious cover are derived from high resolution IKONOS imagery that only covers limited areas in the urban core and some urban fringe areas. The regression approach generated slightly better results in the areas with high resolution IKONOS training data. This was anticipated, because high-resolution data were used in both network training and testing. The relationships between sub-pixel proportions and the input spectral signals are simply learned through training samples (with sub-pixel proportions specified as the training targets). In the neural network classification approach, however, the assumption is made that posterior probabilities are equal to sub-pixel proportions. This assumption may or

may not be true, depending on the characteristics of the study site and the information class of interest. Schowengerdt (1996) presents the importance of spectral signature separability – the approach is valid only if classes of interest have high spectral separability. In addition, the characteristics of training data may not be representative for the study site, including the class likelihood distributions and class prior probabilities. Although the accuracy of this approach is lower than for that of the regression approach, the difference in accuracy is not substantial, and for many objectives, this loss in accuracy may be worth the savings in time and costs associated with the regression approach.

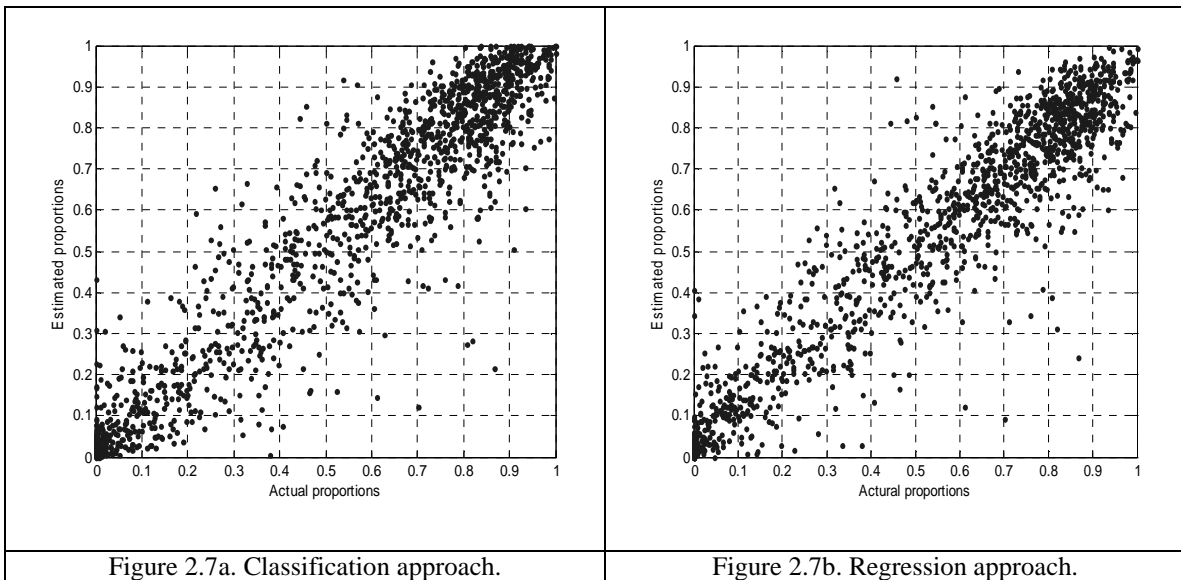


Figure 2.7. Accuracy Assessment of Neural Network Classification and Regression Approaches

Figure 2.8a and 2.8b show the results for the entire Bangkok city and surrounding areas using the neural network classification and the regression approach, respectively. Initial visual interpretation indicates that urban areas or impervious cover is clearly discernible from the results of neural network classification approach. For neural network regression approach, however, there appears to be confusion between impervious cover

and several other land use/cover types (i.e., soil, cleared rice field, and even water class). This is to be expected since all training pixels for the regression approach are randomly selected and limited by the spatial extents of high resolution IKONOS imagery. Therefore, the network may generate uncertain outputs if input patterns are novel to the trained network. In practice, it is difficult to obtain high resolution data to cover large spatial extents and then produce sub-pixel proportional covers for network training. Data availability and poor generalizability can be major challenges in the use of neural network regression for mapping large urban environments.

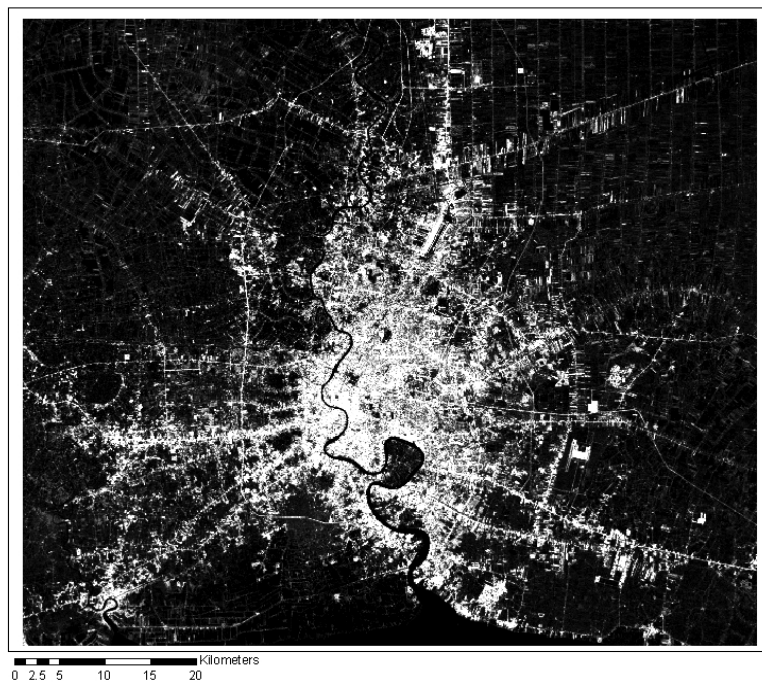


Figure 2.8a. Neural network classification approach

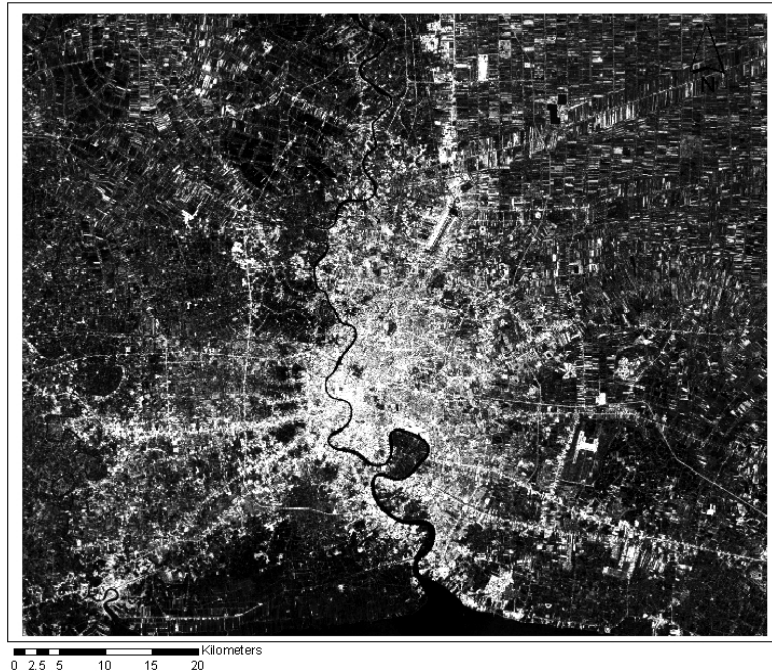


Figure 2.8b. Neural network regression approach

Figure 2.8. Imperviousness Derived from 1999 Landsat ETM image using Neural Network Classification and Regression Approaches.

One potential solution for the improvement of the neural network regression approach is to incorporate more training samples. For instance, more training pixels can be identified from areas at the urban fringe or at rural setting, especially for those pixels confused in the initial classification. The target values can be set as 0 (i.e., 0% of impervious cover) for these additional training pixels (i.e., agricultural fields). However, visual interpretation of initial classification results shows that almost all other land cover types need to be evaluated, including agricultural fields, bare soil, and even water. In other words, the sample selection procedure at this step is simply to repeat the same training data collection conducted in the neural network classification approach. After collecting large numbers of training samples, the network is re-trained and the Landsat

ETM image is re-classified. The result is shown in Figure 2.9, which is similar to the impervious cover derived from the neural network classification approach.

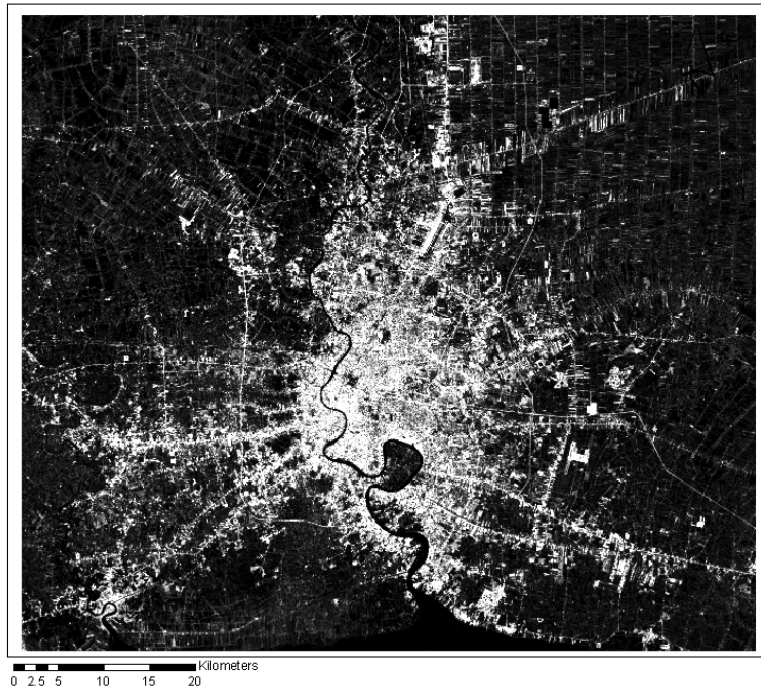


Figure 2.9. Improved Classification Results from Neural Network Regression Approach.

The neural network classification approach is also used to derive the proportional impervious cover from Landsat-5 TM (1993) and Landsat-7 ETM (2002) imagery. Figure 2.10 shows the proportional impervious cover for 1993 and 2002, respectively. On the left-side of Figure 2.10 is Landsat TM/ETM images, whereas on the right-side is the derived impervious cover.

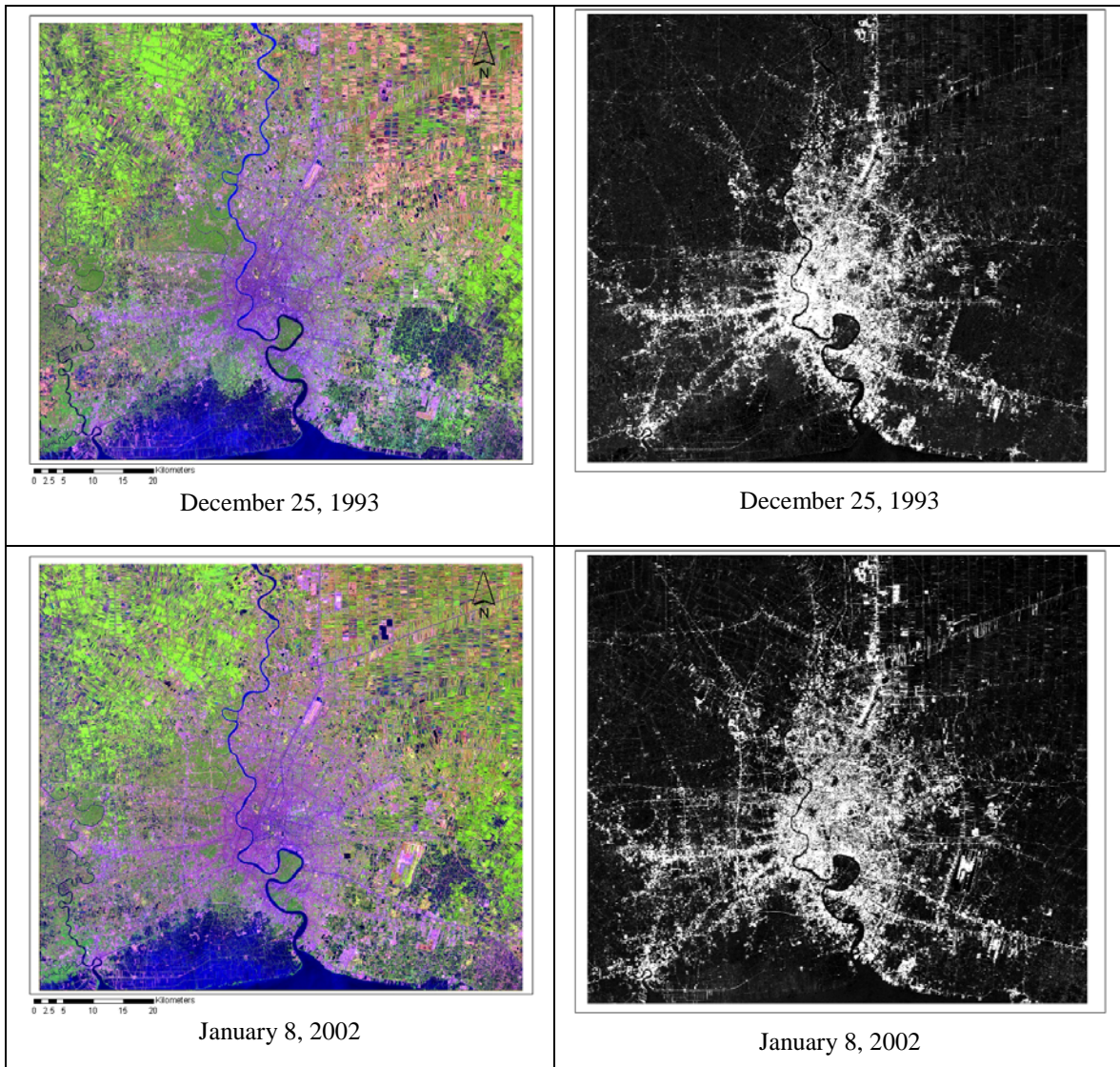


Figure 2.10. Landsat TM/ETM images and Imperviousness of Bangkok from 1993 and 2002.

Change-detection analysis is simply conducted by comparing the difference in the proportional impervious cover for each pixel from different time-periods. Figure 2.11 shows the fuzzy representation of land cover change. Overall, there are more urban developments from 1993 to 1999 than from 1999 to 2002. The acquisition dates for the 1999 and 2002 images are November 16, 1999 and January 8, 2002, respectively. Therefore, the actual difference between these two images is only about 2 years, and dramatic urban development and change rarely occurs within this short period. Due to

complexity of scene-spatial/scale-ground object relationships, the fuzzy representation of land cover change may be considered a more realistic approach than traditional per-pixel analysis. However, it should be noted that the sub-pixel classification accuracy is about 11-percent for the 3 by 3 window size (90m). The accuracy of sub-pixel classification at 30m spatial resolution may be even lower than this number. Also, the mis-registration between images may introduce additional uncertainty in change-detection analysis, especially for pixel-by-pixel comparisons (Townshend et al., 1992). Therefore, the urban change in fuzzy representation needs to be interpreted with caution. For instance, an increase of proportional impervious cover less than 22-percent may or may not be a real change due to uncertainty in sub-pixel classification.

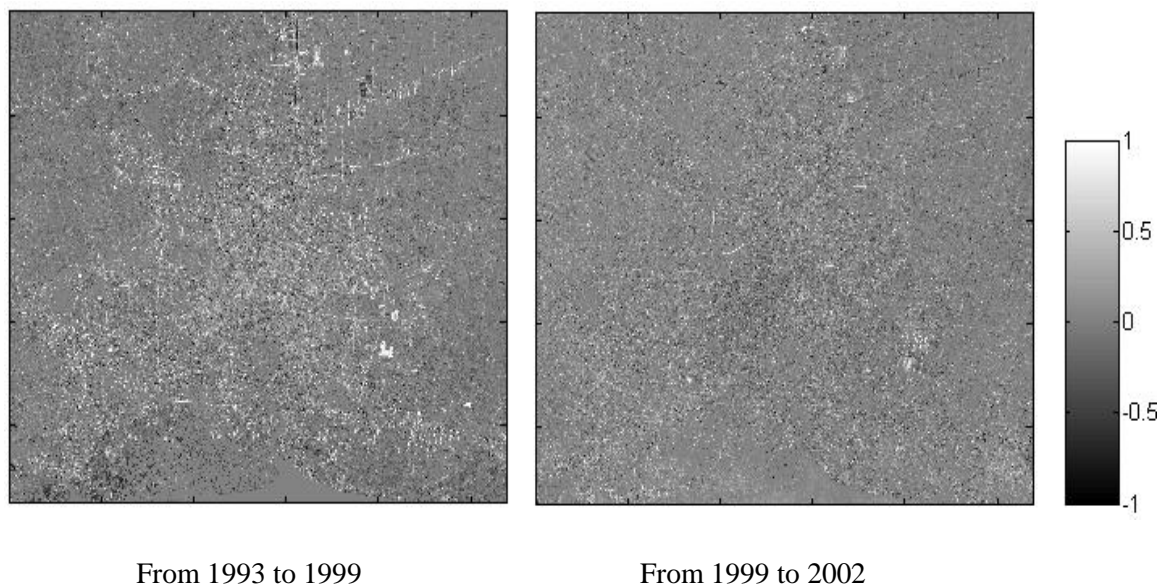


Figure 2.11. Fuzzy Representation of Image Change Detection (Imperviousness) from 1993 to 1999 and 1999 to 2002.

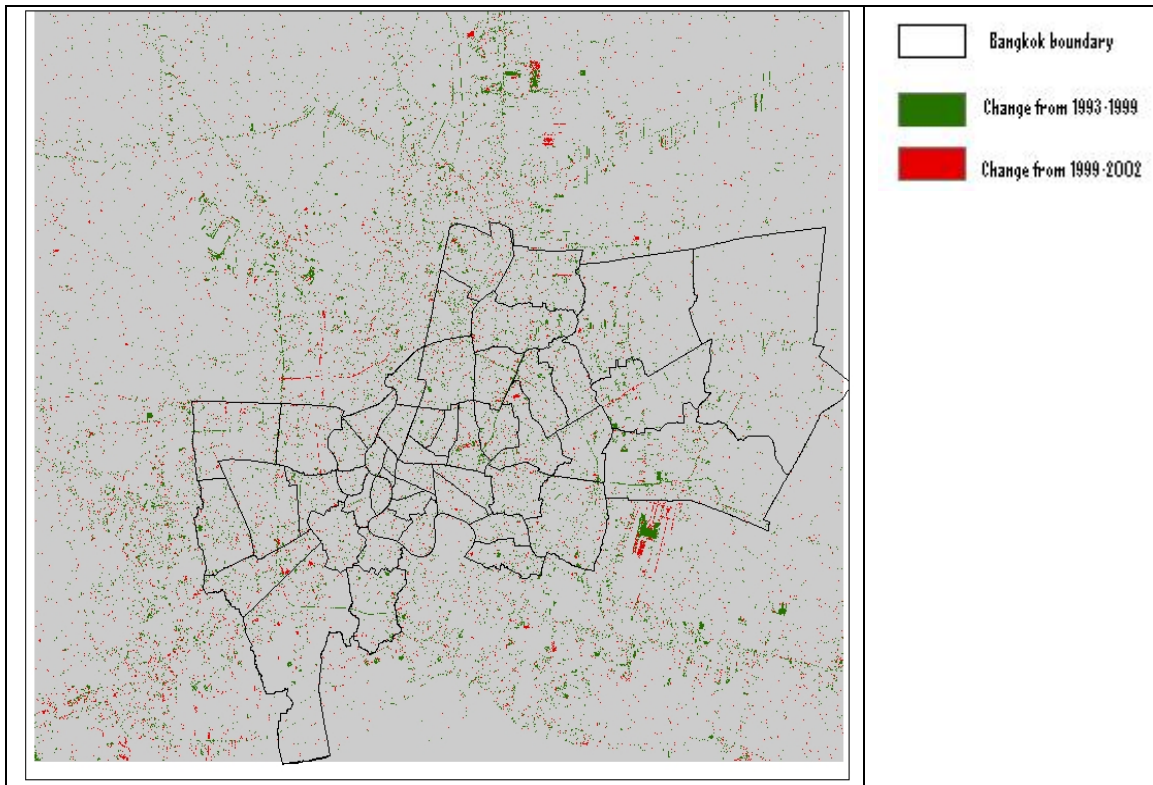


Figure 2.12. Per-Pixel Change Detection (Imperviousness) from 1993 to 1999 and 1999 to 2002

The fuzzy representation of urban change can be easily converted to traditional per-pixel change maps. A threshold of 0.5 is applied for the proportional change map. A pixel is considered to be a significant change pixel, if there is an increase of 50-percent impervious cover. Figure 2.12 shows urban development from 1993 to 2002 using the per-pixel approach. Pixels in green indicate urban growth from 1993 to 1999; pixels in red indicate urban growth from 1999 to 2002. The metropolitan growth has extended well beyond official Bangkok boundaries. Administrative boundaries seem to be irrelevant in studying the dynamics of urban growth (McGee 1991, 1995). For the entire study area, the total area of impervious cover is 560km², 708² and 779² km for 1993, 1999, and 2002, respectively. The annual growth rate is 4-percent from 1993 to 1999 and 5-percent from 1999 to 2002.

2.6 Conclusion

Sub-pixel proportions are estimated through neural network regression and neural network classification approaches. Although the regression approach generated slightly better results (i.e., lower RMSE values) in the areas with high resolution IKONOS training data, the classification approach also achieved acceptable accuracy. In addition, the neural network regression approach requires high-resolution data in the network training process. The data availability and poor generalizability may seriously impact the implementation of the neural network regression approach for mapping in large urban environments. The neural network classification approach, on the other-hand, is a straightforward supervised classification. It does not require that sub-pixel proportions be known in the network training stage. Therefore, the training pixels can be identified in a more relaxed manner. This can be advantageous for mapping large urban environments using time-series remote sensing data.

To generate accurate sub-pixel fraction estimates using the neural network classification approach, two practical concerns are recommended. First, evaluate the impacts of training sample size and the class likelihood distribution on the sub-pixel classification results. Second, the impacts of varying prior probabilities in the training set should also be examined. High-resolution IKONOS data are only used to validate the classification results. Through this case study, a large sample size and spectral heterogeneity in the training set were found to be important for deriving consistent sub-pixel estimations. A large improvement in the performance of the classification was realized as compared to previous studies that used limited training samples from spectrally homogeneous areas. The prior probability in the training set may also affect

classification performance, but its impacts are less than those from training sample size. In practice, however, it is impossible to define specific sample size for each land cover/use class and the prior probabilities are often unknown for the study areas. Therefore, a solution is to collect large numbers of training samples and evaluate the classification results based on ground truth or references derived from high-resolution images. The network architecture and other training protocols also need to be examined. The entire process requires large amounts of time and it is probably the most challenging question for the users and researchers of neural networks. In this research, the neural network classification approach is also employed to derive proportional impervious cover for a Landsat TM and ETM image time-series for Bangkok, Thailand. The urban changes are represented using both fuzzy and per-pixel approaches. It is found that most urban developments are located outside of the Bangkok city boundary. Traditional urban analysis or modeling using administrative boundaries may not be ideal for studying the dynamics of urban environments.

References

- Adams, J.B., Sabol, D., Kapos, V., Fliho, R.A., Roberts, D.A., Smith, M.O. (1995). Classification of multispectral images based on fractions of endmembers: application to land-cover change in the Brazilian Amazon. *Remote Sensing of Environment* 52, 137-154.
- Atkinson, P.M., Cutler, M.E.J., Lewis, H. (1997). Mapping sub-pixel proportional land cover with AVHRR imagery. *International Journal of Remote Sensing*, 18(4), 917-935.
- Bishop, C.M. (1994). Novelty detection and neural network validation. *Vision, Image and Signal Processing, IEE Proceedings*, 141(4), 217-222.
- Bishop, C.M. (1995). *Neural Networks for Pattern Recognition*. Clarendon press. Oxford.
- Carpenter, G.A., Gopal, S., Macomber, S., Martens, S., Woodcock, C.E. (1999). A neural network method for mixture estimation for vegetation mapping. *Remote Sensing of Environment* 70, 138-152.
- DeFries, R., Townshend, J., Hansen, M. (1999). Continuous fields of vegetation characteristics at the global scale at 1-km resolution. *Journal of Geophysical Research*, 104, 16911-16923.
- Duda, R.O., Hart, P.E., Stork, D.G. (2001). *Pattern Classification*. John Wiley & Sons, Inc.
- Fernandes, R., Fraser, R., Latifovic, R., Cihlar, J., Beaubien, J., & Du, Y. (2004). Approaches to fractional land cover and continuous field mapping: a comparative assessment over the BOREAS study region. *Remote Sensing of Environment* 89, 234-251.
- Fisher, P., Pathirana, S. (1990). An evaluation of fuzzy membership of landcover classes in the suburban zone. *Remote Sensing of Environment* 34, 121-132.
- Foody, G.M., Compbell, N.A., Trodd, N.M., Wood, T.F.(1992). Derivation and applications of probabilistic measures of class membership from the maximum likelihood classification. *Photogrammetric Engineering and Remote Sensing*, 58(9): 1335-1341.
- Foody, G.M., McCulloch, M.B., Yates, W.B. (1995). The effect of training set size and composition on artificial neural network classification. *International Journal of Remote Sensing*, 16(9), 1707-1723.

- Foody, G.M. (1996). Relating the land-cover composition of mixed pixels to artificial neural network classification output. *Photogrammetric Engineering and Remote Sensing*, 62(5), 491-499.
- Foody, G.M. (1997). Fully fuzzy supervised classification of land cover from remotely sensed imagery with an artificial neural network. *Neural Computing and Applications*, 5, 238-247.
- Frizzelle, B.G., Moody, A. (2001). Mapping continuous distributions of land cover – A comparison of maximum-likelihood estimation and artificial neural networks. *Photogrammetric Engineering and Remote Sensing*, 67(6), 693-705.
- Gong, P., Howarth, P.J. (1990). An assessment of some factors influencing multispectral land-cover classification. *Photogrammetric Engineering and Remote Sensing*, 56, 597-603.
- Gopal, S., Woodcock, C. (1996). Remote sensing of forest change using artificial neural networks. *IEEE Transactions on Geoscience and Remote Sensing* 34(2), 398-404.
- Gopal, S., Woodcock, C., Strahler, A. (1999). Fuzzy ARTMAP classification of global land cover from the 1 degree AVHRR data set. *Remote Sensing of Environment*, 67, 223– 243.
- Huang, C., Davis, L.S., Townshend, J.R.G. (2002). An assessment of support vector machines for land cover classification. *International Journal of Remote Sensing*, 23(4), 725-749.
- Ju, J., Kolaczyk, E.D., Gopal, S. (2003). Gaussian mixture discriminant analysis and sub-pixel land cover characterization in remote sensing. *Remote Sensing of Environment* 84, 550-560.
- Landgrebe, D.A. (2003). *Signal Theory Methods in Multispectral Remote Sensing*. John Wiley & Sons, Inc.
- Lee, S., Lathrop, R.G. (2006). Subpixel analysis of Landsat ETM/sup +/- using self-organizing map (SOM) neural networks for urban land cover characterization. *IEEE Transactions on Geoscience and remote sensing*, 44(6), 1642-1654.
- Liu, W., Seto, K., Wu, E.Y., Gopal, S., Woodcock, C.E. (2004). ART-MMAP: a neural network approach to subpixel classification. *IEEE Transactions on Geoscience and Remote Sensing*, 42(9), 1976-1983.
- Liu, W. (2005). Comparison of non-linear mixture models: sub-pixel classification. *Remote Sensing of Environment*, 94,145-154.

- Lo, C. P., Faber, B. (1997), Integration of Landsat Thematic Mapper and Census Data for quality of life assessment. *Remote Sensing of Environment*, 62, 143–157.
- Lo, C.P., Choi, J. (2004). A hybrid approach to urban land use/cover mapping using Landsat 7 Enhanced Thematic Mapper Plus (ETM+) images. *International Journal of Remote sensing*, 25(14), 2687-2700.
- McIver, D.K., Friedl, M.A. (2002). Using prior probabilities in decision-tree classification of remotely sensed data. *Remote Sensing of Environment*, 81,253-261.
- Moody, A., Gopal, S., Strahler, A.H. (1996). Artificial neural network response to mixed pixels in coarse-resolution satellite data. *Remote Sensing of Environment* 58,329-343.
- Paola, J., Schowengerdt, R.A. (1995). A detailed comparison of backpropagation neural network and maximum-likelihood classifiers for urban land use classification. *IEEE Transactions on Geoscience and remote sensing*, 33(4), 981-996.
- Phinn, S., Stanford, M., Scarth, P. (2002). Monitoring the composition of urban environments based on the vegetaion-impervious surface-soil (VIS) model by subpixel analysis techniques. *International Journal of Remote sensing*, 23(20), 4131-4153.
- Richards, J. A., Jia, X. (1999). *Remote Sensing Digital Image Analysis*. Springer.
- Richard, M.D., Lippmann, R.P. (1991). Neural network classifiers estimate Bayesian a Posteriori probabilities. *Neural Computation*, 3, 461-483.
- Ridd, M.K. (1995). Exploring a V-I-S (vegetation-impervious surface-soil) model for urban ecosystem analysis through remote sensing: Comparative anatomy for cities. *International Journal of Remote Sensing* 16(12), 2165–2185.
- Rumelhart, D.E., Hinton, G.E., Williams, R.J. (1986). *Learning internal representation by error propagation in Parallel Distributed Processing: Explorations in the Microstructures of Cognition*. MIT press, Cambridge, MA, pp.318-362.
- Schowengerdt, R.A. (1996). On the estimation of spatial-spectral mixing with classifier likelihood functions. *Pattern Recognition Letters*, 17, 1379-1387.
- Small, C. (2001). Estimation of urban vegetation abundance by spectral mixture analysis. *International Journal of Remote Sensing*, 22(7), 1305-1334.
- Smith, M.O., Ustin, S.L., Adams, J.B., Gillespie, A.R. (1990). Vegetation in deserts: A regional measure of abundance from multispectral images. *Remote Sensing of Environment* 31, 1-26.

- Song, C. (2005). Spectral mixture analysis for subpixel vegetation fractions in the urban environment: how to incorporate endmember variability? *Remote Sensing of Environment*, 95, 248-263.
- Strahler, A.H. (1980). The use of prior probabilities in maximum likelihood classification of remotely sensed data. *Remote Sensing of Environment*, 10, 135-163.
- Townshend, J.R.G., Justice, C.O., Gurney, C., McManus, J. (1992). The impact of misregistration on change detection. *IEEE Transactions on Geoscience and Remote Sensing*, 30(5), 1054–1060.
- Wang, F. (1990). Fuzzy supervised classification of remote sensing images. *IEEE Transactions on Geoscience and Remote Sensing*, 28(2), 194-201.
- Ward, D., Phinn, S.R., Murray, A.T., (2000). Monitoring growth in rapidly urbanizing areas using remotely sensed data. *Professional Geographer* 52: 371-386.
- Warner, T.A., Shank, M. (1997). An evaluation of the potential for fuzzy classification of multispectral data using artificial neural networks. *Photogrammetric Engineering and Remote Sensing*, 63(11), 1285-1294.
- Wu, C., Murray, A.T. (2003). Estimating impervious surface distribution by spectral mixture analysis. *Remote Sensing of Environment* 84,493-505.
- Xian, G., Crane, M. (2005). Assessments of urban growth in the Tampa Bay watershed using remote sensing data. *Remote Sensing of Environment*, 97, 203-215.
- Yang, X., Lo, C.P. (2002). Using a time series of satellite imagery to detect land use and land cover changes in Atlanta, Georgia metropolitan area. *International Journal of Remote Sensing*, 23(9), 1775-1798.
- Zhang, J., Foody, G.M. (1998). A fuzzy classification of sub-urban land cover from remotely sensed imagery. *International Journal of Remote Sensing*, 19, 2271-2738.
- Zhang, J., Foody, G.M. (2001). Full-fuzzy supervised classification of sub-urban land cover from remotely sensed imagery: statistical and artificial neural network approaches. *International Journal of Remote Sensing*, 22(4), 615-628.

CHAPTER 3

BUILDING HEIGHT ESTIMATION USING SHADOW INFORMATION

3.1 Introduction

The classification of remotely-sensed data is generally conducted at the two-dimensional or 2-D level in which a target pixel or object is assigned to each of the predefined land use/cover categories such as impervious cover, water, vegetation and soil cover (e.g., Ridd, 1995). In a more detailed land use classification, individual pixels may be classified as agriculture, forest, residential/commercial and roads and parking lots (e.g., Landgrebe, 2003; Paola and Schowengerdt, 1995). In this type of 2-D land use/cover mapping, a high-rise building and a single-story structure may be classified as the same land cover category (i.e., impervious cover). The building height information has generally not received sufficient attention in remote sensing of urban places, particularly satellite-based remote sensing. The ability to characterize the three-dimensional or 3-D urban setting may provide very useful, and even essential, information for assessing urban structure and socio-demographic implications of urban areas that are of particular interests to urban planners and researchers in social, population, and environmental studies (Delaney, 2000; Gruen and Nevatia, 1998; Shiode, 2001).

The use of aerial photogrammetry techniques is the most common approach to derive 3-D structural information. Manual interpretation of building height from aerial photography is a time-consuming and expensive task that often relies on the application

of standard equations and devices such as stereoscopes, stereoplotters, and parallax wedges (Paine and Kiser, 2003). Over the past 30-years, automatic building extraction and building height estimation have been one of the main challenges in the fields of photogrammetry and computer vision (e.g., Baillard, 1999; Gruen et al., 1995; Mohan and Nevatia, 1989; Noronha and Nevatia, 2001). One approach to estimate building height is to examine shadows cast by the structure on aerial photograph (e.g., Avery, 1977; Huertas and R. Nevatia, 1988; Irvin et al., 1989). The building height can be estimated from the shadow length using simple trigonometry. The shadow approach is appealing, because shadows often have relatively homogeneous spectral responses (i.e., dark areas) compared to spectral patterns from buildings. Therefore, the segmentation of shadow is relatively easier to accomplish than direct building extraction and building height estimation (i.e., Huertas and R. Nevatia, 1988; Lin et al., 1994; McGlone et al., 1994; Yi-Hsing and Wang 2003).

A few researchers have used satellite-borne remote sensing data to estimate building height. For instance, Shettigara and Sumerling (1998) derived building heights using shadow information on a SPOT panchromatic image. However, shadow detection from medium spatial-resolution satellite imagery (e.g., SPOT, Landsat TM/ETM) is difficult, because the shadow size may be less than the size of a single pixel. The size, shape, and boundary of a building's shadow may not be well defined in a medium spatial resolution image. The newly available high resolution imagery (e.g., IKONOS) has improved spatial resolution to 1-m to 4-m. These data offer new opportunities for building height estimation using shadow information, however, until recently very few studies have used IKONS images for 3-D building height estimation. Fraser et al. (2002)

conducted traditional photogrammetric analysis using 1-m panchromatic IKONOS stereo images, but the data availability (i.e., stereo-pair) and the variability of scene-to-scene image quality are main concerns. The shadow analysis, however, shows significant potential as an alternative approach for building height estimation or 3-D urban mapping. The main purpose of this chapter is to design a semi-automated approach for shadow detection and building height estimation using IKONOS imagery.

There are three main challenges for the automatic shadow detection and building height estimation. First, the classification of high resolution imagery is a difficult task due to the high information content of high-resolution data (Schowengerdt, 1997). Pixels of a homogeneous land cover patch may have heterogeneous spectral responses (i.e., roof structures). A “salt and pepper” effect is a main concern using traditional per-pixel classifiers that are generally employed for image classification (Bauer et al., 2001; Stuckens et al., 2000). Second, the spectral responses of shadows are very similar to those from other dark features such as a water body. Although the shadows can be identified using visual interpretation, often based on neighboring buildings or texture information, it is difficult to delineate shadow and water automatically (e.g., Sawaya et al. 2003). Third, there is a need to develop computer algorithms to estimate shadow length and building height in an automatic manner. This is especially important for a large study area such as Bangkok, Thailand. Manual interpretation of shadow length can be extremely expensive and time consuming, if large numbers of buildings are involved.

One potential approach for shadow detection on high resolution imagery is to use the “per-field” classification approach (Ballard and Brown, 1982; Janssen, 1994; Roberts, 1970; Tilton, 1989; Woodcock et al., 1992). Per-field classification employs not only

spectral information, but also the spatial concepts such as shape and neighborhood information to segment an image. Recently developed commercial software, *eCognition*, provides a user-friendly environment to generate and analyze images through an object-based image analysis (i.e., OBIA) approach (Blaschke et al. 2000; eCognition User Guide 2003). OBIA has been increasingly used in high-resolution image classifications (e.g., Walsh et al., in press). This study examines the use of OBIA in a complex urban setting. The main purpose is to identify shadow objects from high resolution IKONOS images. In addition to the spectral information, a number of spatial indices, such as size, shape, and spatial neighbors are used to separate shadow and water objects, a challenge in remote sensing image analyses. The building height is estimated using the relationship between building location, shadow, and solar position (e.g., elevation angle and azimuth angle). The high-rise buildings in Bangkok, Thailand are of particular interests.

3.2 Data

Two IKONOS images were used in this study. The image acquisition dates are May 08, 1999 and November 27, 2002. The November 27, 2002 image is of high quality with no clouds and haze, while the May 08, 1999 image has some clouds present. The spatial extent of each IKONOS image is approximately $11\text{km} \times 11\text{km}$. There is a $10\text{km} \times 6\text{km}$ overlap area between the two images. However, a substantial portion of the overlap area for the 1999 image has cloud cover. Therefore, it is not feasible to conduct a stereo-pair image analysis. In addition, these two images cover the entire core area of Bangkok, as well as some fringe areas of the city (Figure 3.1). Thus, single image-based shadow analysis is used to provide 3-D information for a larger spatial extent (i.e., $16 \times 10 \text{ km}$).

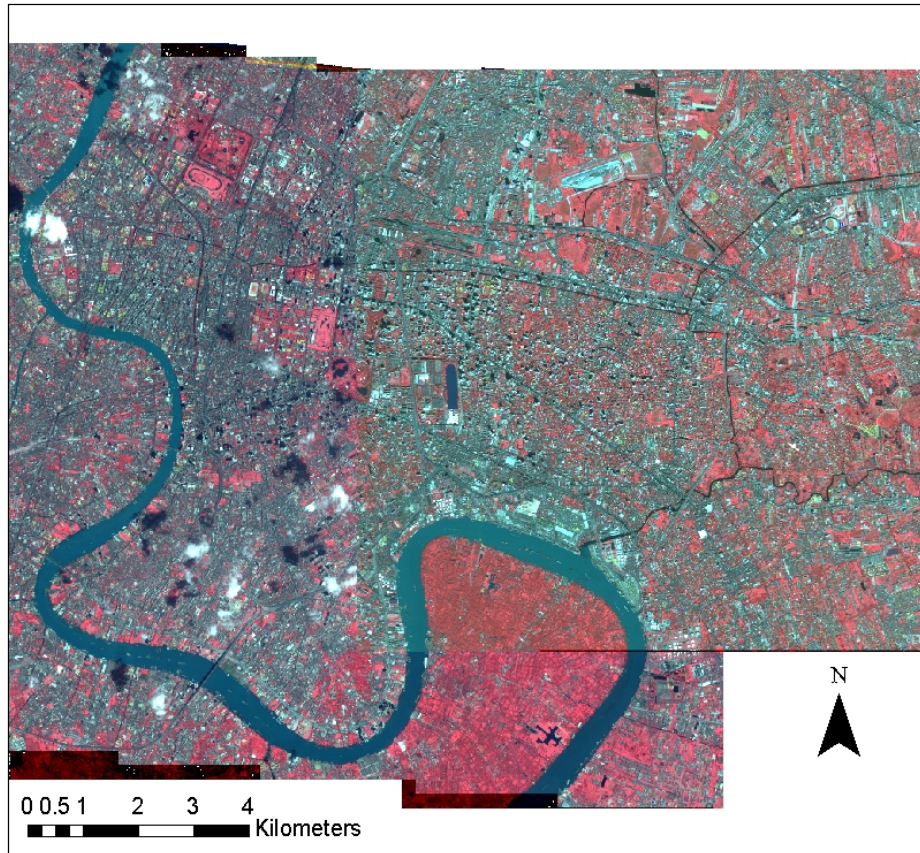


Figure 3.1. IKONOS Image from 1999 and 2002 (Band 4, 3, and 2 composite).

An IKONOS image has a spatial resolution of 4-m for the multi-spectral bands. The spatial resolution of satellite remote sensing systems have greatly improved and now approached those of medium-scale aerial photography. IKONOS has three spectral bands from the visible spectrum and one band from the near-infrared spectrum. In addition to the multi-spectral bands, there is also a panchromatic band with a spatial resolution of 1-m. The radiometric resolution is 11-bit. The improvements of spatial, spectral, and radiometric resolutions are critical for detailed 2-D and 3-D land use/cover classification in compact urban setting. The information describing the sun azimuth angle and sun elevation angle are obtained from image header files. Table 3.1 presents ephemeris data

about image acquisition time, sun elevation angle, and sun azimuth angle for both images.

Table 3.1:

IKONOS Image Acquisition Date, Sun Azimuth Angle and Sun Elevation Angle

	1999 image	2002 image
Acquisition date	May 08, 1999	November 27, 2002
Sun azimuth (degree)	78.1385	154.2802
Sun elevation (degree)	67.0952	51.5396

3.3 Method

The 2002 image was used as the primary dataset for the shadow detection and building height estimation. The image was first classified using an OBIA classification method. The classification results were evaluated by the standard error matrix. The spectrally confusing classes (i.e., shadow and water) were further analyzed using object size, shape, and spatial neighbor information. A simple thresholding method was employed to separate shadow and water objects. The “clean” shadow objects were then processed by a derived computer algorithm to generate shadow length and building height for high-rise buildings in Bangkok.

3.3.1 Image Segmentation

OBIA emphasizes image segments or objects. Individual pixels are grouped into meaningful objects based on spectral statistics and textural information (Blaschke et al., 2000). The first commercial software for OBIA is *eCognition* and now referred to as *Definiens Professional*. One main advantage of OBIA is its ability in multi-resolution segmentation. Multi-resolution segmentation uses a region-merging approach starting with 1-pixel objects. The resultant image objects can be considered as homogenous

image regions with regard to spectral statistics, texture, shape, and neighbor information (eCognition User guide, 2003). The image objects, instead of individual pixels, are the inputs for the image classification. Training samples (i.e., image objects) need to be identified for different land use/cover types. The input feature may include spectral information and additional object attributes such as shape, texture, and the spatial relationship between the objects.

The multi-resolution segmentation was first used to generate image objects. A number of parameters need to be defined in this process, including scale, color/shape, and smoothness/compactness. The parameter setting directly affects the size and the shape of image objects. It is impossible to define these parameters using prior knowledge, as trial-error tests are routinely used. For a specific image, large scale factors typically produce large image objects. A relatively small scale factor (i.e., 8) was used, thus small image objects such as individual buildings or shadows are discernable through visual interpretation. Color/shape (i.e., 0.3 and 0.7 respectively) and smoothness/compactness (i.e., 0.4 and 0.6 respectively) were defined. Four spectral bands were weighted equally in the image segmentation process.

The resultant image objects, from the image segmentation process, were used as inputs for classification. A six-class classification scheme was employed. Land cover types include shadow, water, vegetation, high albedo impervious cover, low albedo impervious cover, and soil. Training samples (i.e., image objects) were identified using visual interpretation. Both panchromatic and multi-spectral bands of IKONOS were used as reference. The classification is primarily based on the spectral statistics (i.e., mean value of spectral response) of image objects. A nearest neighbor classifier was employed

for the classification task. It should be noted that *eCognition* uses a fuzzy logic approach where each image object has a set of membership values with regard to the classification scheme. The image objects were labeled according to the highest membership value. The classification results were assessed using a standard error matrix. A total of 30 random pixels were selected for each of the land cover classes. These “test” pixels were examined by visual interpretation using IKONOS panchromatic and multi-spectral bands as reference.

3.3.2 Shadow Detection

Both shadow and water classes appear dark in the image. Spectral responses from these two classes are very similar, thus, it is difficult to separate these two classes using spectral information only. A number of object attributes such as size, shape, and spatial neighbor are employed to separate shadow and water objects. The object size/shape/spatial neighbor analysis is based on the classified image, instead of initial image segmentation results. For instance, all the spatially-connected pixels from the water class were treated as a single image object. A river, therefore, may become a single image object. The object size was used first to delineate extremely large objects such as rivers, streams, and large water bodies, such as lakes and ponds. These objects were discarded, because the sizes of most shadow objects from high-rise buildings are substantially smaller. The remaining image objects from shadow and water classes were then merged into a single water/shadow class. The object sizes were recalculated. Thresholding was employed to remove extremely small objects (i.e., less than 10 pixel) as small shadow objects are often related to low buildings.

The remaining image objects were further examined using shape indices. Visual interpretation of the IKONOS image shows that the shadows from low buildings in residential areas typically have an elongated linear shape, while those from high-rise buildings have a disk shape (Figure 3.2). A Perimeter-Area ratio was used to differentiate these two types of objects. In addition, some small streams may also show a linear shape, which can be detected using the same shape index. In addition to the Perimeter-Area ratio index, an Object Length index was also examined for the water/shadow objects. The Length index was calculated as the largest distance among individual pixels for a given image object. Similarly, thresholding was used to define potential shadow objects from high-rise buildings. All other shadow/water objects were discarded.

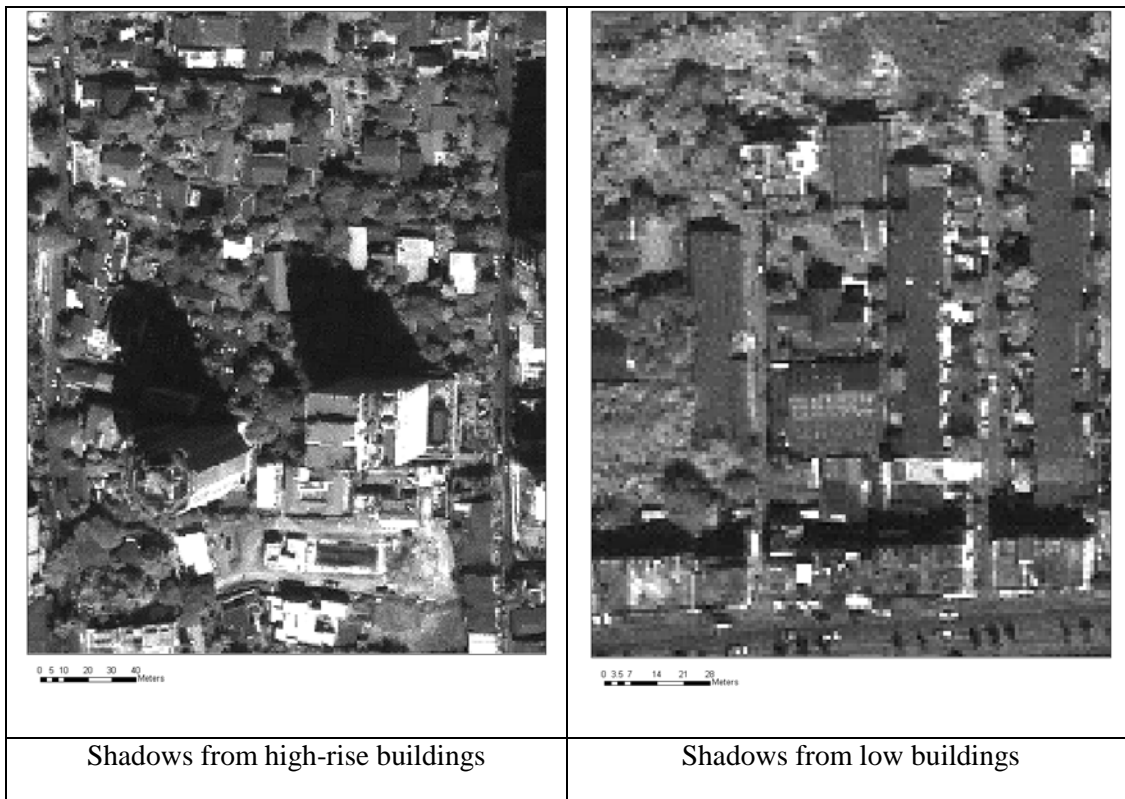


Figure 3.2. Examples of Shadow Objects for High- and Low- rise Buildings from IKONOS.

The spatial relationship of neighboring objects was also examined. An image object is considered a shadow if an impervious cover object is located in its “neighborhood” and in the sun-side direction. The object size, shape and spatial neighbor together serve as thresholds to generate a “clean” shadow dataset for building height estimation.

3.3.3 Shadow Length and Building Height Estimation

The shadow objects were first smoothed by removing the “pixel spurs”. The shadow length was then measured according to the sun-azimuth angle. A computer algorithm was designed for the task. First, the perimeter pixels were identified for each input shadow object. The distances and azimuth angles were calculated for all possible combinations between two perimeter pixels. However, only the largest distance measure in the defined azimuth angle range (i.e., 152~156 degrees) were retained as the shadow length. This measurement may be problematic for buildings with multileveled rectangular solids, but the approach is simple and efficient. The shadow lengths derived from this automatic computer algorithm were compared with the results from manual interpretation of the IKONOS image. Specifically, 20-percent of the shadow objects are randomly selected and shadow length was manually measured for each object.

The simplest method of building height estimation is to use trigonometry to link shadow length and building height. One key assumption is that the surface on which shadows fall is flat, which is the case for Bangkok. The topography of Bangkok is a low-lying, flat surface. Equation 1 shows a simple model of sun-building-shadow relationships:

$$H = L \times \tan (\theta)$$

Equation 1

where L is the length of the shadow and θ is the sun elevation angle. Sun elevation angle is directly available from the IKONOS image header file. In this approach, the accuracy level of building height measurements depends on the shadow length estimations.

3.4 Results

3.4.1 Image Segmentation

Multi-resolution image segmentation generated a total of 996,640 image objects. The object size varies greatly over the image. These image objects were labeled according to the strength of class membership outputs. Figure 3.3 shows a subset of initial classification results using the OBIA approach.

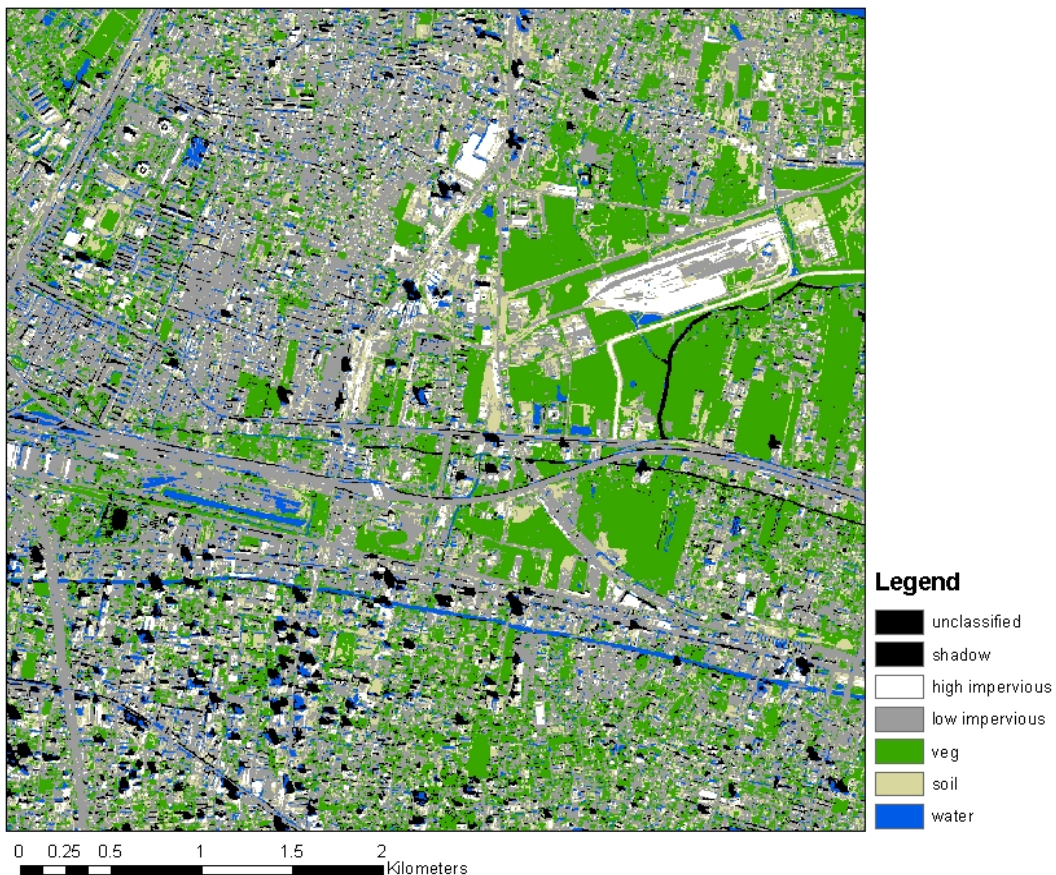


Figure 3.3. Image Classification Results from OBIA.

The classification results show more homogenous patches and less “salt and pepper” effects than a traditional per-pixel classifier (i.e., ISODATA), especially for the vegetation cover. A classification error matrix is presented in Table 3.2. The overall classification accuracy is 84-percent. The users’ and producers’ accuracy for the shadow class is 87-percent and 74-percent, respectively. The users’ and producers’ accuracy for the water class is 73-percent and 85-percent, respectively. The error matrix also suggests that the main difficulty is the confusion between shadow and water classes, as it is difficult to delineate shadow from water class using spectral information only. This is expected since the spectral responses from these two classes are very similar (Sawaya et al., 2003). There is also obvious confusion between the soil class and low albedo impervious class. However, the total amount of soil cover is very limited, because the image primarily covers the central area of Bangkok. Thus, there is no need to re-train or re-classify the soil class.

Table 3.2:

Error Matrix for Image Classification

	Ground Truth						
	Shadow	Water	Imp_high	Imp_low	Vegetation	Soil	Total
Shadow	26	4	0	0	0	0	30
Water	7	22	0	0	1	0	30
Imp_high	0	0	29	1	0	0	30
Imp_low	2	0	0	24	3	1	30
Vegetation	0	0	0	0	29	1	30
Soil	0	0	0	8	1	21	30
	35	26	29	33	34	23	180

3.4.2 Shadow Detection

The results are quite acceptable for a general land use/cover classification. However, the confusion between water and shadow class makes it impossible to conduct

building height estimation directly. For instance, many shadow pixels were labeled as water in the initial image classification and vice versa. Therefore, the size, shape, and spatial neighborhood information were further used to separate shadow and water objects. Figure 3.4 shows the distribution of water objects from the 2002 IKONOS image. Large rivers and streams are obvious in the image, however, there are also large numbers of small objects scattered across the entire image. These small objects can be ponds and shadow objects from nearby buildings and trees. The sizes of these water/shadow objects were calculated. A threshold of 500 pixels was used to delineate large rivers, streams, and lakes and ponds from other small objects. Figure 3.5 shows the derived large water objects. The largest object is located in the lower left corner of image -- a segment of the Chao Phya River. The image objects in the shadow layer are relatively small and homogeneous in their size distribution.



Figure 3.4. Water objects from the initial classification.



Figure 3.5. Derived large rivers, streams and ponds.

After removing the extremely large water objects, the remaining small water/shadow objects from the water layer were combined with the previously classified shadow layer. Therefore, a single layer of shadow/water was generated. New image objects were reconstructed for this shadow/water layer by linking spatially connected pixels. The total number of water/shadow objects is 52,840. The sizes of these objects range from 1 to 1,564 pixels.

A histogram plot of object size suggests that there are large numbers of water/shadow objects with a relatively small size (i.e., less than 10 pixels). Small shadow objects may be cast by low buildings or trees, and therefore discarded for building height estimation. This procedure reduced the total number of objects to 12,906. Perimeter-Area Ratio was used to define the shape complexity of these objects. Figure 3.6 shows the histogram plot of the Perimeter-Area ratio for the water/shadow objects. A large number of objects (48,539) have a Perimeter-Area Ratio of 1. The remaining objects show an

interesting bimodal (2 peak) form. Figure 3.7 shows Perimeter-Area ratio of objects using an R-G-B color ramp. Red suggests high values of the Perimeter-Area ratio, and blue indicates low values of the Perimeter-Area ratio. The color representation clearly shows that shadows from high-rise buildings have a characteristic Perimeter-Area ratio range (i.e., 0.2~0.5). Figure 3.8 further illustrates the contrast of spatial objects with regard to the Perimeter-Area ratio. Linear objects typically have high values of Perimeter-Area ratio (i.e., 1), while shadows from high-rise buildings have a low or intermediate Perimeter-Area ratio (i.e., 0.2~0.5). A threshold of 0.5 was used to remove linear-shaped objects from the image. In addition, a Length index was calculated for the remaining shadow/water objects. The Length index was found to be useful in the detection of the elongated stream segments. A threshold of 60 was applied to remove stream segments.

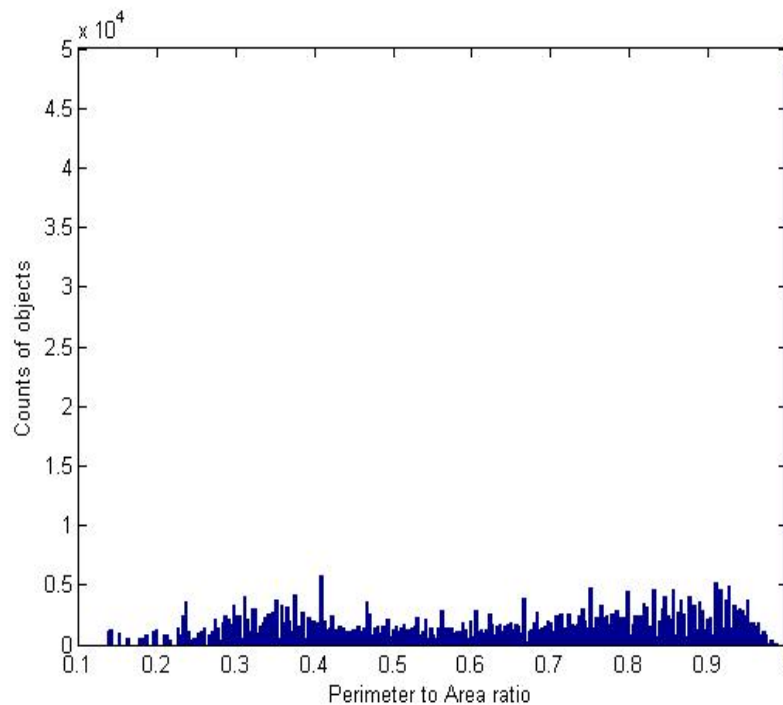


Figure 3.6. Histogram Plot of the Perimeter-Area Ratio for Water/Shadow Object.

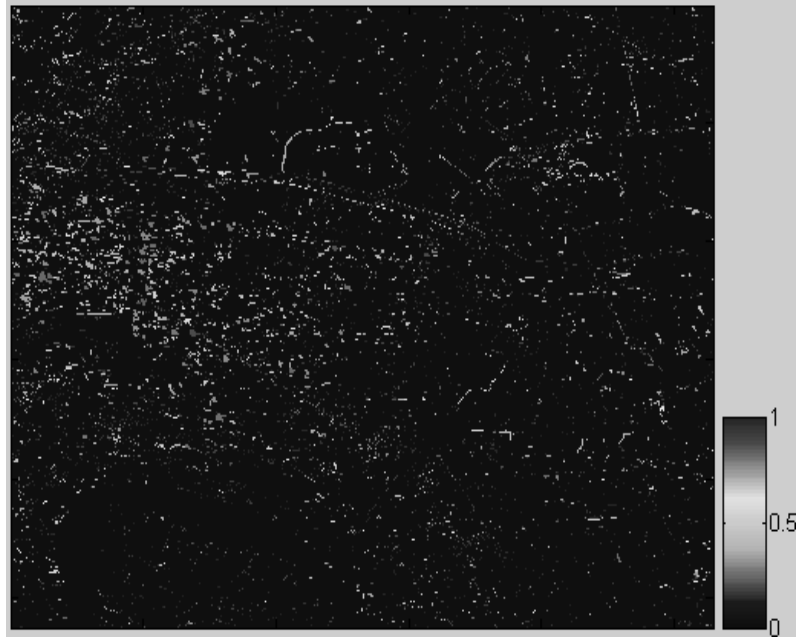


Figure 3.7. Color Ramp of the Perimeter-Area Ratio for Water/Shadow Objects.

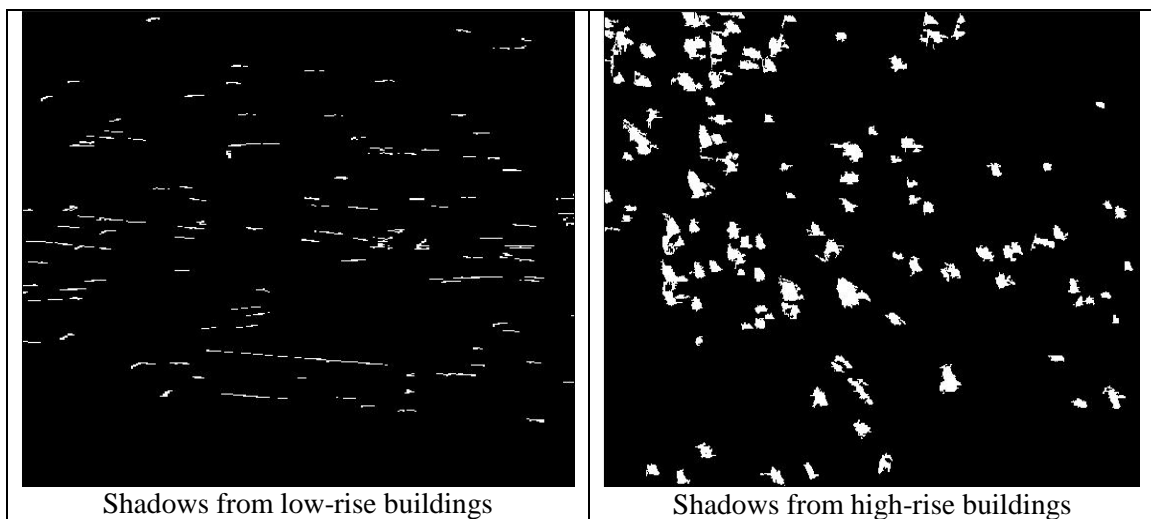


Figure 3.8. Comparison of Shadow Objects from High- and Low-rise Buildings

The remaining objects were overlaid on the panchromatic IKONOS image. Most objects matched very well with the shadows of high-rise buildings. However, it was found that some small ponds have very similar shape characteristics compared to those from high-rise buildings, especially in the urban-rural fringe areas, as indicated in Figure 3.9. Spatial neighborhood information was used to separate water ponds with shadows. The fundamental assumption of the sun-angle shadow method is that buildings and their

shadows must be spatial neighbors. A shadow/water image object is considered a shadow only if an impervious cover object is located in its neighborhood and in the sun-side direction. This approach successfully removed most ponds, because they are surrounded by other land cover types, especially vegetation cover. The remaining objects were considered to be “clean”. Each represents a shadow object for a specific high-rise building or a relatively high building (Figure 3.10). The total number of the remaining objects is 455.

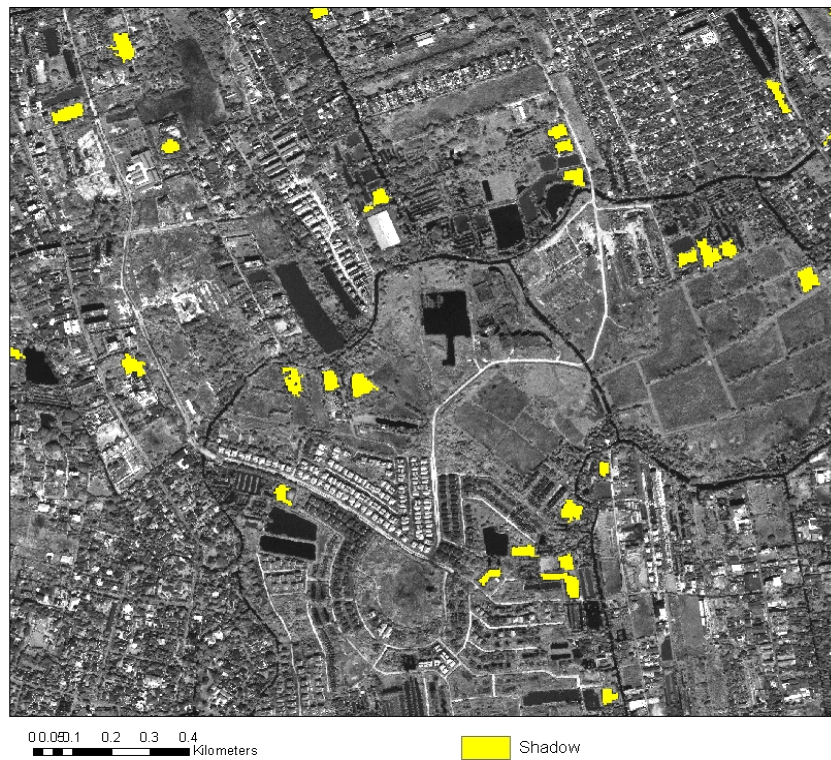


Figure 3.9. Spatial Neighborhoods of Small Water Ponds in Urban-rural Fringe Areas

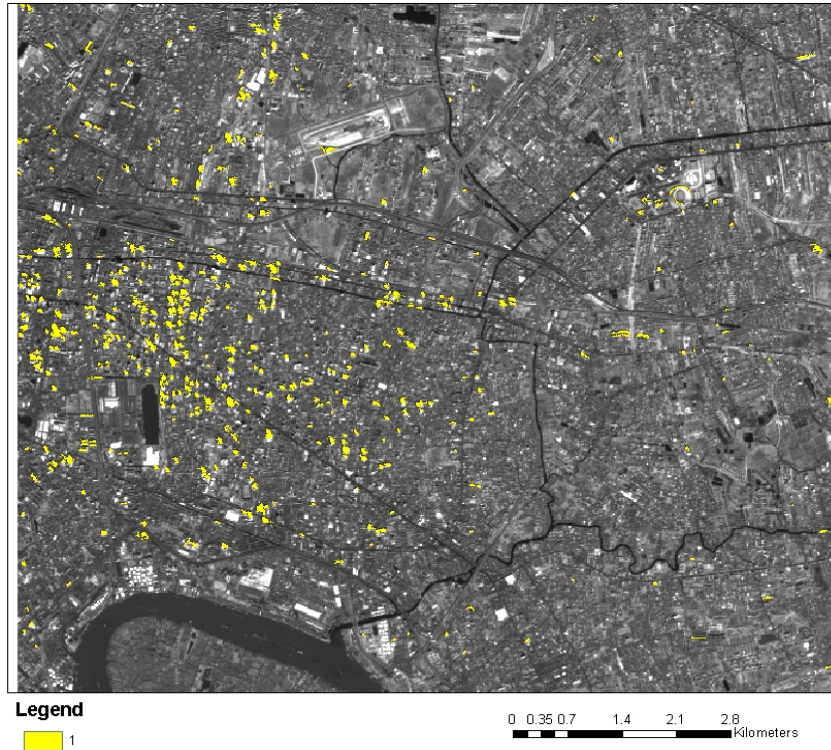


Figure 3.10. “Clean” Shadow Objects from High-rise Buildings.

Table 3.3 presents a set of threshold values and the remaining numbers of objects after each step of size, shape, and spatial neighbor analysis. The threshold of object size removed extremely large objects (i.e., rivers) and extremely small objects (i.e. shadows from low buildings or trees). Perimeter-Area ratio and Length index were used to remove elongated linear features. Finally, the spatial neighbor information was used to validate the relationship between shadow objects and impervious cover objects.

Table 3.3:

Threshold Values and the Remaining Image Objects

	Size(pixel) Large	Size (pixel) Small	Perimeter- Area ratio	Length (pixel)	Spatial neighbor
Threshold	<500	>10	0.2-0.5	<60	-
The number of remaining objects	52840	12906	489	477	455

3.4.3 Shadow Length and Building Height Estimation

The shadow objects were first smoothed by removing the “pixel spurs”. Perimeter pixels were then identified for each shadow object. The distances and azimuth angles were calculated for all possible combinations between two perimeter pixels. The largest distance measure in the defined azimuth-angle range (i.e., 152~156 degrees) was retained as the shadow length. Figure 3.11 shows examples of shadow objects (in yellow) and their perimeter pixels (in red). The shortest and longest shadow lengths are 17.89-m and 193.20-m, respectively. This shadow-length detection method is different from methods previously applied to aerial photography by Irvin et al. (1989). In their study, the mean value of shadow length at sun azimuth-angle was estimated. Although no accuracy level was reported in their study, the results may underestimate the building height. Massalabi et al. (2004) used the manual interpretation of shadow length, but it can be time consuming and expensive.

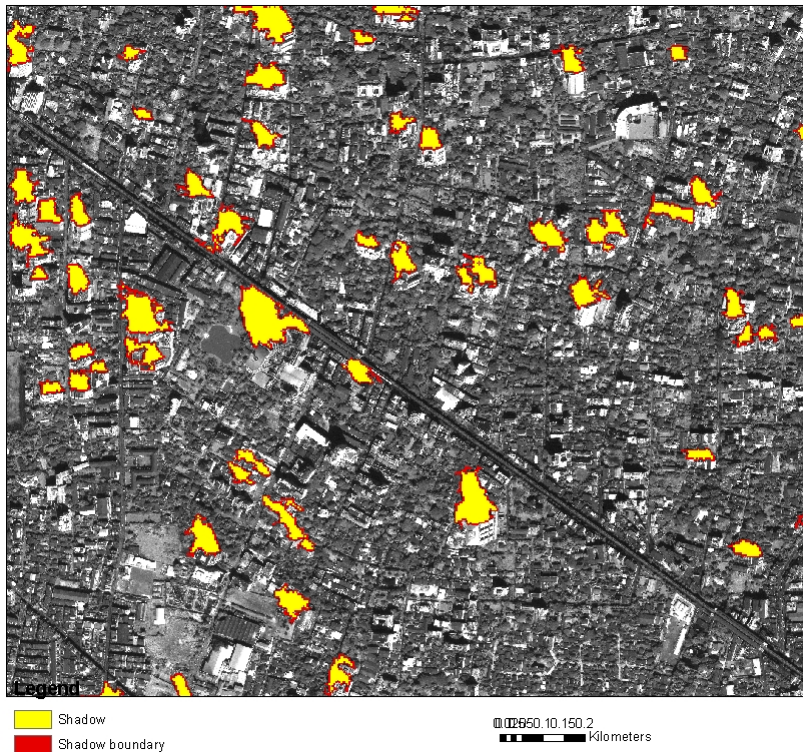


Figure 3.11. The Perimeter Pixels from Shadow Objects

A total of 85 shadows were randomly selected and their lengths were measured manually. Four shadows were found to be falsely identified: one was water and the other three were dark impervious materials. The manually interpreted shadow lengths and the automatic detected values are plotted in Figure 3.12. The correlation coefficient is 0.9460, and 62.5-percent of buildings have less than 4-m error. Recall that IKONOS multi-spectral bands (4-m spatial resolution) are being used for shadow identification and measurements, as such, the error is quite small. In addition, the performance of the shadow length measurement appears to be relatively consistent, and there is no obvious error distribution across different building heights.

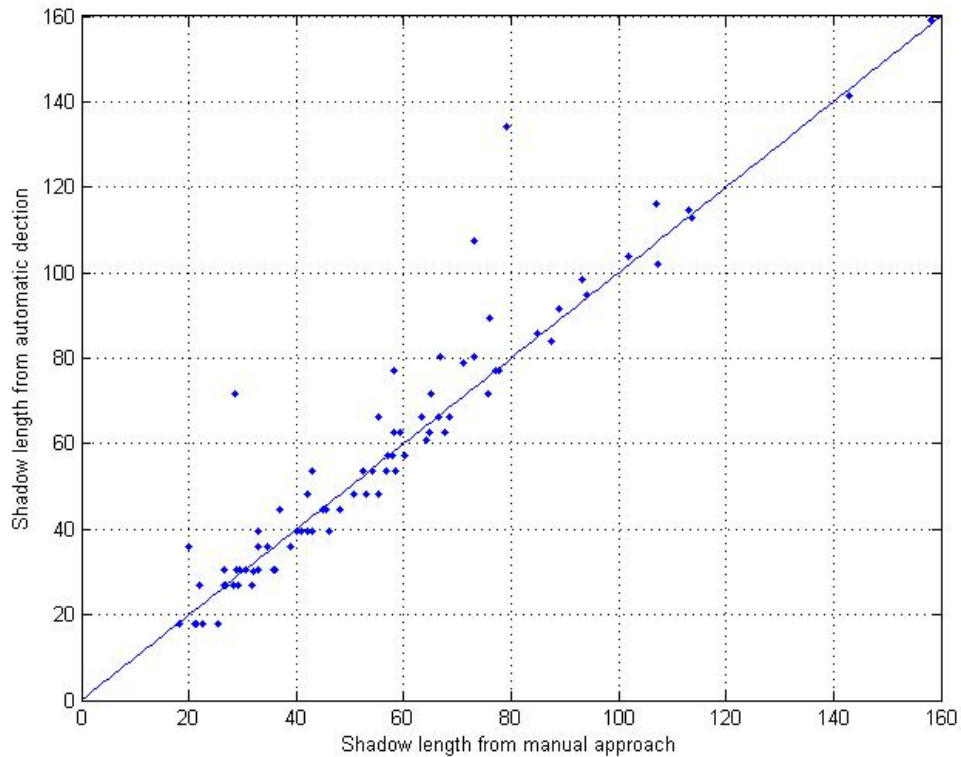


Figure 3.12. Accuracy Evaluation of the Shadow Length Estimation

Figure 3.12 also suggests that there are several buildings where the automatic algorithm produced large errors. These shadow objects and buildings were identified for

further analysis. Figures 3.13a, 3.13b, and 3.13c show different scenarios of high-rise buildings' relative positions, orientations, and the resultant shadow sizes and shapes. A common problem is that two individual buildings' shadows are merged into a single shadow object. This will cause two obvious errors. First, one of the buildings will not be identified. Second, the shadow length from automatic detection may generate large error estimates (i.e., overestimation of shadow length). Figure 3.13d shows another type of error, where shadow objects are connected to a dark surface area (i.e., water body). Both error types are difficult to correct using the automatic approach. For the first type of error, a potential solution is to decompose a shadow object. However, it is a very complicated problem and there is no universal method/algorithm that can be applied to all images or study areas (Irvin, 1989; Lin et al, 1999). Another solution is to incorporate multiple images obtained at different sun elevation/azimuth angles. Different shadow position, size, and shape may be potentially useful for the analysis (i.e., Lee and Lei, 1990). Overall, the approach developed here can generate shadow length with high accuracy for most isolated high-rise buildings, but the performance is problematic for clustered high-rise buildings. In some case, the shadow object can be fragmented and this can lead to extraneous shadow length estimations, but these are common problems for all automatic or semi-automatic shadow/building extractions. In fact, it is widely recognized that most previous works in aerial photography analysis only focuses on very simple scenes and detached buildings (Baillard, 1999). Few automatic systems have been developed to extract buildings or estimate building heights in a dense and complex urban setting.

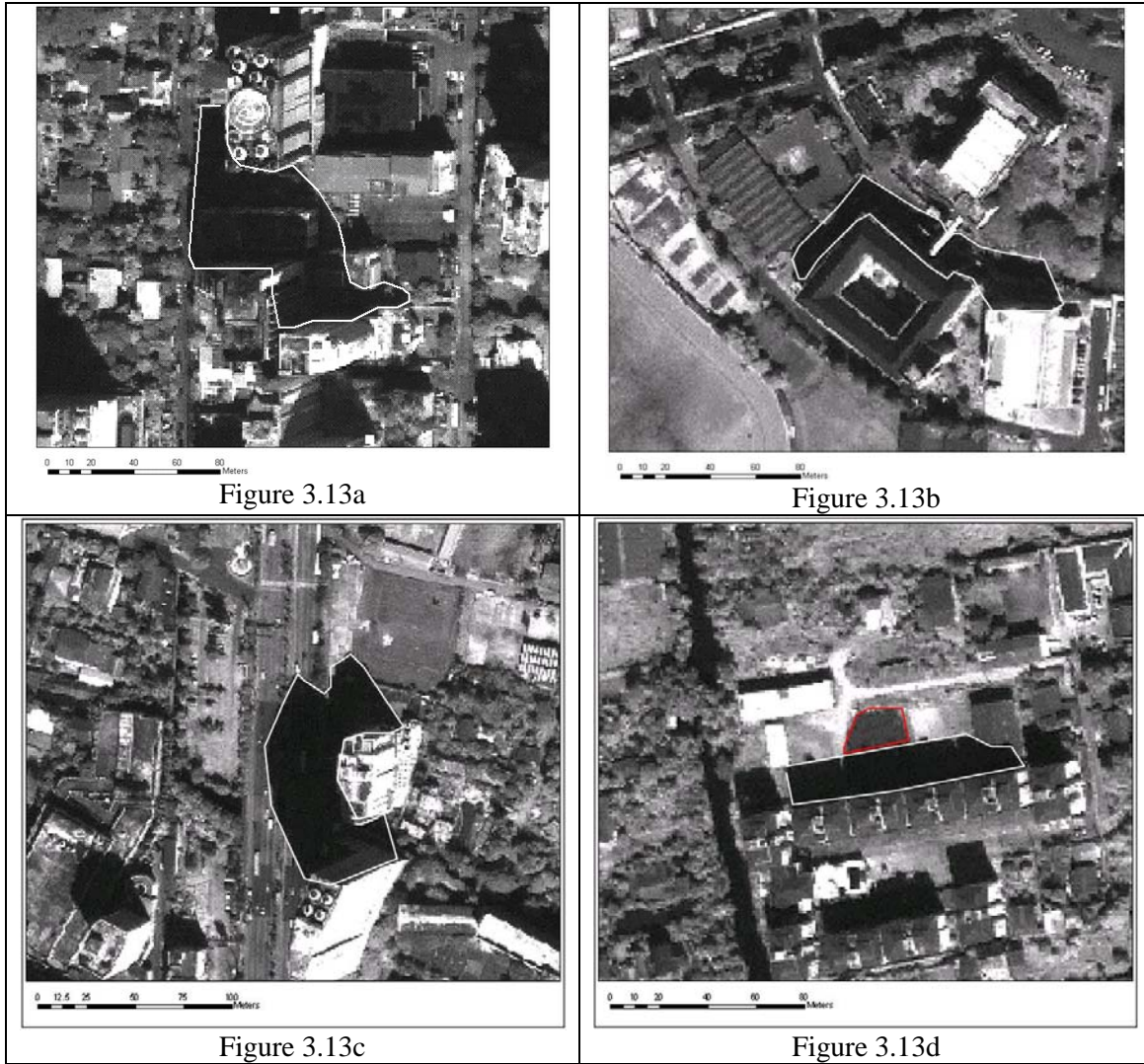


Figure 3.13. Error Sources of Shadow Length Estimation.

It should be noted that a good match between automatic estimated shadow length and visually interpreted shadow length does not guarantee a good estimation of actual building height. The size and shape of shadow objects can be affected by many factors, including the surface cover types on the ground, the building structure (i.e., sharp-pointed structure), the relative position of buildings (isolated or clustered), sun elevation/azimuth angle, and sensor elevation/azimuth angle. To further assess the accuracy of building height estimation, actual building heights were obtained by accessing government/city information by colleagues at IPSR (Institute for Population and Social Research),

Thailand. Building heights were obtained for a total of 21 high-rises from the Bangkok central business district (CBD), especially in the Sukhumvit area. The actual building heights and the automatic detected values are plotted in Figure 3.14. The correlation coefficient is 0.97. In sum, 57-percent of buildings have less than 4-m error and 67-percent of buildings have less than 8-m error.

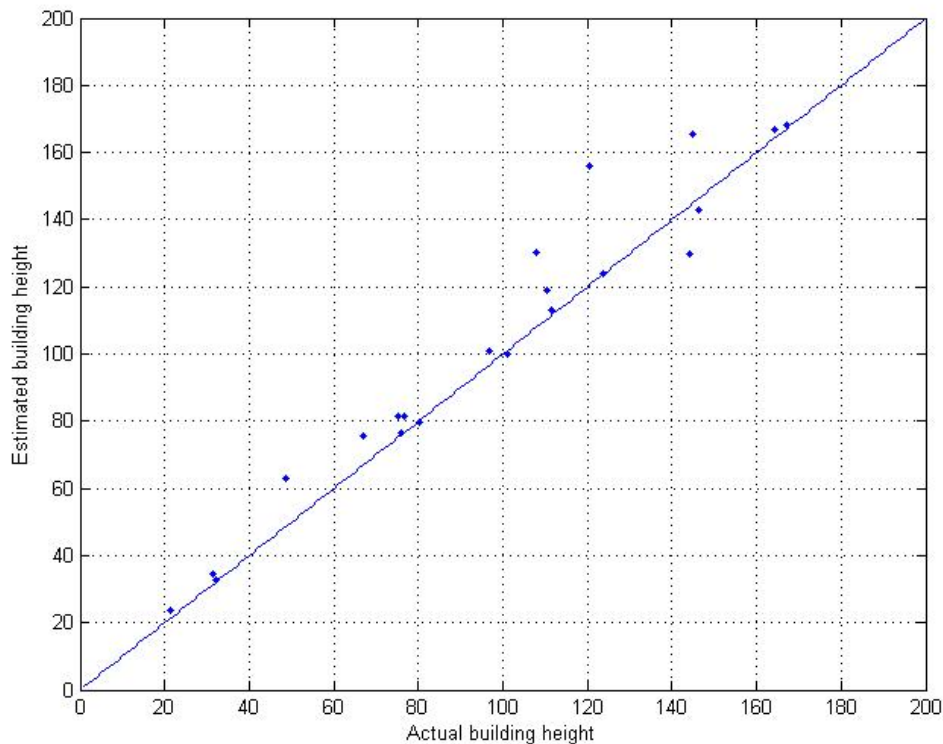


Figure 3.14. Accuracy Evaluation of the Building Height Estimation.

There is an error pattern of overestimation for almost all buildings. A careful visual interpretation of the panchromatic IKONOS band shows that the self-shadowing is one of the main error sources. Proportions of buildings were classified as shadows in the multi-spectral image segmentation and the overestimation of shadow length leads to the errors in building height estimation. The pixel size imposed (i.e., 4-m) may also affect the

shadow identification. A pixel may have mixed spectral signals from different land cover types that can cause difficulties and errors in image classification. There are 3 buildings that show extremely large errors (i.e., >15-m difference) between the actual and the estimated building heights. These are caused by the spatial clustering of high-rise buildings. It is probably the most challenging question for the shadow-based method. The high level of the fusion/fragmentation of shadow objects may cause large uncertainty of building height estimation. The surface terrain information is also important. The method suggested in this study may not be appropriate for cities with high levels of terrain variation, where a very detailed digital elevation model may be needed to correct the terrain effects on the shadows. Shettigara and Sumerling (1998) also addressed the importance of the sensor azimuth, sensor elevation angle, and building orientation for building height estimation. In any case, the estimated building height needs to be evaluated using actual building height.

The shadow detection and shadow length estimation methods were extended to the May 1999 image. As a result, a total of 903 shadow objects were identified and linked to high-rise buildings or relatively high buildings for Bangkok. The building height was simply estimated using a trigonometry method described previously. A simple 3-D urban map for the Bangkok city was generated. Figure 3.15 show 3-D images (i.e., from multiple viewpoints) of Bangkok, Thailand. Landsat ETM image (2002) and road coverage were used as background. 3-D objects or markers were placed in the map by reading height information from each building. It should be noted that all buildings were simply represented using uniform objects/markers (in grey). This data provide additional information for urban structure analysis. For instance, most high-rise buildings are

clustered in the central business area (CBD) in Bangkok. The 3-D urban map can be useful for the identification of CBD area. This will be further discussed in the next chapter.

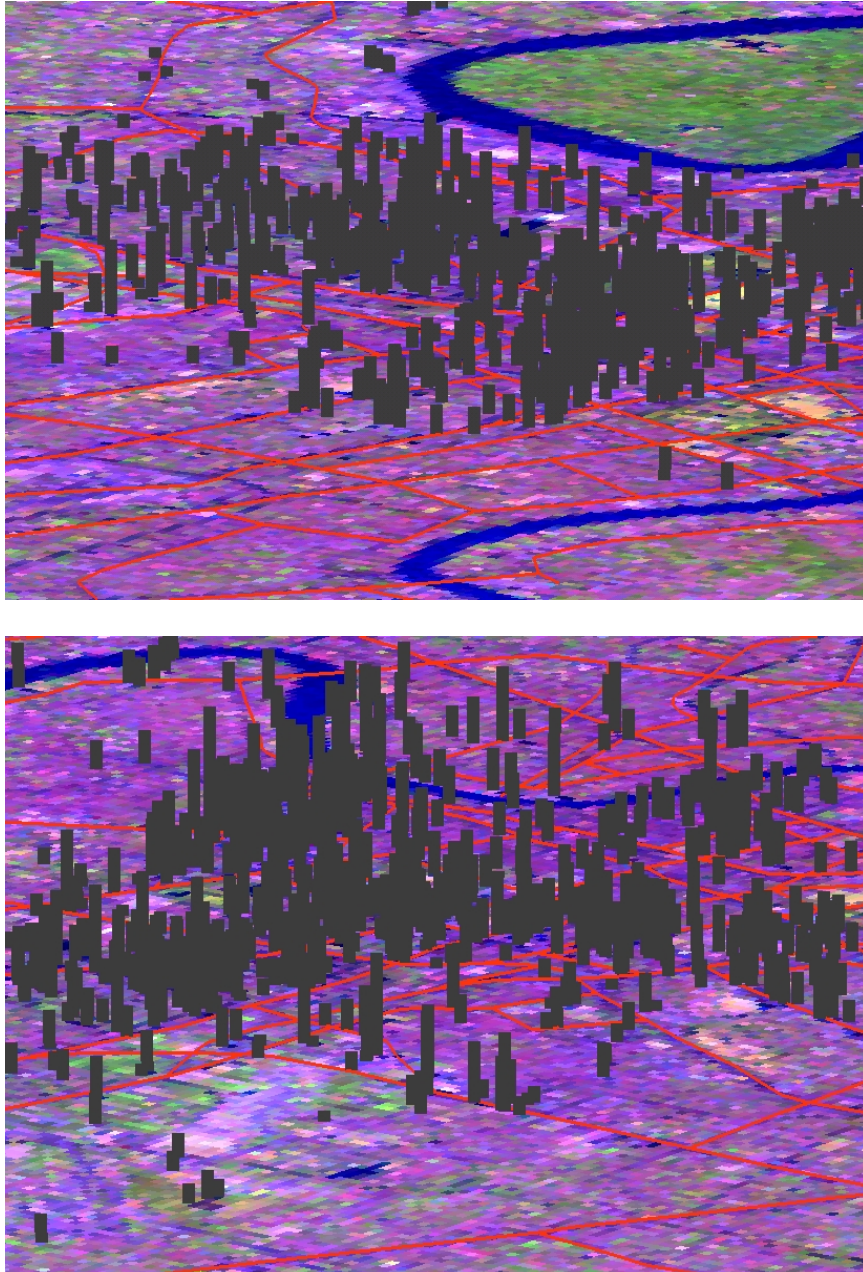


Figure 3.15. 3-D urban view of Bangkok, Thailand

3.5 Conclusions

Building height or 3-D urban information can provide very useful information for assessing urban structure and socio-demographic implications of urban areas. Shadow analysis is one of several methods used in traditional aerial photography analysis. However, few studies have used shadow information from satellite remote sensing data to derive building height. The recently available high-resolution remote sensing data (i.e., IKONOS, QuickBird) provides increased spatial and radiometric resolution. Thus, traditional photogrammetry techniques such as shadow analysis may be used to estimate 3-D building information from 2-D satellite images.

This chapter examined advanced image classification methods for the automatic detection of shadow objects from high-resolution IKONOS image. Object-based image analysis (OBIA) was first used to segment a high-resolution image. The main advantage of OBIA is that it incorporates both spectral and spatial information for image classification. This often leads to better classification results, especially in urban setting where spatial and spectral variation is the main concern. In addition, a number of size, shape, and spatial neighborhood information were used to delineate shadow objects from water objects. This type of rule-based classification generated a “clean” shadow dataset. Computer algorithms were developed to measure shadow length automatically. This can be useful if large numbers of shadows/buildings are involved for analysis. Overall, the method produced excellent shadow detections and shadow length measurements, especially for high or isolated buildings. However, the approach is problematic for clustered high-rise buildings. The shadows from different buildings may merge into a single large shadow object. The automatic system designed in this study generated poor

results for this case. While there are still many challenges in automatic building height estimation, this study suggested that shadow information on a 2-D image may provide very useful information with regard to 3-D building height. A semi-automatic system was developed that incorporates object-based image analysis, object size/shape/spatial neighbor analysis, automatic shadow length detection, and building height estimation. The results are potentially useful for urban structure/function analysis. For instance, the urban center or CBD area in Bangkok may be identified using building height information.

Reference

- Awry, T.E. (1977). *Innerprefutroii of Aeriul Photographs Minneapolia*. MN: Burgess Publishing Company.
- Baillard, C., Maître, H. (2002). 3-D Reconstruction of Urban Scenes from Aerial Stereo Imagery: A Focusing Strategy. *Computer Vision and Image Understanding* 76 (3), 244-258.
- Ballard, A., Brown, C.M. (1982). *Computer Vision*. Prentice-Hall Inc., Englewood Cliffs, NJ, 523 pp.
- Blaschke, T., Lang, S., Lorup, E., Stobl, J., Zeil, P. (2000), Object-oriented image processing in an integrated GIS/remote sensing environment and perspectives for environmental applications. In: Cremers, A. and Greve, K. (editors), *Environmental Information for Planning, Politics and the Public*, Verlag, Marburg, 2, 555-570.
- Donnay, J.P., Barnsley, M.J., Longley, P.A. (2001). *Remote Sensing and Urban Analysis*. Taylor & Francis.
- Fraser, C.S., Baitsavias, E., Gruen, A. (2002). Processing of IKONOS imagery for sub-metre 3D positioning and building extraction. *ISPRS Journal of Photogrammetry and Remote Sensing*, 56, 177–194.
- Gruen A., Kübler O., Agouris P. (editors). (1995). *Automatic Extraction of Man-Made Objects from Aerial and Space Images*. Birkhäuser Verlag, Basel.
- Gruen, A., Nevatia, R. (1998). Special Issue on Automatic Building Extraction from Aerial Images. *Computer Vision and Image Understanding* 72:2.
- Huertas, A., Nevatia, R. (1988). Detecting buildings in aerial images. *Comput. Vision, Graphics, Image Processing*, 41 (2), 131-152.
- Irvin, R., McKeown, D. (1989). Methods for exploiting the Relationship Between Buildings and their Shadows in Aerial Imagery. *IEEE Transactions on Systems, Man and Cybernetics*, 19(6): 1564-1575.
- Janssen, L.L.F. (1994). *Methodology for Updating Terrain Object Data from Remote Sensing Data*. Ph.D. Thesis. Landbouw Universiteit Wageningen, Wageningen, The Netherlands.
- Landgrebe, D.A. (2003). *Signal Theory Methods in Multispectral Remote Sensing*. Hoboken, NJ: Wiley.
- Lin, C., Huertas, A., Nevatia, R. (1994). Detection of buildings using perceptual grouping and shadows. *Proc. Computer Vision and Pattern Recognition*, 62–69.

- Lin, C.A., Nevatia, R. (1998). Building Detection and Description from a Single Intensity Image. *Computer Vision and Image Understanding*, 72 (2), 101-121,
- Massalabi, A., He, D.C., Bénié, G.B., Beaudry, E. (2004). Detecting information under and from shadow in panchromatic Ikonos images of the city of Sherbrooke. *Geoscience and Remote Sensing Symposium, IGARSS*, 3, 2000-2003.
- McGlone, J.C., Shufelt, J.A. (1994). Projective and Object space geometry for monocular building extraction. *Proc. Computer Vision and Pattern Recognition*, 54–61.
- Mohan, R., Nevatia, R. (1989). Using perceptual organization to extract 3D structures. *IEEE Trans. Patt. Anal. Mach. Intell.*, 11, 1121-1139.
- Noronha, S., Nevatia, R. (2001). Detection and Modeling of Buildings from Multiple Aerial Images. *IEEE Trans. Pattern Analysis and Machine Intelligence (PAMI)*, 23 (5), 501-518.
- Paine, D.P., Kiser, J.D. (2003). *Aerial photography and image interpretation*. Second edition. John Wiley and Sons, Hoboken, New Jersey, USA.
- Paola, J., Schowengerdt, R.A. (1995). A detailed comparison of backpropagation neural network and maximum-likelihood classifiers for urban land use classification. *IEEE Transactions on Geoscience and remote sensing*, 33(4), 981-996.
- Ridd, M.K. (1995). Exploring a V-I-S (vegetation-impervious surface-soil) model for urban ecosystem analysis through remote sensing: Comparative anatomy for cities. *International Journal of Remote Sensing* 16(12), 2165–2185.
- Roberts, L.G. (1970). Machine Perception of Three Dimensional Solids. In: J.T. Tippett, D.A. Berkowitz, L.C. Clapp (editors), *Optical and Electro-Optical Image Processing*, MIT Press, Cambridge, MA, 159–197.
- Sawaya, K., Olmanson, L., Holden, G., Sieracki, J., Heinert, N., Bauer, M. (2003). Extending satellite remote sensing to local scales: Land and water resource management using high resolution imagery. *Remote Sensing of Environment*, 88, 144-156.
- Schowengerdt, R.A. (1997). *Remote Sensing: Models and Methods for Image Processing*. Academic, San Diego.
- Shettigara, V.K., Sumerling, G. M. (1998). Height determination of extended objects using shadows in SPOT images. *Photogrammetric Engineering and Remote Sensing*, 64, 35± 44.
- Shiode, N. (2001). 3D Urban Models: Recent Developments in the Digital Modeling of Urban Environments in Three-Dimensions. *GeoJournal*, 52 (3), 263-269.

- Stuckens, J., Coppin, P.R., Bauer, M.E. (2000). Integrating contextual information with per-pixel classification for improved land cover classification. *Remote Sensing of Environment* 71, 282–296.
- Tilton, J.C. (1989). Image segmentation by iterative parallel region growing and splitting. In: *Proceedings of the International Geoscience and Remote Sensing Symposium (IGARSS)*. Vancouver, Canada, 2235–2238.
- Tseng, Y.-H., Wang, S. (2003). Semiautomated building extraction based on CSG model-image fitting. *Photogrammetric Engineering and Remote Sensing*, 69. 171-180.
- Walsh, S.J., W.F. Welsh, T.P. Evans, B. Entwisle, and R.R. Rindfuss. (1999). Scale Dependent Relationships between Population and Environment in Northeastern Thailand. *Photogrammetric Engineering and Remote Sensing*, 65(1): 97-105.
- Woodcock, C., Harward, V.J. (1992). Nested-hierarchical scene models and image segmentation. *International Journal of Remote Sensing*, 13(16), 3167-3187.

CHAPTER 4

URBAN FORM ANALYSIS

4.1 Introduction

In urban studies, administration officials, city managers, and urban researchers are often concerned with the analysis of urban form, because of the implicit and explicit links to urban function. The compactness and diversity of urban form may have direct and indirect impacts on energy demand and environmental consequences (Anderson, 1996). For instance, urban sprawl is generally considered an inefficient urban form in that low density suburban development may generate long commutes, traffic congestion, and air pollution. Urban sprawl also can contribute to the decay of downtown areas and a reduction in social interactions (Brueckner, 2000). In addition, dispersed urban development can affect urban runoff, fragmentation of land cover, and a reduction in local species diversity (Lassila, 1999). Dale et al. (2000) provides a review of the direct effects of urban growth pattern on ecosystem form and function.

Despite these main concerns, there are still fundamental questions about urban form that remains unanswered. First, the measurement criteria of urban form may vary among researchers. Urban form may have different definitions and implications for researchers that range from urban planning, urban geography, urban ecology, and urban sociology (e.g., Alberti, 1999; Batty and Longley 1988; Harvey and Clark 1965; Mills, 1981; Song and Knaap 2004; von Thünen, 1825). Researchers have employed a variety of measurements or indices to characterize urban form. The input datasets may include

population statistics, land use and land cover patterns from remote sensing systems, and GIS coverages such as road networks and locations of shops and industrial, commercial, and residential uses. The most commonly used indices include measures of density, pattern, and proximity (Fulton et al., 2002; Galster et al., 2001; Song and Knaap, 2004). AS such, a high diversity of measurement criteria and approaches makes the comparison of urban form very difficult across space and time. Second, the measurements or indices are often derived by city boundaries, district/census tracts, and ZIP code areas (Krizek, 2003). However, these units all have arbitrary shapes and boundaries that may or may not offer meaningful representations of actual urban forms and their dynamics. For instance, the city of Bangkok has extended its geographic reach well beyond its administrative boundary to include surrounding provinces. This also leads to an important concept of scale-dependence in which measurement units influence the nature of pattern-process relations (i.e., Walsh et al., 1999). Urban form may be defined at local to regional scales (Krizek, 2003), and each has different implications on human and natural processes. Third, there is a large gap between the characterization of urban form and the analysis of urban function. The causes, consequences, and feedback mechanisms of urban form on the social and biophysical processes have not been thoroughly examined. For instance, land use/cover transformations are an important process that has direct impacts on the urban form. On the other hand, the spread of land use/cover change may also be affected by urban form and/or landscape heterogeneity.

The coupling of scale, pattern, and process in urban settings is rooted in landscape ecology (Risser et al., 1984; Turner, 1989). Landscape ecology theory argues that landscape patterns should be addressed at their “characteristic” scales or ranges of spatial

(or temporal) scales that are autocorrelated so that associated processes can be described (e.g., Allen and Starr, 1982; O'Neill et al., 1986; Turner et al., 1990; Urban et al., 1987; Walsh et al., 1999). Landscape pattern analysis in urban setting is relatively new compared to its wide application in natural environments (Seto and Fragkias, 2005). Recently, the concept of urban-rural gradients, proposed by McDonnell and Pickett (1990), has been increasingly used to examine urbanization and ecological conditions. The basic concept of urban-rural gradients incorporates humans as a component of “natural” ecosystems. The theory and methods of landscape ecology, therefore, can be directly used to assess the pattern-process interactions in urban setting. Many urban-rural gradients studies assess the composition and spatial organization of land use/cover along one or more linear transects across a metropolitan area (Conway and Hackworth, 2007; Luck and Wu, 2002). Researchers have studied the variations of species diversity and water quality along these transects (Sukopp, 1998; Wear et al., 1998). In addition, the study of “patchiness” and their dynamics along transects provides a convenient way to organize question of spatial heterogeneity vs. homogeneity. This allows researchers to characterize the relationships between observed patterns and underlying processes across different spatial scales (Wu and Loucks, 1995; Zipperrer et al., 2000). The inputs into the urban-rural gradient analysis largely depend on the research objective and data availability. Derived remotely-sensed land use/cover classification is often used as an input to urban-rural gradient analyses, although it is not uncommon to incorporate road networks, dwelling units, population, and other socio-demographic dataset for more advanced studies of urban analysis (e.g., Conway and Hackworth, 2007). For most

developing countries, however, data availability and data quality are considerable concerns.

A fundamental assumption of urban-rural gradient analysis is that cities are mono-centric. However, urban forms in the real world can be more complicated, especially for large cities or metropolitan areas. For instance, researchers have defined three key urban forms: concentric city, radial city, and multinucleated city (Burgess, 1925; Hoyt, 1939). More recent studies of urban forms also include fractal city (Batty and Longley, 1994) and self-organization city (Portugali, 2000; Schweitzer, 1997). As a result, it is very difficult to characterize overall urban form using the customary limited number of transects, because the location, width, length, and orientation of transects may be subjectively designed. The imposed length/width of transects also ignores the fact that pattern-process interactions are scale-dependent. There is a need, therefore, to develop alternative strategies for characterizing the overall urban-rural gradients with higher consistency and robustness. A multi-scale approach is of particular interest as it reflects landscape ecology theory: the interplay of scale-pattern-process relations and an interconnected area of urban-rural landscapes. In addition, urban-rural gradients are typically characterized using one image or a single snapshot of the landscape in time. In practice, researchers are more interested in the temporal dynamics of urban form that responds to social, natural and/or ecological processes. Until now, few multi-temporal, urban-rural gradient analyses have been conducted, and the advantage of high temporal resolution, remote sensing data has yet to be fully utilized in the study of urban settings.

In landscape ecology, a consistent challenge is to find appropriate measures of landscape composition/structure that can be linked to underlying processes (Gustafson,

1998; Turner et al., 1991). Hundreds of landscape pattern metric indices have been developed to quantify area, shape, connectivity, and diversity characteristics at class, patch, and landscape-levels (O'Neill et al., 1988). Empirical analysis shows the relative importance of indices for specific applications (Gustafson, 1998). However, measurement of pattern indices is very sensitive to land use/cover classification schemes and classification accuracy assessments (Wu, 2000). The inconsistency of urban classification schemes and accuracies make it difficult to compare urban forms across space and time. Recently, the impervious cover mapping of urban space has received increased attention in the remote sensing literature. Simple measurements such as density and spatial structure of imperviousness may provide a useful basis for urban form analysis and urban feature identification (i.e., urban core, inner zone, urban fringe, peripheral clusters, and rural). It should be noted that some urban features/functions may not be discernible using imperviousness as the only input. For instance, the urban core or the central business districts (CBD) is often characterized by clustered high-rise buildings. However, there is no 3-D or building height information in a traditional 2-D impervious cover map. Therefore, it may be difficult to delineate the CBD from the urban fringe or peripheral clusters based on present imperviousness as a single description variable. Urban form characterization also provides a general framework to study the process of urban space filling (Donnay et al., 2001). The relationships between urban form and land use/cover change are considered as pattern-process interactions that operate on multiple spatial and temporal scales. One simple approach to characterize these interactions is to examine the linkage between the newly urbanized pixels and their neighborhoods or pre-existing urban form. Specifically, the urban change pixels can be

grouped into several classes based on urban form at immediate, local, and regional spatial scales. The concept is similar to that proposed by Wilson et al.'s (2003) in which urban change pixels are labeled as structural infilling, diffusive expansion, and isolated urban growth based on the conditions of neighborhood pixels.

This chapter is designed to examine and improve urban form characterization using multi-scale landscape pattern metrics. The study site is Bangkok, Thailand. The empirical testing is discussed through three objectives: (1) traditional transect sampling is used to examine urban-rural gradients for Bangkok, Thailand; pattern indices are calculated and compared across space and time; (2) the urban-rural gradients are examined over the entire remote sensing image of the Greater Bangkok Area using a moving window strategy; urban features (i.e., core, inner zone, fringe, and rural) are identified using 2-D and 3-D maps as inputs; the temporal change of urban features is also considered; (3) the relationships between the locations of urban change pixels and pre-existing urban form/structure are examined from 1993-2002 at multiple spatial scales.

4.2 Study Area

Bangkok is Thailand's largest metropolitan area. It has experienced rapid population growth and urban growth since the mid-1970s. The urban area continues to expand outwardly, mainly along three major transport corridors (southwest, southeast, and north of the city). Population growth, including both natural growth and in-migration, is one of the main contributing factors to this areal expansion (Choiejit, 2005; Nanthamongkolchai, 1999;). The average household size in Bangkok has also decreased during the past three decades (NSO, 2000). This demographic shift demands more housing units and additional built-up areas. Furthermore, researchers indicated that the

lack of coordination between the public sector (i.e., transportation planning policy) and private sector (i.e., residential/commercial development) may be responsible for the inefficient urban land use patterns or urban forms seen across the landscape. In fact, urban area of Bangkok has encroached into five surrounding provinces, including Nonthaburi, Pathumthani, Samutprakarn, Nakhonpathom, and Samutsakorn. As a result, Bangkok has emerged as a primate city and the Greater Bangkok region that describes the areal expansion of the space, geographic reach, and functional influence. Administrative boundary of Bangkok city bears little resemblance of urban form or urban functions.

4.3 Data

This chapter uses sub-pixel classification results (see Chapter 2) and building height information (see Chapter 3) for the analysis of urban form. Two Landsat TM/ETM images (1993 and 2002) were initially classified using a neural network, sub-pixel classification approach in which land use/cover are represented as percent impervious cover at the sub-pixel (30-m) level. Chapter 2 provided details of land use/cover classification methods and results. Most landscape pattern studies require discrete input values (e.g., 0 or 1). Therefore, the sub-pixel classification results were converted into discrete impervious/non-impervious cover using a threshold value of 0.5 that reduces the uncertainty in image classification. The landscape pattern metrics are highly sensitive to image classification errors, especially when large numbers of land use/cover types are involved (Wu, 2000). Building height information was derived from photogrammetric analyses of two high-resolution IKONOS images (May 2000 and November 2002). These two IKONOS images cover a relatively large portion of the central Bangkok area, where most high-rise buildings are located. A total of 901 high-rise buildings were identified.

The heights of the tallest and the lowest buildings in the study area as of the two image dates are 299-m and 38-m, respectively. The detailed method and results of building height estimation were provided in Chapter 3.

4.4 Method

4.4.1 Sampling Transect-Based Urban-Rural Gradients

Two 3-km transects belt were designed to sample the urban-rural gradient in Bangkok (Figure 4.1). Both transects are oriented in a west to east direction. For Transect A, the center line is located approximately 30-km north of the Bangkok city center. The transect bisects a main transport corridor and crosses urban fringe area, however, a majority of the transect is characterized as agricultural, rural landscape. Transect B traverses the central city area of Bangkok. It also follows a main transport corridor that is oriented in a west-east direction. Previous research suggested that land development in Bangkok has followed this main transport corridor (Guest et al., 2000), and, as such, high variability of landscape structure is hypothesized along Transect B over time. A moving window approach is used to analyze landscape patterns along these two transects. The size of the moving window is 3×3-km. Fragstats software (McGarigal and Marks, 1993) was used to calculate landscape pattern indices for each moving window. Three indices were measured: the percentage of impervious cover, mean patch size, and patch number. The pattern indices are calculated at class level. The percentage of impervious cover within each moving window suggests a general level of urban development, while the mean patch size and patch number provide information about landscape fragmentation (Riitters, 1995). The landscape pattern indices are plotted against the distance to the

origin (west edge of the transect). The curves of landscape pattern indices are evaluated, providing insights into the spatial/temporal dynamics of landscape structure.

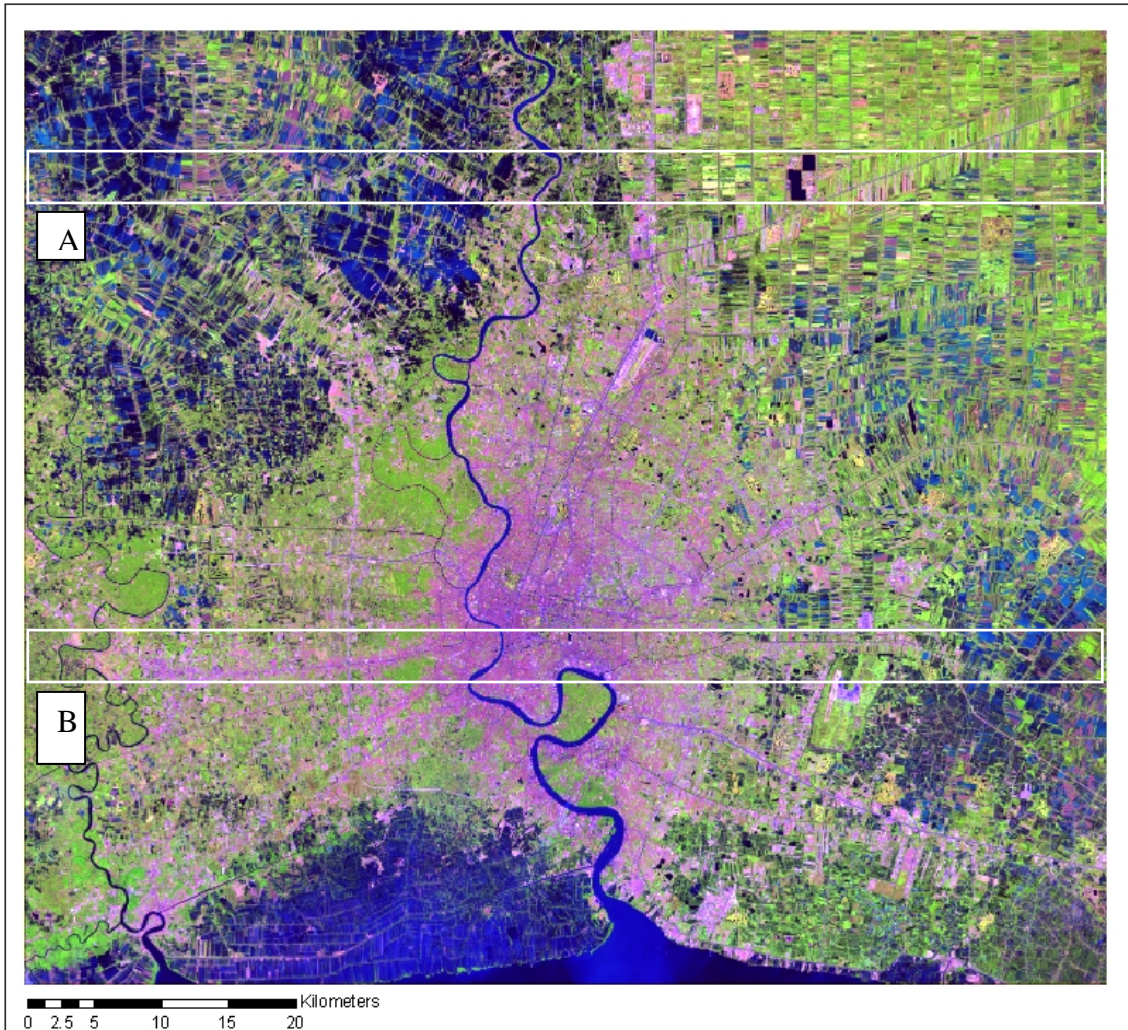


Figure 4.1. Transects for urban-rural gradient analysis.

4.4.2 Overall Urban-Rural Gradients and Urban Feature Identification

The sampling transect approach provides a measurement of landscape pattern for limited areas. The orientation, position, width, and length of the transects are subjective to and constrained by the design. Therefore, urban-rural gradient analysis was applied to the entire image. The approach is similar to an image convolution operation in which a

moving window is positioned over each pixel as the focal cell of the image, so the landscape pattern indices can be calculated for the defined neighboring through the window size. As indicated, three pattern indices are calculated: the percentage of impervious cover, mean patch size and patch number. Thus, three resultant landscape pattern images are generated: a density image, a mean patch size image, and a patch number image. For these images, the pixel values represent the compositional and structural information of defined neighborhoods (i.e., 3-km buffer). The image “convolution” operation is simply an extension of the sampling transect approach. To examine the effects of window size on the landscape pattern metrics indices and their effectiveness in describing urban form, four different window sizes (150-m, 500-m, 1500-m and 3000-m) were examined, because different window sizes provide spatial structure information at different scales.

Two approaches are used to identify urban features (i.e., urban core, inner zone, urban fringe, and rural areas). The first approach reclassifies the landscape pattern images. For instance, urban core area may have high values of mean patch size for impervious cover, while a rural landscape may have lower values. Using different threshold values, the landscape pattern image can be reclassified into several regions. Each of these regions has similar characteristics in terms of urban landscape structure. This approach quantifies urban features from the perspective of spatial organization of urban space. Using the percentage of impervious index as an example, urban core can be simply identified using a threshold value that is three standard deviations above the mean value. Visual interpretation can be used to specify the threshold values. Landscape pattern images from different time periods (i.e., density image from 1993 and 2002) can

be classified using the same set of threshold values for comparison purposes. Thus, the changes of urban features and spatial pattern can be monitored through time. Urban features may vary in locations and spatial extents if different landscape pattern indices are used for classification. In this study, the density and mean patch size indices are employed for urban feature classification and analysis consistency.

In the second approach, the building height information is used as an alternative input to analyze urban features. The locations of high rise buildings are treated as individual points. Their areal distribution is mapped using a kernel smoothing technique (Bailey, 1995). A kernel sizes of 3000-m is used. Within the moving kernel, the distances to the kernel center are calculated for the high-rise buildings, and the intensity value of the center-point is derived as a function of the weighted distances. This approach allows the variation of high-rise building intensity over Bangkok to be examined. The urban core area is defined by thresholding the intensity image. The temporal change of urban features is not examined using this approach due to limitations of data availability. There is no high-resolution data available for the study area in early 1990.

4.4.3 Urban Change Pixels and Pre-Existing Urban Form

To examine the spatial relationships between urban change pixels and pre-existing urban form or urban gradients, the change detection results from 1993 to 2002 are overlaid on landscape pattern images from 1993. The total number of change pixels from 1993 to 2002 is 175,926. To reduce the data volume and computational cost, 10-percent of change pixels are selected for urban space infilling and expansion analysis. For comparison purpose, the same numbers of pixels are randomly selected for stable urban and stable non-urban classes for the periods of analysis. These randomly selected pixels

serve as control samples to evaluate whether there are significant differences between the change pixels and non-change pixels with regard to the pre-existing urban form. Simple boxplots were used as the primary data exploration method. The comparisons were conducted for different window sizes, ranging from 150-m to 3000-m. A small window size (i.e. 150-m) provides urban structure information at immediate pixel neighborhoods, while large window size (i.e., 3000-m) allows high level urban structures, such as urban core/fringe, to be examined. The operation at a small window size is similar to the urban growth modeling work conducted by Wilson et al. (2003). The change pixels are grouped into three main urban growth patterns: urban infilling growth, diffusive expansion growth, and isolated growth. Infilling growth is defined as an “urbanized pixel” surrounded by more than 50-percent existing urban pixels, whereas isolated growth is defined as an “urbanized pixel” surrounded by 0-percent existing urban pixels. All other change pixels are labeled as diffusive expansion growth.

4.5 Result

4.5.1 Urban-Rural Gradients from Sampling Transects

Figure 4.2 shows plots of pattern metrics derived for Transect A and Transect B. Both transects are orientated along a west-east direction. The X-axis indicates the distance to the origin (about 40-km to Bangkok city center), and the Y-axis indicates the measurements of the selected pattern indices: the percentage of impervious cover, mean patch size, and patch number. Transect A is located in an urban fringe area. There is a main transport route oriented across transect A at about 47-km from the west edge of the transect. The location of this transport corridor can be easily identified by examining the peak values of impervious cover density and mean patch size presented in Figure 4.2.

Urban development is represented as the gaps between the blue line (1993) and the red line (2002). For transect A, the urban growth is primarily located near the transport route, between the distance of 35-km and 60-km from the west edge of the transect. Other regions (0~35-km and 60~80-km) from the west edge of the transect can be considered as a rural-dominated landscape, because the percentage of the impervious cover is quite low (i.e., less than 5-percent). Overall, the level of urban development in Transect B is much higher than in Transect A, as indicated by higher values of imperviousness. For Transect B, the peak value of percent imperviousness is located around 37-km from the west edge of the transect. Visual interpretation of Landsat TM/ETM (1993 and 2002) images confirms that the location of the peak value matches well with the high density urban space in central Bangkok area or the city center. There are also several peak values around 15-km, 25-km, 47-km, and 60-km from the west edge of the transect. These peak values match well with important urban features such as peripheral urban clusters, transport intersections, and other major urban developments. There is a peripheral cluster located at 15-km from the west edge of the transect, and two major road interactions are located at 25-km and 47-km, respectively. A new airport is developing around 60-km. The curves of impervious density show a high level of oscillation along Transect B. This is largely due to the location of Transect B that follows a main transport route that is oriented from west to east. The urban development along this transport route is complex. It is also interesting to see that impervious density is generally stable between 27-km to 45-km from the west edge of the transect from 1993 to 2002. Most urban development actually occurs beyond this range (i.e., at least 10-km away from the urban center). The mean patch size curves look smoother than those for the impervious density index. This

is misleading, because of the data range. For Transect B, the highest mean patch value is around 1,700 (at 37-km), which is substantially higher than values from other regions. The plots at the bottom of Figure 4.2 show patch numbers along transect A and B, respectively. The curves are much more complicated than those for density indices and mean patch size indices. It is difficult to delineate urban center and rural area, because the urban center may also have smaller numbers of impervious patches, although their patch size may be significantly larger than those for rural area. Through time, there are obvious increases of patch numbers between 0~37-km and 60~80-km from the west edge of the transect for Transect A and Transect B, respectively.

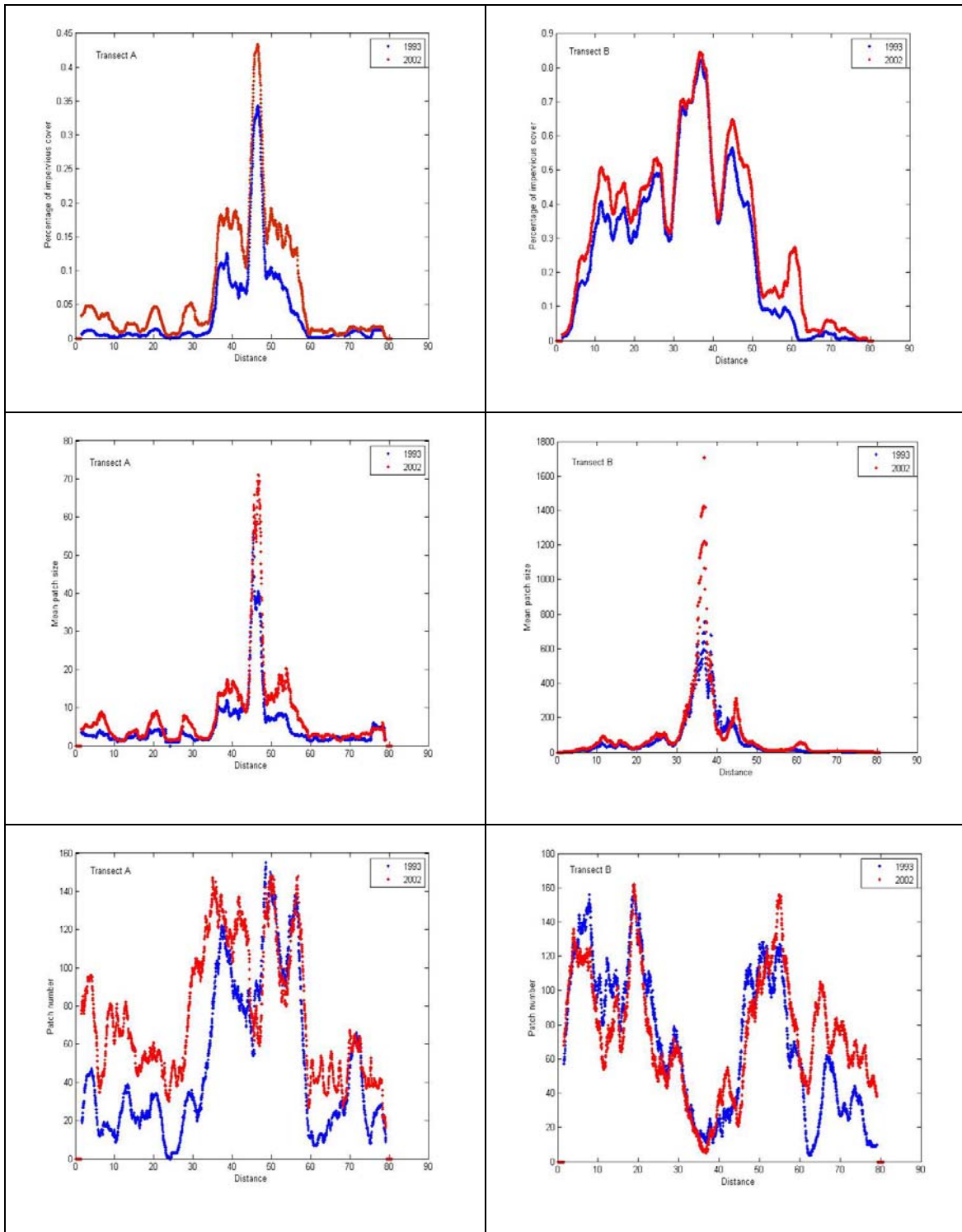


Figure 4.2. The density, mean patch size, and patch number of Impervious Cover along Transects A and B

The landscape pattern indices derived for these two transects show very different characteristics with regard to the spatial and temporal dynamics. For instance, Transect A indicates abrupt contrasts between urban and rural landscape, while Transect B shows high oscillations due to the presence of peripheral clusters, road intersections, and other urban developments across space. In fact, it is difficult to capture general urban form based on the limited number of sampling transects, especially for large metropolitan that often have more complicated urban forms than a simple concentric urban shape (Conway and Hackworth, 2007).

4.5.2 Urban-Rural Gradients for Entire Image and Urban Feature Identification

Figure 4.3 shows resultant landscape pattern images using a moving window or image convolution approach for the entire Greater Bangkok area represented in the satellite images. The mean value of impervious density increases from 0.11 in 1993 to 0.14 in 2002 (top panel). A visual interpretation of 1993 and 2002 density images shows the expansion of the road network and the development of several peripheral urban clusters in the eastern part of Bangkok. For mean patch size, the mean value increases from 17.01 in 1993 to 26.8 in 2002 (middle panel). There is one cluster with an extremely high mean patch size in 1993 image. The cluster is located in the middle of Bangkok city and near the Chao Phraya River. An additional cluster has developed from 1993 to 2002. It is located to the northeast of the initial cluster. The mean value of the patch number also increases from 56 to 72 during this period (lower panel). This generally indicates an increased level of land fragmentation, which is clearly shown in Figure 3 (lower panel). The fragmentation of rural landscape is particularly obvious.

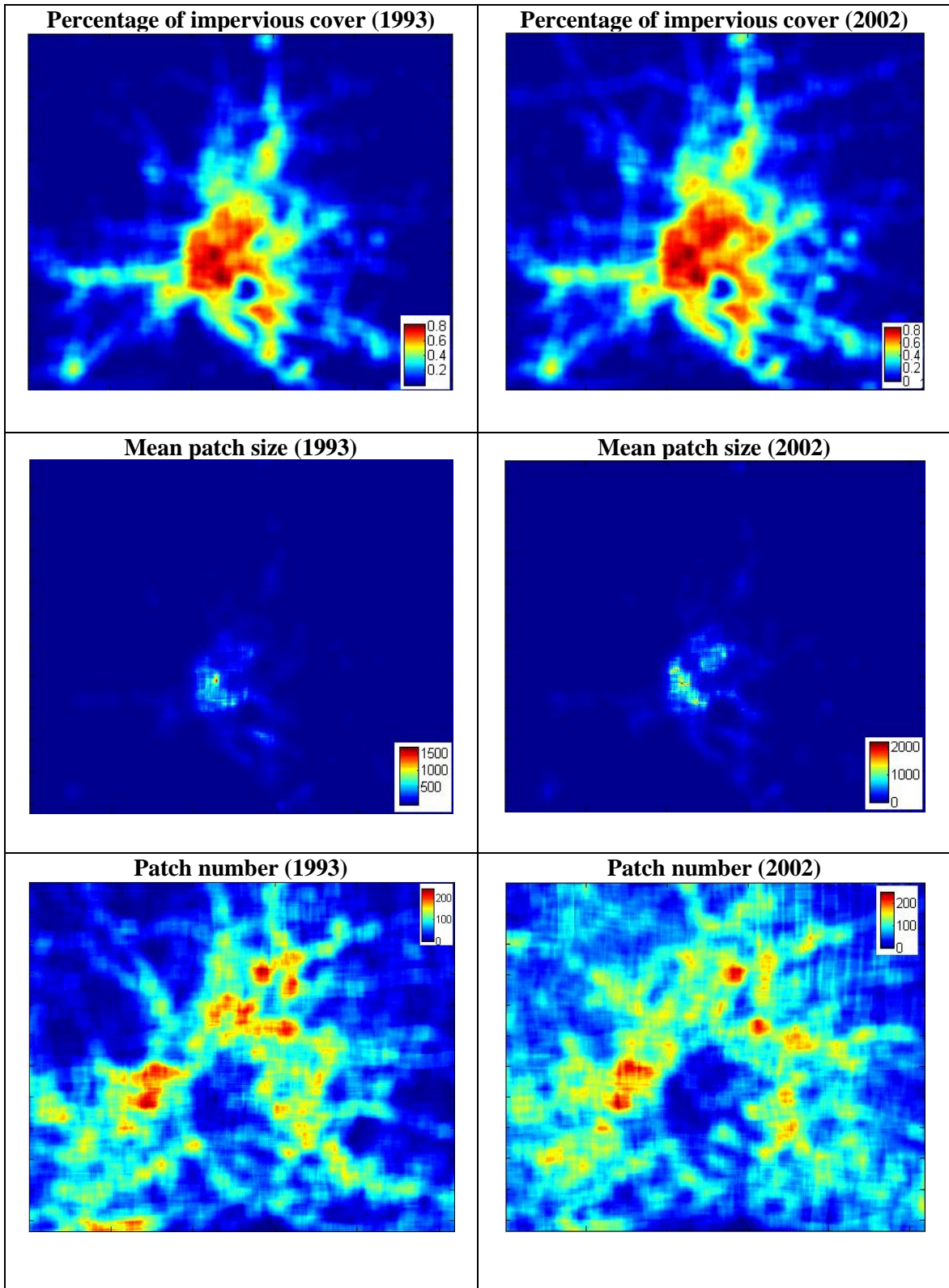


Figure 4.3. Urban-rural gradients analysis using moving window (3-km window size) approach: density, mean patch size, and patch number of impervious cover

The impact of window size are examined using a range of window sizes: 150-m, 500-m, 1500-m and 3000-m. Using the derived density image for 1993 as an example, Figure 4 shows that small window size (i.e., 150-m) characterizes the local variation in imperviousness as the resultant image appears very similar to the original input image (i.e., impervious cover from 2002). It should be noted that the edge effect for a small window size may introduce uncertainty (Urban et al. 2001). Therefore, spatial structure information derived from small window size can be difficult for interpretation. The images are much smoother if large window sizes (i.e., 1500-m, 3000-m) are employed. It is not possible to define a window size as a-prior knowledge. Geo-statistical method such as a semivariogram may be employed for data exploration. However, it is also useful to examine a range of window sizes or a multi-scale approach that captures urban structure at different levels. In practice, the resultant landscape pattern images should be examined using satellite images and other GIS dataset (e.g., road network) as a reference. A larger window size should be used if the overall urban-rural gradients are of interests, while a smaller window size emphasizes urban structure for each pixel's immediate neighborhood locale. In this study, the window size of 3000-m was appropriate to assess the urban-rural gradients that characterize the city of Bangkok. The general contrast of the urban/rural landscape can be easily identified, while key urban features such as peripheral clusters are retained as well.

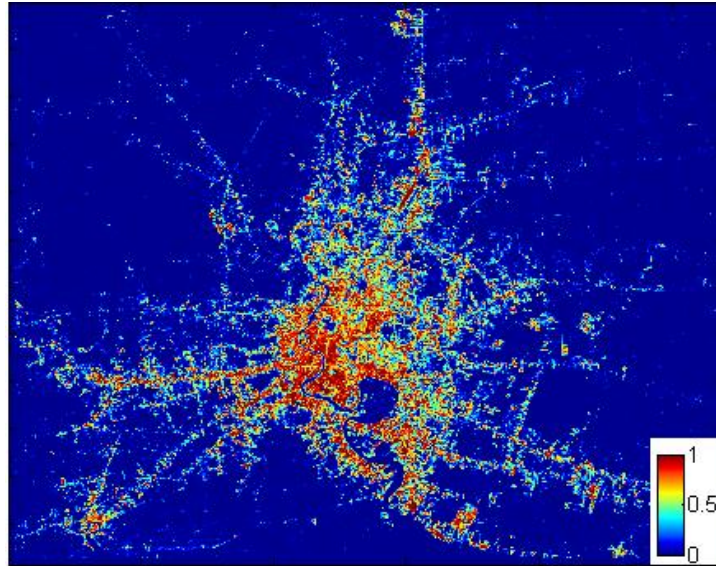


Figure 4.4. Impervious Density Image of 1993 (with 150-m window size).

The urban features are classified by applying different threshold values to landscape pattern images. For the 1993 impervious density image, the mean value for the entire image is 0.11 and the standard deviation is 0.16. The threshold value for the urban core area was defined as 0.6, which is three standard deviations above the mean value. The urban fringe area was defined as the mean value (0.11) and one standard deviation above the mean (0.27). The region of Bangkok that has the density value between the urban core and the urban fringe is labeled as inner zone and has a range of value extending from 0.27-0.6. All other regions with a density measure of less than 0.11 are assigned to the rural area. Figures 4.5a and 4.5b show the urban core, inner zone, urban fringe and rural areas for 1993 and 2002 images, respectively. The urban features are also classified using mean patch size pattern images. Figures 4.5c and 4.5d show the locations and areal distributions of urban features defined by the mean patch size index. The shape, location, orientation, and area of urban features can be different depending on the inputs (e.g., density image or mean patch size image). Using 2002 urban features as an example,

the inner zone and urban fringe areas derived from the density image show much higher levels of connectivity than those from the mean patch size image. Although threshold values can be modified to reshape urban feature, the fundamental differences between the compositional and structural information of the landscape remain. Both can be useful for quantifying the level or form of urban development. The urban feature statistics can also be compared for different metropolitan areas over space and time to examine pattern – process relations across a range of settings and conditions.

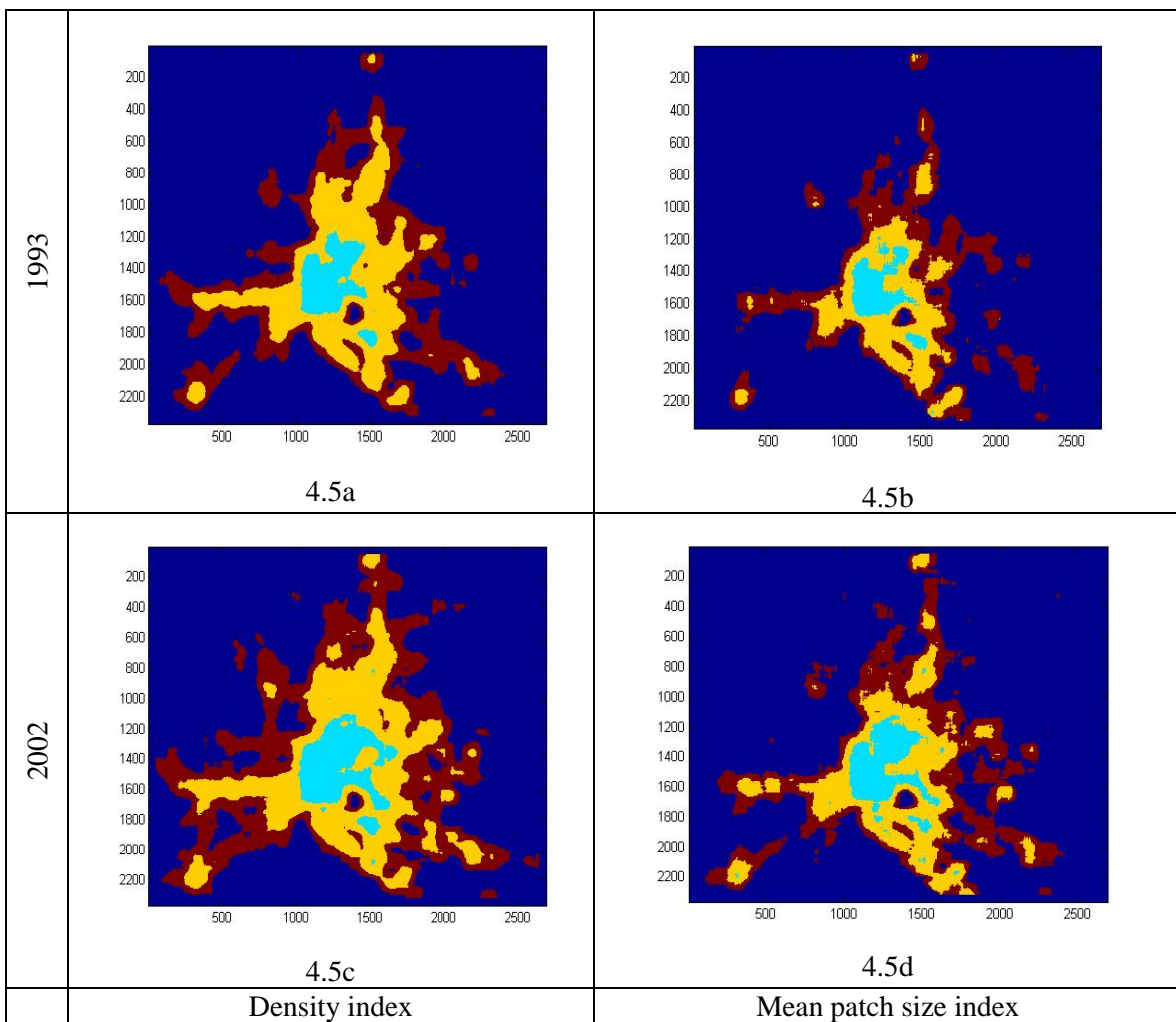


Figure 4.5. Urban Feature Identification Using Density and Mean Patch Size Indices: Urban Core, Inner Zone, Urban Fringe, and Rural Areas.

The shape of the urban area is highly irregular for Bangkok. It has a dense core area and urban development that extends towards east, west, and north directions, mainly along three transportation corridors. The locations and area extents of urban features change from 1993 to 2002. General trends include the conversion from inner zone to urban core, urban fringe to inner zone, and rural area to urban fringe. Using the density image as an input, Table 4.1 shows areal distributions of these urban features for 1993 and 2002. It should be noted that there is another city, Samut sakhon, located at the southwest corner of the image. Considerable urban built-up areas have been developed along the transport routes between Bangkok and Samut sakhon since the early 1990s. As a result, the urban fringe areas of these two cities have merged and Samut sakhon appears as a peripheral cluster of Bangkok.

Table 4.1:

Areal Distribution of Urban Features for 1993 and 2002

	Urban core	Inner zone	Urban fringe	Rural
1993	0.0239	0.1095	0.1383	0.7283
2002	0.0379	0.1412	0.1975	0.6234

Using a moving window approach, an intensity image was generated to represent the spatial clustering of high-rise buildings in Bangkok, Thailand. Figure 4.6 shows an overlay of the intensity image and previously defined urban core areas using the impervious density index. It is interesting to note that the areas with most high-rise buildings do not match well locations with the highest impervious density. In other

words, the locations of urban core areas may be different depending on the inputs: 2-D impervious cover or 3-D building height. In Bangkok, high-rise buildings are often clustered in the Central Business Districts (CBD), most of them are office buildings, hotels, and luxury condominiums. In a traditional 2-D land use/cover map, these high-rise buildings may be simply grouped into the same urban class (i.e., impervious cover), although the function of a high-rise building can be very different from a single-story structure. Therefore, it may be difficult to delineate the CBD area from fringe areas or peripheral clusters using only 2-D impervious cover information. This will be another challenge for the physical characterization of urban form or features from remotely-sensed imagery. Urban mapping in 3-D may offer a significant potential for the identification of meaningful urban functions (e.g., CBD), because of the capability to characterize building area for demographics studies.

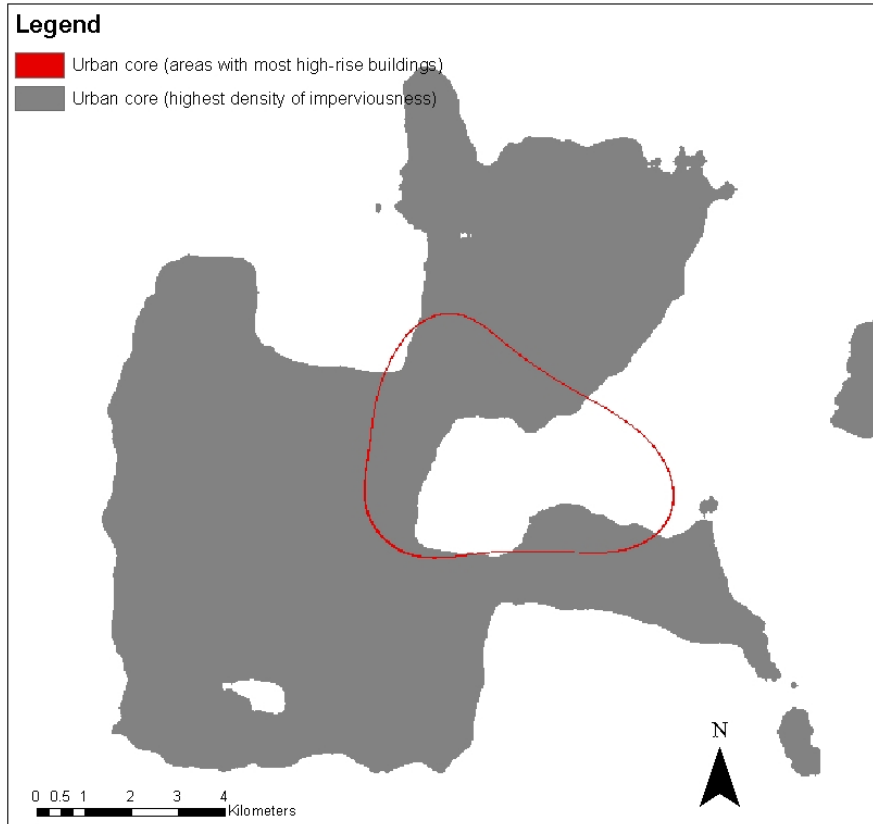
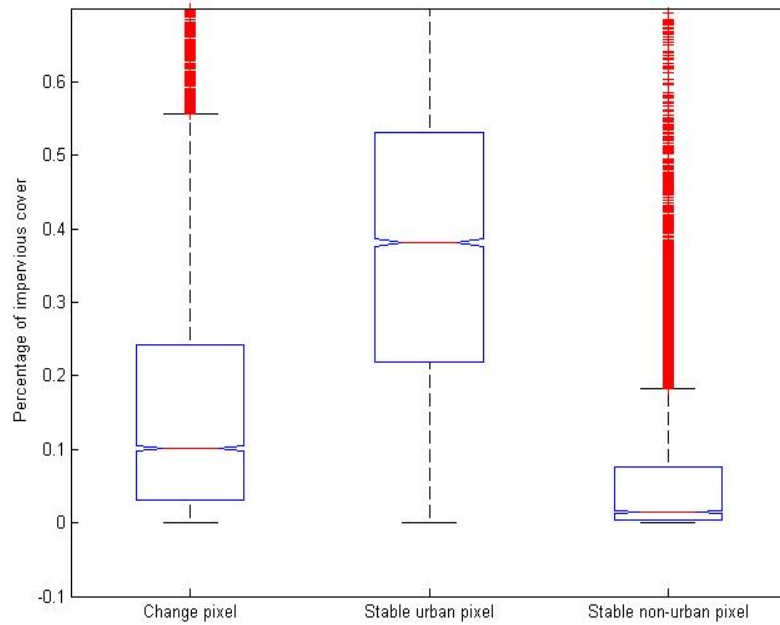


Figure 4.6. Comparison of Urban Core Areas Derived from 2-D and 3-D Inputs.

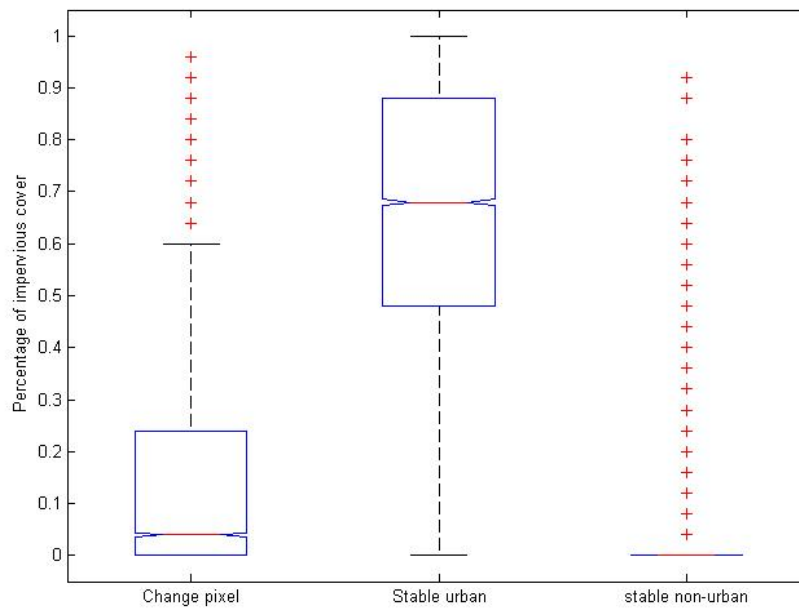
4.5.3 Urban Change and Urban Form

To examine the relationship between urban change pixels and pre-existing urban form, 17,000 random pixels were selected from the total number of change pixels from 1993 to 2002. The same numbers of random pixels were selected from stable urban class areas and from stable non-urban class areas. Within predefined window sizes, three indices were calculated for these sample pixels, including the percentage of impervious cover, mean patch size, and patch number. Figure 4.7 shows the boxplots for these indices. Overall, the density indices for change pixels are substantially lower than those from stable urban class. The stable non-urban class has the lowest overall density indices and the boxplot for this class is highly skewed. The mean patch size index shows similar

characteristics as the impervious cover density index. The stable urban class has the largest mean patch size over a range of window sizes from 150-m to 3000-m, and the stable non-urban class has, in general, the lowest mean patch size. In addition, the overlap between the three classes becomes smaller as the window size decreases. This is anticipated, because a larger window size emphasizes the variability of the landscape at a larger scale and local variations may be smoothed. However, it is still useful to examine the large scale contextual information for the locations of the change pixels, as it provides a general distribution of change pixels along rural-urban gradients or urban form/features. Using previously defined urban features (i.e., density based urban features) as zoning boundaries, the distribution of change pixels are 2-percent, 18-percent, 25-percent and 55-percent for the urban core, inner zone, fringe, and rural area, respectively. The patch numbers are similar for the change pixel and the stable urban pixel. Both classes have relatively higher values of patch numbers than the stable non-urban class. It should be noted that the patch number indices at small window size (i.e., 150-m) are clustered at fairly low values (0 or 1). This will not be very useful for examining the relationships between urban change and urban structure/form.

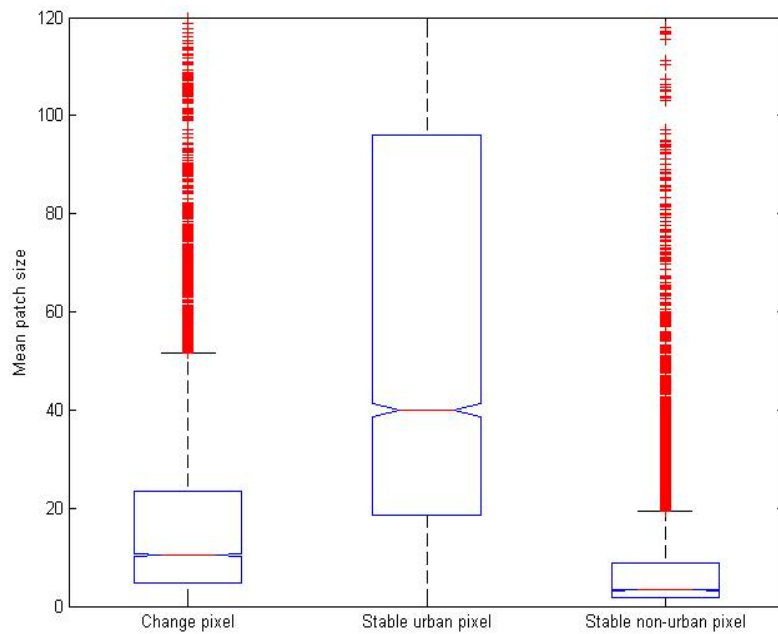


3000-m Window Size

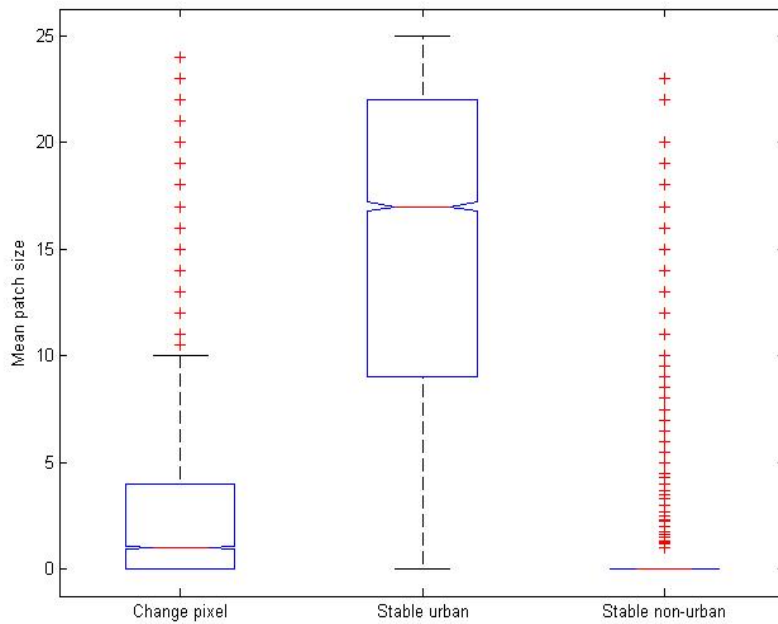


150-m Window Size

Figure 4.7a. Percentage of impervious cover for the spatial neighborhoods of the change, stable urban and stable non-urban pixels.

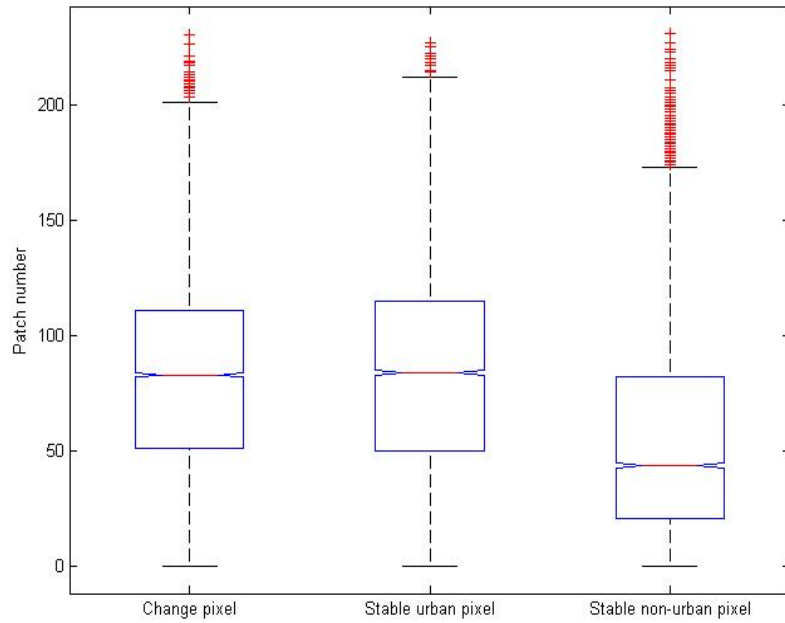


3000-m Window Size

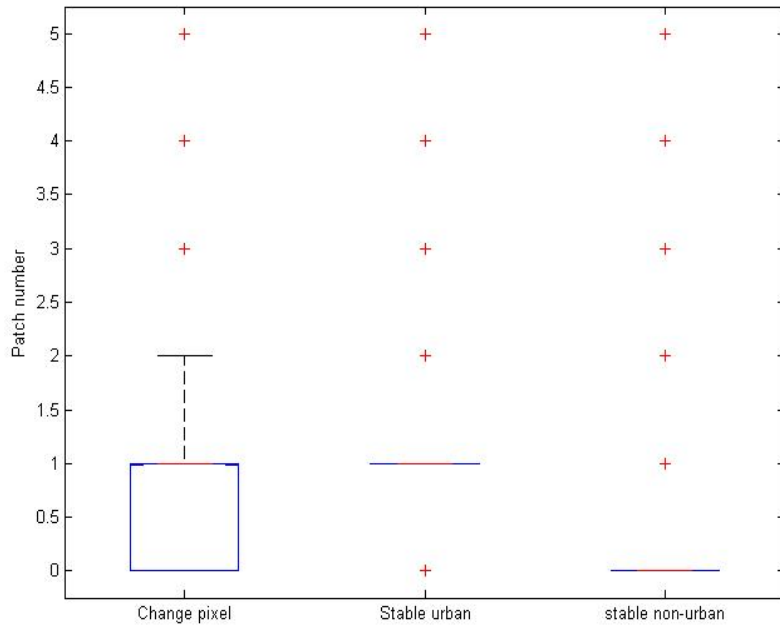


150-m Window Size

Figure 4.7b. Mean patch size of impervious cover for the spatial neighborhoods of the change, stable urban and stable non-urban pixels.



3000-m Window Size



150-m Window Size

Figure 4.7c. Patch number of impervious cover for the spatial neighborhoods of the change, stable urban and stable non-urban pixels.

The indices derived at the small window size (i.e., 150-m) can be used for characterizing conceptual urban growth models, such as infilling growth, diffusive expansion growth, and isolated growth (Wilson et al., 2003). In this study, 8-percent of change pixels can be labeled as infilling growth. For these pixels, the density of impervious cover in a 150-m window size is equal or above 50-percent. 45-percent change pixels can be considered as diffusive expansion growth, because these pixels are located in areas with between 0~50-percent impervious cover density. All the remaining change pixels (47-percent) are labeled as isolated growth. The contribution of diffusive expansion growth and isolated growth are almost identical, and they are substantially higher than infilling growth. This may suggest that Bangkok has increased its level of urban sprawl through time.

4.6 Conclusion

Urban-rural gradients in Bangkok, Thailand was initially examined through a transect sampling approach. Three landscape pattern indices were measured along two transects. The density of impervious cover provides, in general, the level of urban development, while mean patch size and patch number indicate landscape fragmentation. Pattern indices show very different characteristics (i.e., abrupt transition/oscillation) depending on the location of the transects. Thus, it is difficult to capture the overall urban form using a limited number of transects. A moving window or “convolution” approach was employed for the entire image. Pattern indices were calculated within each moving window. Urban features (i.e., urban core, inner zone, urban fringe, and rural) were then defined as regions with similar characteristics of impervious density or spatial structure. The temporal dynamics of urban features were also examined. The area expansion of

urban core, inner zone, and urban fringe are obvious from 1993 to 2002, although the measurements exclusively rely on physical characteristics of urban space. The urban core of Bangkok was also defined using 3-D building height information. It was found that the location and areal distribution of the urban core can be different depending on the inputs (i.e., 2-D impervious map vs. 3-D building height). The measurement of urban features allows researchers to compare urban form, or the level of development, across space and time. In addition, the approach provides a general framework to study the relationship between urban change process and urban form/pattern. Simple boxplot analysis shows that there are significant differences among urban change pixels, stable urban pixels, and stable non-urban pixels with regard to their spatial context or neighboring urban structure. The relationships are scale-dependent. Urban structures at local neighborhoods are useful for characterizing urban growth models such as infilling, diffusive expansion, and isolated growth. Large scale urban structure provides an overall picture of urban growth. The distribution of change pixels along rural-urban gradients or urban form/features can be summarized and compared.

Reference

- Alberti, M. (1999). Urban patterns and environmental performance: what do we know? *Journal of Planning Education and Research* 19,151 – 163.
- Allen, T.F.H., Starr, T.B. (1982). *Hierarchy: Perspectives for Ecological Complexity*. University of Chicago Press, Chicago.
- Anderson, W.P., Kanaroglou, P.S., Miller, E.J. (1996). Urban form, energy and the environment: a review of issues, evidence and policy. *Urban Studies*, 33, 7–35.
- Batty, M., Longley, P.A. (1994). *Fractal cities: A geometry of form and function*. London: Academic Press.
- Batty, M., Longley, P.A. (1988). The morphology of urban land-use. *Environmental Planning B*, 15: 461-488.
- Brueckner, J.K. (2000). Urban sprawl: diagnosis and remedies. *International Regional Science Review* 23, 160–171.
- Burgess, E.W. (1925). The growth of the city: an introduction to a research project. *The city*. R. E. Park, E. W. Burgess, R. D. McKenzie (editors). University of Chicago Press, Chicago, IL. 47-62.
- Choiejit, R., Teungfung, R. (2005). *Urban growth and commuting patterns of the poor in Bangkok*. Worldbank.
- Conway, T., Hackworth, J. (2007). Urban pattern and land cover variation in the greater Toronto area. *The Canadian Geographer/Le Géographe canadien* 51 (1), 43–57.
- Dale, V.H., Brown, S, Haeuber, R.A., Hobbs, N.T., Huntly, N., Naiman, R.J., Rlebsame, W.E., Turner, M.G., Valone, T.J. (2000). Ecological principles and guidelines for managing the use of land. *Ecological Application* 10: 639-670.
- Donnay, J.P., Barnsley, M.J., Longley, P.A. (2001). *Remote Sensing and Urban Analysis*. Taylor & Francis.
- Fulton, W., Pendall, R., Nguyen, M., Harrison, A. (2002). *Who sprawls most? How growth patterns differ across the U.S.* Wasbington, DC: Brookings Institute.
- Galster, G. (2001). On the nature of neighborhood, *Urban Studies*, 38, 2111–2124.
- Gustafson, E.J. (1998). Quantifying landscape spatial pattern: what is the state of the art? *Ecosystems* 1: 143–156.

- Harvey, R.O., Clark, W.A.V. (1965). The Nature and Economics of Urban Sprawl. *Land Economics*, 41: 1-10.
- Hoyt, H. (1939). *The structure and growth of residential neighborhoods in American cities*. Federal Housing Administration, Washington, D.C.
- Krizek, K. (2003). Residential relocation and changes in urban travel: Does neighborhood-scale urban form matter? *Journal of the American Planning Association* 69: 265-281
- Lassila, K.D. (1999). The new suburbanites: how American plants and animals are threatened by sprawl. *Amicus Journal* 21:16–20.
- Luck, M., Wu J. (2002). A gradient analysis of urban landscape pattern: A case study from the Phoenix metropolitan region, Arizona,USA. *Landscape Ecology* 17: 327–339.
- McDonnell, M.J., Pickett, S.T.A. (1990). Ecosystem structure and function along urban-rural gradients: an unexploited opportunity for ecology. *Ecology* 71:1232–37.
- McGarigal, K., Marks, B.J. (1993). FRAGSTATS: spatial pattern analysis program for quantifying landscape structure (version 1.0). Oregon State University, Forest Science Department, Corvallis.
- Mills, D.E. (1981). Growth, speculation and sprawl in a monocentric city. *Journal of Urban Economics*, 8: 201-226.
- O'Neill, R.V., DeAngelis, D. L., Waide, J. B., Allen, T. F. H. (1986). *A Hierarchical Concept of the Ecosystem*. Princeton University Press, Princeton, NJ.
- O'Neill, R.V., Milne, B.T., Turner, M.G., Gardner, R.H. (1988) Resource utilization scales and landscape patterns. *Landscape Ecology*, 2, 63-69.
- Portugali, J. (2000). *Self-Organization and the City*. Springer, Berlin.
- Riitters, K.H, O'Neill, R.V, Hunsaker, C.T, Wickham, J.D, Yankee, D.H, Timins, S.P, Jones, K.B, Jackson, B.L. (1995). A factor analysis of landscape pattern and structure metrics. *Landscape Ecology* 10: 23-39.
- Risser, P.G., J. R. Karr, Forman, R.T.T. (1984). *Landscape ecology: directions and approaches*. Illinois Natural History Survey Special Publication, Champaign, Illinois.
- Schowengerdt, R.A. (1997), *Remote Sensing: Models and Methods for Image Processing*. Academic, San Diego.
- Schweitzer, F. (1997). *Self-Organization of Complex Structures*. Gordon and Breach, Amsterdam, The Netherlands.

- Seto, K.C., Fragkias, M. (2005). Quantifying spatiotemporal patterns of urban land-use change in four cities of China with time series landscape metrics. *Landscape Ecology* 20:871–88.
- Song, Y., Knaap, G.J.. (2004). Measuring urban form: is Portland winning the battle against urban sprawl? *Journal of the American Planning Association* 70(2): 210- 225.
- Sukopp, H. (1998). *Urban ecology—scientific and practical aspects*. Springer, Berlin.
- Thunen, J. VON. (1825). *Der Isolierte Staat in Beziehung auf Landwirthschaft und Natioalokonomie*. Hamburg.
- Turner, M.G. (1989). Landscape ecology: the effect of pattern on process. *Annu. Rev. Ecol. Syst.* 20:171-197.
- Turner, M.G. (1990). Spatial and temporal analysis of landscape patterns. *Landscape Ecology* 4: 21-30.
- Turner, M.G., Gardner, R.H. (1991). *Quantitative Methods in Landscape Ecology*. Springer, New York, New York, USA.
- Urban, D.L., O'Neill, R.V., Shugart, H.H. (1987). *Landscape Ecology - BioScience* 37: 119-127.
- Walsh, S.J., W.F. Welsh, T.P. Evans, B. Entwisle, R.R. Rindfuss. (1999). Scale Dependent Relationships between Population and Environment in Northeastern Thailand. *Photogrammetric Engineering and Remote Sensing*, 65(1): 97-105.
- Wear, D.N., Turner, M.G., Naiman, R.J. (1998). Land cover along an urban-rural gradient: implications for water quality. *Ecological Applications* 8, 619–630.
- Wilson, J.S., Clay, M., Martin, E., Struckey, D., Vedder-Risch, K. (2003). Evaluating environmental influences of zoning in urban ecosystems with remote sensing. *Remote Sensing of Environment*, 86, 303-321.
- Wu, J., Loucks, O.L. (1995). From balance-of-nature to hierarchical patch dynamics: A paradigm shift in ecology. *Q. Rev. Biol.* 70: 439–466.
- Wu, J. (2000). *Landscape Ecology: Pattern, Process, Scale and Hierarchy*. Higher Education Press, Beijing, China.
- Zipperer, W.C., Wu, J., Pouyat, R.V. and Pickett, S.T.A. (2000). The application of ecological principles to urban and urbanizing landscapes. *Ecological Applications* 10: 685–688.

CHAPTER 5

SPATIAL CLUSTERING AND URBAN SETTINGS OF RURAL MIGRANTS IN BANGKOK, THAILAND¹

5.1 Introduction

Rural migration to urban places continues to fuel urbanization in developing countries, although natural increase and reclassification also have roles to play (Cohen et al., 2003; White et al., 2003; United Nations, 2004). Rapid urbanization can generate negative consequences through dramatic increases in population density that may outstrip infrastructure development. Related effects of urbanization can include environmental degradation, deterioration of land and water quality, loss of open green-space, alteration of urban hydrology, air pollution, and general degradation of the quality of life in urban settings. While urban places offer a number of pull-factors (e.g., manufacturing and construction jobs) to migrants that encourage their arrival, rural places, the source of much of the in-migration to Bangkok and other urban destinations, experience a number of push-factors (e.g., lack of good agricultural land for new households) that increase the propensity of people to leave their villages for urban settings. Often, remittances are returned to the origin household by family migrants, thereby, affecting rural household assets, and perhaps rural land use/land cover (LULC) patterns.

¹ The research work described in this chapter has been accepted for publication in *Geocarto International* (Shao et al., in press).

The data used in this paper are from an ongoing longitudinal study of social change in Nang Rong district, Northeast Thailand (Entwisle et al., 1998; Rindfuss et al., 2004, 2005; Walsh et al., 2005; www.cpc.unc.edu/projects/nangrong). As part of the 2000/01 round of survey data collection, migrants from 22 of the 51 study villages were followed to the top urban destinations: metropolitan Bangkok (Thailand's capital), the Eastern Seaboard (three provinces that the government has designated as an economic development zone), Korat (the largest city in the Northeast), and Buriram (a provincial capital). The overwhelming majority of urban migrants were in Bangkok. The migrants who were followed included those who resided in the 22 Nang Rong villages in either or both 1984 and 1994, but were not resident in 2000. Approximately 70 percent of these migrants were found and interviewed.

In August 2003, GPS coordinates were collected for the migrants from the 22 study villages who settled in Bangkok. These coordinates were for the addresses recorded when the migrants were interviewed in 2000/01, and, for the most part, represented their place of residence; for a few, it is their job location. Through the migrant follow-up questionnaire, the GPS coordinates of the surveyed locations in Bangkok, and data from earlier survey rounds, a rural-to-urban link was established. Because of this geolocal link, urban migrants can be assessed relative to geographic location and other demographic attributes in their destination and/or origin. This unique characteristic of the Nang Rong data set offers the opportunity for insights into the spatial pattern and geographic proximity of urban migrants from Nang Rong district relative to urban features such as roads, rivers, and development zones, as well as, the social and

demographic characteristics of the migrants relative to each other and to their origin villages.

This study examines selected social, spatial, and spectral characteristics of migrants, and their origin and destination locations within the context of a wide ranging set of questions including: How is the nature of LULC change in Nang Rong associated with the pattern of out-migration to cities within metropolitan Bangkok? Are migrants choosing to settle in newly urbanized areas in the cities, or in pre-existing places, possibly more familiar to earlier migrants from the same or spatially- and/or socially-connected villages? What are the spatial links between migrants in destinations and the home locations of migrants? To what extent can the concepts, techniques, and data of spatial analysis be brought to bear on the study of migration and land use in rural and urban places? And, how might such information help us understand the social demography of urban areas, the interrelationships between rural and urban places, and the bridge between traditional demographic data sources and geo-spatial data and spatial digital technologies?

The basic intent of this research is to conduct a descriptive social, spatial, and spectral analysis of migrants and their geographical settings surveyed and geo-located in Bangkok, and linked to their rural villages, as part of the 2000/01 Nang Rong survey. The first objective is to examine the spatial pattern of Nang Rong migrants in Bangkok by testing alternative approaches for characterizing the spatial pattern of all migrants and migrants linked to their 22 origin villages. Questions to be addressed include: (a) do the spatial patterns of migrants in Bangkok suggest spatial-social connections between migrants from the same source village as a consequence of spatial clustering in the

destination urban setting; and (b) how does the level of spatial clustering correlate with socio-demographic characteristics of rural-urban migrants? The second objective examines the use of satellite remote sensing to characterize urban environments that surround migrant locations (i.e., spatial neighborhoods) with particular emphasis on the degree and spatial pattern of impervious surfaces within a defined spatial window or kernel around the geo-located migrants' location. Specific questions to address include (a) what are the physical characteristics of the migrants' neighborhood environments in terms of impervious surface and the spatial organization of imperviousness, and (b) how do selected demographic variables and geographic variables correlate with migrants' neighborhood characteristics?

5.2 Geographic Setting

Nang Rong district is located in northeastern Thailand (Figure 5.1). Until well into the second half of the Twentieth Century, Nang Rong was a frontier area, with available, ambiguously titled, forested land. Even today, most villagers are farmers, growing rice and upland crops such as cassava, sugar cane, kenaf, and corn. As is true for Thailand as a whole, Nang Rong is in the final phase of the demographic transition, with low mortality and replacement level fertility (Knodel, Chamrathirong, and Debavalya, 1987; Hirschman et al., 1994). Mortality declined prior to fertility, and the steepest declines were infant and child mortality. Such an age pattern of decline is equivalent to an increase in fertility. As a result of these demographic processes in Nang Rong, there is a generation that is larger than preceding and subsequent generations. Coupled with the closing of the frontier, the stage was set for substantial out-migration from Nang Rong. Migration, both permanent moves to Bangkok and other urban areas, and temporary

movement, are common (Fuller et al., 1985; Fuller, 1990; Guest et al., 1994; Korinek et al., 2005). Further, seasonal migration is affected by the rhythm of agricultural activities in Nang Rong. The dominant crop is paddy rice, and there is almost no irrigation. The climate is monsoonal, with rains arriving late spring – early summer. The rice harvest typically occurs in December, and then there is a long dry season, with few agricultural activities prior to the start of the next rainy season. This dry season is a traditional time for Nang Rong residents to seasonally migrate in search of short-term employment prior to the next rainy season.



Figure 5.1. Nang Rong district, northeastern Thailand.

Bangkok is located in the central part of Thailand along the Chao Phraya River (Figure 5.2). Since the mid-1980s, direct foreign investments in manufactured exports created substantial employment in manufacturing, construction, and service sectors in

Bangkok and vicinity (Douglas, 1995). The economic efficiency of the metropolis and urban life draw large numbers of migrants from northeast Thailand and elsewhere. Bangkok now exceeds 9 million inhabitants and uncontrolled urban growth has been a major concern of the Thai government (UN Thailand ,2005). Urban problems, such as air/water pollution, traffic congestion, infrastructure deficiency, and environmental degradation have been exacerbated by increased population density in recent years.



Figure 5.2. Bangkok, Thailand: a Landsat TM view

5.3 Spatial Data

In 2003, 1022 migrants' locations in Bangkok were collected using GPS technology. Among these locations where GPS coordinates were collected, 100 points were recorded at migrants' work addresses; these points are not included in the analyses reported here. There are also 18 migrants whose addresses have missing data values.

These 18 records are deleted from the dataset. The remaining 904 migrants' geographic positions were collected at their home address. In some case, two or more migrants were at the same address, resulting in one GPS point location to represent more than one migrant. Thus, the actual number of GPS points ($n = 747$) used in this analysis is less than the number of migrants. Note that the focus of this paper is migrants and each migrant is treated as an individual observation. We also use satellite data to describe the composition and spatial organization of migrants' urban environments. Two Landsat ETM images (both from January 08, 2002) and one IKONOS image (November, 2002) were obtained. A mosaic of the two Landsat ETM images was produced, and an areal subset of $2,500 \times 2,500$ pixels was created to cover the Greater Bangkok Metropolitan Area and its surrounding provinces. The IKONOS image, with 4-meter spatial resolution, was used to generate training statistics and to test samples for Landsat ETM image classification. It should be noted that the IKONOS image only covers approximately a 10×10 km area, primarily the urban center of Bangkok.

5.4 Background

5.4.1 Migration and Urbanization

Urbanization and urban growth, more generally, is the consequence of three factors: rural–urban migration, differential natural increase, and re-classification of the urban administrative area as a consequence of planned and actual uses (Cohen et al., 2003; United Nations, 2004; White et al., 2003). In Thailand, over the past several decades, rural-urban migration has been a major contributor to urban growth (Phongpaichit, 1993), especially the growth of Bangkok. Over the same period, rural-urban migration has been a major contributor to population loss in rural areas, notably

those of the Northeast region (Susangkarn and Chalamwong, 1996), where Nang Rong is located. The migrants in our analyses, originating in rural Nang Rong and moving to Bangkok, are participants in Thailand's largest internal migration stream (Guest, 1996; Pejaranonda et al., 1995).

The impact of rural-urban migration on cities and other urban places, whether positive (e.g., Bilsborrow, 1996) or negative (e.g., Stern et al., 1992), as well as the impact of cities on them, will depend on how long migrants stay and where they settle. Some migrants are permanent, others are temporary (Guest, 1996; Korinek et al., 2005). Some live close to other migrants, others are dispersed. What is more, these two aspects of the migration stream are linked: the extent to which migrants live in close proximity to one another, and provide assistance to one another, affects the length of stay in the destination (Korinek et al., 2005). This study applies spatial analyses and GIS techniques to examine the residential clustering of migrants from Nang Rong.

Although spatial point pattern analysis has been intensively studied in spatial statistics (e.g., Bailey 1995; Cressie 1991; Diggle, 1983; Romesburg, 1989), ecology (e.g., Davis et al., 2000), and epidemiology (e.g., Gatrell et al., 1996), its application to migrants' individual location is relatively new. We study patterns of residential clustering in relation to origin villages, asking whether migrants from the same village are more likely to live in close proximity than those from different villages. The origin village represents a social context for migration and a set of social ties that travel with the migrant from the origin to the destination. A common origin can be viewed as one set of social ties, or social network, although not the only one (see Korinek et al., 2005).

Spatially explicit investigations of social ties are rare (see Faust et al. 2000 as an example of a social network analysis that operated within a spatial context).

5.4.2 Remote Sensing of Urban Places

Remote sensing has long been used to characterize urban settings by mapping land use and land cover (e.g., Forster, 1983; Mesev, 1998; Paola and Schowengerdt, 1995). The thematic maps generated from satellite images can be further used to study urban form (Batty and Longley, 1994) and urban growth (Ward et al., 2000, Xian et al., 2000). Empirical models have also been developed to link biophysical and social-demographic variables (Forster, 1983; Jensen et al., 1999; Weeks et al., 2005). Due to the heterogeneous land cover surfaces and their complex spatial organization, many urban pixels have mixed spectral signals from two or more land cover types. This is especially the case when images with low or medium spatial resolution are employed for classification. Therefore, traditional per-pixel classification is questionable in representing urban landscapes and estimating built-up areas. Ridd (1995) proposed a conceptual vegetation - impervious surface - soil model (V-I-S) to un-mix the pixels. This type of linear spectral mixture modeling has received intensive study, and imperviousness is considered the most important indicator of urban structure (Rashed et al., 2001; Small, 2001; Wu and Murray, 2003).

In addition to linear spectral mixture modeling, numerous other models have been employed to derive land cover proportions at the sub-pixel level. Neural networks (Atkinson et al., 1997; Foody, 1996; Liu et al., 2004) and decision trees (DeFries et al., 1999; Xian et al., 2005) are of particular interest, because no assumptions are made about the nature of the spectral mixture and the function is simply “learned” from training

samples. If the size of the training sample is relatively large and representative, neural network based models often work well. We apply the neural network approach in the sub-pixel classification to derive impervious cover for Bangkok, and extend our preliminary and descriptive analyses to social demographic processes.

5.5 Methods

5.5.1 Point Pattern Analysis of Migrants' Locations

The migrants' locational data set is relatively large ($n = 904$). Multiple observations representing migrants' locations are referenced at the same GPS location (i.e., several migrants may share the same dwelling unit). In addition, many types of attributes (i.e., age, sex, education level, occupation, and origin village) are linked to each migrant. A spatial statistical approach was used to perform a point pattern analysis of their geo-coded locations. First, we considered the rural-urban migrants as a single group. Their areal distribution was mapped using a kernel smoothing technique (Bailey 1995). Kernel sizes of 1000-meters and 2000-meters were tested. Within the moving kernels, the migrants' distances to the kernel center were calculated, and the intensity value of the center point was derived as a function of the weighted distances. This allowed the variation of migrants' intensity over Bangkok and the surrounding areas to be examined within a spatial context.

Social networks from origin villages are inferred based on the spatial clustering of migrants. Nearest neighbor distance was employed as an indicator of spatial clustering. In this study, migrants were stratified based upon 22 origin villages, and the Euclidean distance was computed for each migrant to his/her nearest neighbor from the same origin village. To summarize the spatial clustering by origin village, we simply calculated the

percent of nearest neighbor distance measures that are less than or equal to a specified threshold value (Bailey 1995) using the following equation (1):

$$G(D) = \#(NND \leq D)/n \quad (1)$$

NND indicates a vector of the nearest neighbor distance measures for an origin village. *D* indicates certain threshold distances specified as 500 or 1000 meters. The # symbol simply means counts and *n* is the total number of migrants for the source village. Thus *G*(500m) offers the percent of migrants who have nearest neighbor distances less than or equal to 500 meters. In this study, only two distance thresholds were considered – 500-meters and 1000-meters. We suspect that migrants may interact at relatively local levels and at nearby distances, and so the 0.5-km and 1.0-km distances seemed quite appropriate.

To test the significance of spatial clustering/randomness of migrants from a single village with respect to the total migrant population, we used a Monte Carlo randomization technique (e.g., Davis et al., 2000; Manly, 1991; Romesburg, 1989;). For example, if there are 30 migrants from an origin village, we repeatedly (i.e., 10,000 times) and randomly selected 30 migrants from the entire migrants' data set; *G*-values were calculated for each selection, and the distribution of *G*-values was defined. Assuming a normal distribution, we created 95% confidence intervals from the Monte Carlo simulations. The null hypothesis (*H*₀) is that the *G*-values calculated for the origin village are the same as the randomized simulation. The alternative hypothesis (*H*₁) is that the *G*-values calculated from the origin village are higher than that obtained from the randomized simulation. Accepting *H*₁ indicates spatial clustering of migrants from the same origin village in Nang Rong district.

To further evaluate the variation of spatial clustering/randomness, a correlation matrix was created to indicate how education level, occupation, age, and gender were related to the spatial pattern of migrants. This comparison is at the village level, so the individual socio-demographic variables have been aggregated based on origin villages. The education variable was computed as the percentage of migrants who completed 10 or more years' of education. The occupation variable was computed as the percentage of migrants who were in manufacturing. The percentage of males was used as the sex variable, and mean age was used as the age variable.

5.5.2 Neighborhood Environment of Migrants' Locations

The sub-pixel classification used in this study is a cross-sensor modeling approach, because images with two different spatial resolutions are involved. The IKONOS image was first classified into 30 spectral clusters using an unsupervised classification procedure. These spectral clusters were then grouped into four broad land cover types: impervious cover, vegetation, water/shadow, and soil. This classified IKONOS image was degraded to a $30 \times 30\text{m}$ resolution, providing a “fractional map” for each of the land cover types. The fractional maps were registered to the Landsat ETM imagery so that the location of the $30 \times 30\text{m}$ degraded IKONOS pixel precisely overlaid on the comparable $30 \times 30\text{m}$ Landsat ETM pixel. A multi-layer perceptron (MLP) neural network was employed to model the relationships between the Landsat spectral signals and the fractional maps (e.g. impervious). Specifically, 6 bands of Landsat ETM spectral data were used as the input layer. The output layer had 4 nodes and each node represented one land cover type. The number of nodes at the “hidden layer” was determined through numerous trials. To train the neural network, 3,000 pixels were

randomly selected from the Landsat ETM image, with 2,000 pixels used as the training set and the remaining 1,000 pixels as the validation set. The network was trained through a back-propagation algorithm. A number of practical techniques, such as the number of hidden units, learning rate, momentum, and training iterations were evaluated. The best estimation was obtained with a hidden layer of 10 nodes, a learning rate of 0.01, momentum of 0.8, and 1,200 training iterations. With the trained network, the Landsat ETM images were classified and the resultant impervious cover map was used for further analysis.

The neighborhoods of migrants' locations were defined as kernels with different sizes. Within each kernel, the percentage of impervious cover was calculated. Using FRAGSTATS software, the spatial arrangement of impervious cover was also characterized. Pattern indices, such as mean patch size and patch density, were derived for each spatial definition of neighborhood (i.e., kernel dimension). To perform this analysis, the results from the sub-pixel classification were transformed to “hard” classes and labeled by land use/land cover types using a threshold value of 0.5.

The migrants' neighborhood environment was modeled using multiple regression techniques. Each migrant was treated as an individual observation. The dependent variable was the percentage of impervious land use/land cover as well as the pattern indices for the derived migrants' neighborhoods. Independent variables included a number of socio-demographic characteristics and geographic variables. The socio-demographic variables included age, sex, education, and occupation. Sex and occupation variables were treated as dummy variables in the model. Occupation was equal to 1.0 if the migrant was engaged in manufacturing, and 0.0 for all other jobs. Geographic

variables included the Euclidean distance to primary roads and the Euclidean distance to the city center from the point location of the geocoded migrant's positions in Bangkok. Since the model's performance may be scale dependent, a number of kernel sizes were tested (e.g., 300-, 600-, 900-, 1500-, 2100-, and 3000-meters). A focal filter was used for all calculations centered on the migrant's locations and iteratively assessed. Multiple regression models were developed at each spatial scale (i.e., the kernel dimensions used to represent each migrant's neighborhood).

5.6 Results

5.6.1 Point Pattern Analysis for Migrants' Locations

Considering all the rural-urban migrants as a single group, two different kernel dimensions were tested to generate intensity surfaces for migrants' locations. Figure 3 shows the intensity surfaces of migrants' locations for kernel sizes of 1000-meters and 2000-meters. The smaller kernel size shows a more irregular intensity surface and the pattern of "hot spots" at the local scale. The intensity surface generated by the larger kernel smooths local details and provides a regional view of migrant's locational distribution. We can see in Figure 5.3 that there are local peaks in the intensity surfaces for migrant's locations.

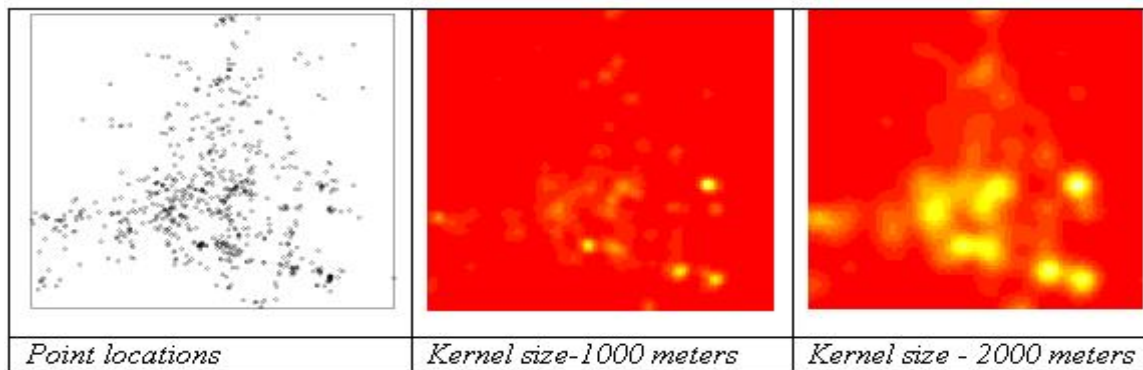


Figure 5.3. Intensity surfaces for migrants' locations in Bangkok.

In Figure 4, we plotted $G(500)$ values (i.e., threshold of 500-meter) against the number of migrants from each source village to ascertain whether migrants from their corresponding source villages were spatially clustered. The x-axis indicates the number of migrants and the y-axis shows $G(500)$ values for different source villages. A $G(500)$ value of 0.8 indicates that 80 percent of the migrants have nearest neighbor distances that are equal to or less than 500-meters. The confidence interval generated from the Monte Carlo simulation is shown as dashed lines. A 95-percent confidence interval ($0.025 \leq p \leq 97.5$) was applied to analyze the spatial clustering or randomness. Figure 4 indicates that 12-villages have significantly higher G -values than the randomized simulation, suggesting a pronounced clustering. In Figure 5, we plotted $G(1000)$ values (i.e., threshold of 1000-meter) against the number of migrants from each source village. Spatial clustering is fairly stable as compared to the $G(500)$ value, i.e., 12 villages show strong spatial clustering at 1000-m. Note that in Figures 5.4 and 5.5, the villages with the most migrants living in Bangkok are considerably more likely to show clustering beyond that which would be expected by chance. This is consistent with the migration literature on the role of social networks in maintaining migration streams (e.g., DeJong, 2000; Hugo, 1981; Korinek et al., 2005; Massey, 1990; Massey et al., 1993).

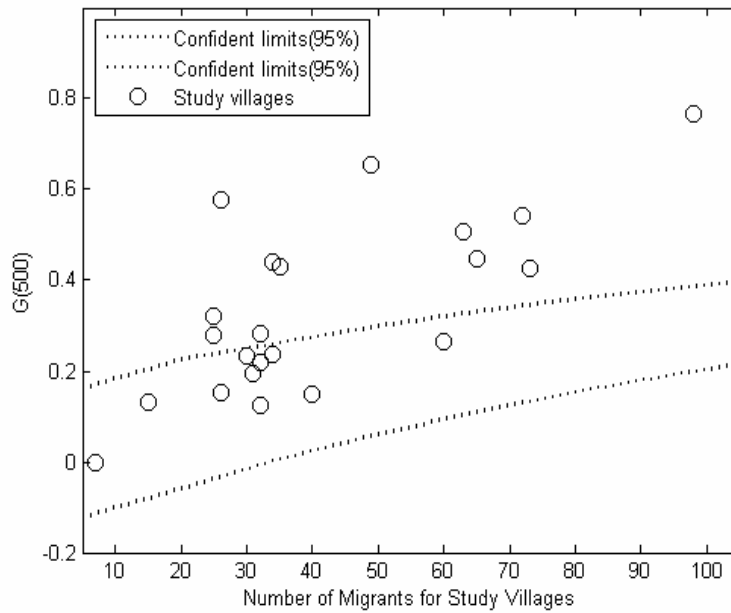


Figure 5.4. Spatial clustering of migrants from origin villages (500-meters threshold)

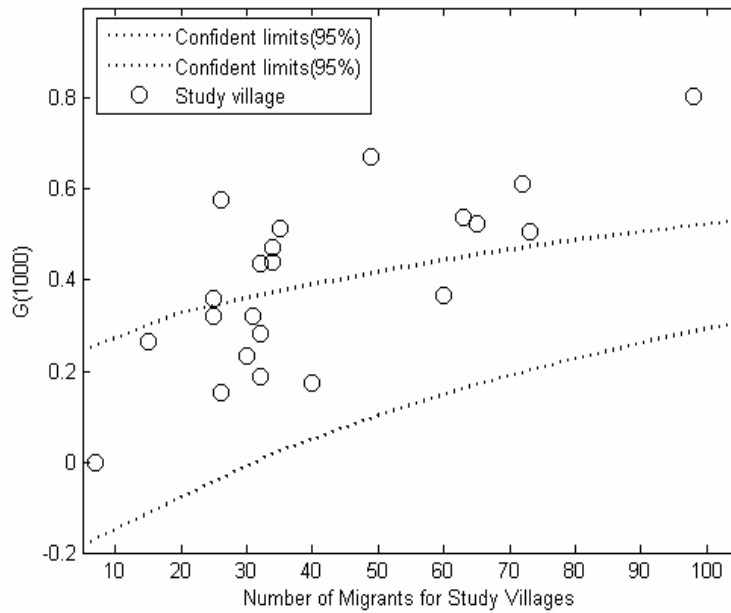


Figure 5.5. Spatial clustering of migrants from origin villages (1000-meters threshold)

To further explain the variation of spatial clustering, the *G*-values were linked to socio-demographic characteristics of the source villages using simple correlation coefficients and p-values (Table 5.1).

Table 5.1: Correlation Coefficients of Spatial Clustering and Socio-demographic Characteristics at the Village Level.

	<i>G</i> (500-meters)	<i>G</i> (1000-meters)
% of migrants in manufacturing	0.60 (p = 0.003)	0.62 (p = 0.002)
% of migrants who completed 10 or more years educati	-0.65 (p = 0.0012)	-0.67 (p = 0.0005)
Mean age	0.23 (p = 0.31)	0.15 (p = 0.51)
% of male	-0.05 (p = 0.81)	-0.08 (p = 0.73)

It can be seen that the occupation variable (the percentage of migrants in manufacturing) is positively correlated with spatial clustering -- the higher the percentage of migrants in manufacturing, the greater the spatial clustering. The education level is negatively correlated with spatial clustering -- the higher the percentage of migrants who completed 10 or more years' of education, the less the degree of spatial clustering. There is almost no correlation between the sex variable and spatial clustering, and the age variable shows a weak correlation, and not statistically significant. No major difference is found in the size of the correlations across two *G*-values.

To interpret these results, it is important to note that a substantial number of the manufacturing establishments in Bangkok are work and residential compounds. They are enclosed by a fence, with a guard at the entrance. The compound contains both the manufacturing facility and a dormitory for the workers, who typically are young and

unmarried. To the extent that social networks link origin and destination, an important role in recruiting factory workers, one would expect the percent in manufacturing to be positively associated with more geographical clustering of migrants.

Education, on the other hand, tends to disperse people. Most of the migrants went through the school system when mandatory education ended at grade 6. Having 10 or more years of education qualifies individuals for a greater diversity of jobs, and the results in Table 1 suggest that this diversity of jobs is also related to greater geographic scatter in their destination.

5.6.2 Neighborhood Environment of Migrants' Locations

The Landsat ETM representation of sub-pixel impervious surface for Bangkok and the surrounding area is shown in Figure 5.6. Light tones indicate higher degrees of imperviousness, whereas darker tones indicate lower degrees of imperviousness. The intensity of urbanization along the river and roads that bisect the image are readily apparent.



Figure 5.6. Impervious cover for Bangkok and surrounding areas.

The following box-plot (Figure 5.7) shows the variation of migrants' neighborhood environments using the percentage of impervious cover as the indicator. Different kernel sizes (i.e., 150 - 3000-meters) were assessed. According to Figure 5, the variation in the percentage of imperviousness decreases with increasing kernel size, as would be expected. However, even using a relatively large kernel size (i.e., 3000-meters), considerable variations in the degree of imperviousness resulted (i.e., a range from 10 to 70 percent).

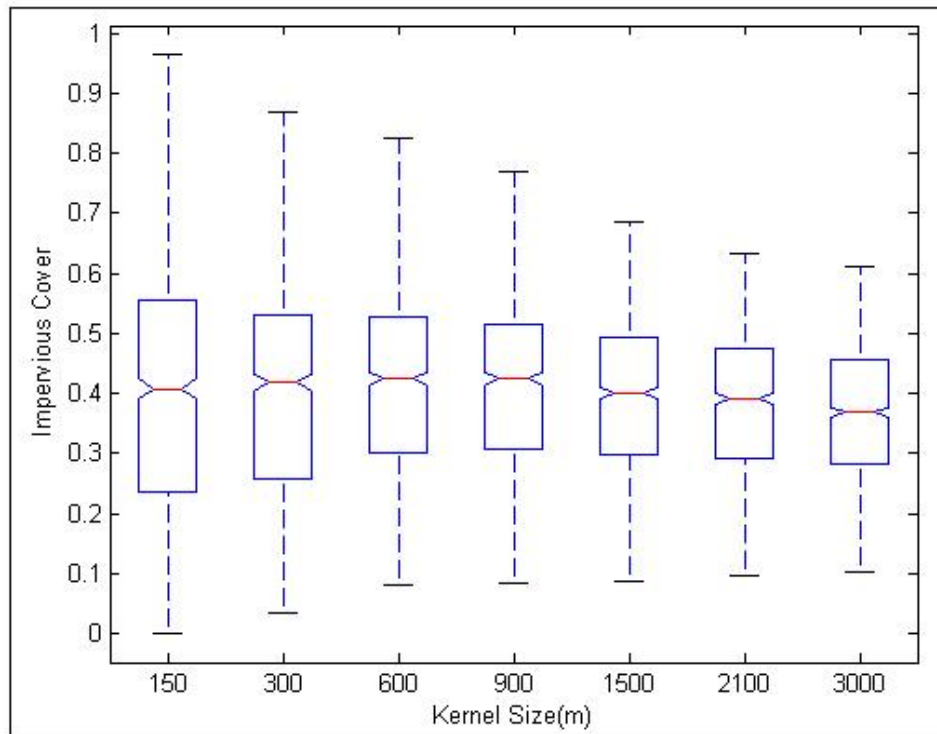


Figure 5.7. Box-plots of the percent impervious cover from varying kernel size.

Multiple regression models were developed to examine the percentage of impervious cover in migrants' neighborhoods as a function of selected socio-demographic (i.e., age, occupation, sex, and education level) and geographic (the log transform of the Euclidean distance to the nearest road and to the city center) variables. City center is arbitrarily specified as the center of the central business district. Each migrant's neighborhood environment is considered to be an individual observation, and the total number of observation is 904. Occupation and sex were treated as dummy variables in the model. Occupation is equal to 1 if the migrant is engaged in manufacturing work, and 0 for all other jobs. Male is coded as 1, and female is coded as 0. Education is the years of school completed. Seven multiple regression models were run, one for each of the

different kernel sizes (i.e., 150- to 3000-meters). Table 5.2 shows model coefficients for the predictor variables and R-squared values.

Table 5.2:
Coefficients for Impervious Cover Percentage Model

	150m	300m	600m	900m	1500m	2000m	3000m
(Intercept)	2.099**	2.112**	2.095**	2.0886**	2.175**	2.192**	2.206**
Distance to center	-0.131**	-0.139**	-0.140**	-0.144**	-0.163**	-0.168**	-0.174**
Distance to road	-0.056**	-0.048**	-0.041**	-0.034**	-0.025**	-0.022**	-0.018**
Occupation	0.061**	0.049**	0.036**	0.034**	0.027**	0.018**	0.002
Sex	-0.002	-0.002	-0.002**	-0.002**	-0.001**	-0.001	-0.001
Age	-0.029	-0.017	-0.011	-0.013	-0.015	-0.015**	-0.015**
Education	0.001	0.000	0.000	0.000	0.001	0.001	0.000
R ²	0.26	0.33	0.39	0.44	0.55	0.63	0.70

**significant at 0.05 level

Variation in the percent of impervious cover percentage is significantly associated with the log distance to the nearest road, the log distance to city center, occupation, sex and age. The geographic variables showed consistent significance at 0.05 level, while the social variables only showed significance at certain kernel sizes. The occupation variable is the most consistently significant of the social variables, and its positive sign is consistent with the large size and compound-like nature of many of the manufacturing establishments in Bangkok. For the distance to the nearest road variable, it has a negative sign and it suggests that the imperviousness is negatively associated with the distance to road. This is consistent with the overall spatial pattern of built-up areas in Bangkok – most developments follow the transportation corridors of the city. Note that the R-squared values increase from 0.26 to 0.70 as the kernel size increases from 150 - to 3000-

meters. It is also worth noting the effect of distance to center increases with kernel size, whereas the effect of distance to road and occupation variable decreases with kernel size.

The spatial pattern of impervious cover within specified kernels can be characterized using a number of pattern indices. Mean patch size was selected to represent the level of fragmentation. Seven regression models were developed for a range of kernel sizes, and the log transformation of mean patch size was used as the response variable. Table 5.3 shows model coefficients for the predictor variables and R-squared values.

Table 5.3:

Coefficients for Spatial Pattern Model

	150m	300m	600m	900m	1500m	2000m	3000m
(Intercept)	8.090**	11.260**	13.19**	13.100**	13.870**	13.76**	13.290**
Distance to center	-0.490**	-0.690**	-0.850**	-0.885**	-1.025**	-1.029**	-0.998**
Distance to road	-0.240**	-0.270**	-0.250**	-0.170**	-0.098**	-0.088**	-0.063**
Occupation	0.202**	0.200**	0.177**	0.156**	0.217**	0.180**	0.094**
Sex	-0.120	-0.056	-0.061	-0.088	-0.067	-0.073	-0.054
Age	-0.009	-0.014**	-0.010	-0.010	-0.006	-0.004	-0.004
Education	0.005	0.001	0.003	0.005	0.006	0.008	0.005
R ²	0.210	0.250	0.340	0.360	0.480	0.550	0.630

**significant at 0.05 level.

Three variables, the log distance to city center, the log distance to the nearest major road, and occupation of the migrant showed significant relationships with the mean patch size. R-squared values increased from 0.21 to 0.63 as the kernel size increased from 150- to 3000-meters. Again, the effect of distance to the city center increases with kernel size, whereas the effect of distance to road and occupation variable decrease with kernel size.

5.7 Conclusions

The unique character of the Nang Rong migrant data set allowed us to quantify the spatial patterns of migrants' locations in Bangkok. Nearest neighbor distance and Monte Carlo simulation were combined to perform the spatial point pattern analyses. Migrants from 12 of the 22 origin villages showed spatial clustering that may indicate strong social networks related to origin villages. The level of spatial clustering was positively correlated with the occupation variable -- the higher the percentage of migrants in manufacturing, the greater the spatial clustering. The education level is negatively correlated with spatial clustering -- the higher the percentage of migrants who completed 10 or more years' of education, the less the degree of spatial clustering. This finding suggests that migrants with high education backgrounds may have greater flexibility in the job market, and they may rely less on village social networks. For age and sex/gender variables, we did not find statistically significant evidence of spatial clustering. Note that these conclusions are based upon village level aggregations.

The neighborhood analysis of migrants' locations was characterized by the percentage and the mean patch size of impervious cover. These neighborhood environment indicators can be modeled as a function of selected socio-demographic and geographic variables. Variation in the percentage of impervious cover is associated with the distance to the nearest major roads, the distance to the city center, age, occupation and sex. The mean patch size was associated with the distance to the nearest major road, the distance to the city center, and occupation. The model's performance is scale-dependent - R-squared values generally increased as the kernel size increased from 150- to 3000-meters.

One of the main contributions of this research is the integration of GPS, GIS, remote sensing, and spatial statistical techniques for the study of rural-urban migration process and migrants' settlement pattern in urban setting. The interpretation of social networks from distance measures and spatial clustering is relatively new. The correlations between spatial clustering and socio-demographic characteristics are consistent with general perceptions with regard to rural-urban migration processes, however, the methods introduced in this research provide quantitative measures to specific aspects of rural-urban migration process (i.e., social network from source villages). One limitation of the neighborhood environment analysis is that the definition of neighborhood is arbitrary. For instance, simple distance buffers may not be appropriate due to the complexity of neighborhoods in the real world, however, the analysis still helps one understand the settlement patterns of rural-urban migrants, the impact of rural-urban migration on cities, as well as the impact of cities on migrants themselves. Overall, the integration of spatial data and analysis to the social research is advantageous from both theoretical and practical perspectives.

References

- Atkinson, P.M., Cutler, M.E.J., Lewis, H. (1997). Mapping sub-pixel proportional land cover with AVHRR imagery. *International Journal of Remote Sensing*, 18: 917-935
- Bailey, T.C., Gatrell, A.C. (1995). *Interactive Spatial Data Analysis*. England, Longman. Scientific & Technical.
- Batty, M., Longley, P.A. (1994). *Fractal Cities: A geometry of form and function*. London: Academic Press.
- Bilsborrow, R. (1996). *Migration, Urbanization, and Development: New Directions and Issues*. United Nations Population Fund and Kluwer.
- Cressie, N.A.C. (1991). *Statistics for Spatial Data*. John Wiley, Chichester.
- Cohen, B., White, M, Montgomery, M.R., McGee, T.G., Yeung, Yue-Man. (2003). *Urban Population Change*. National Research Council, Cities Transformed: Demographic Change and Its Implications in the Developing World. Panel on Urban Population Dynamics, Montgomery, M.R., Stren, R., Cohen, B., and Reed, H.E. (editors). Washington, DC: The National Academies Press, 75-107.
- Davis, J.H., Howe, R.W., Davis G.J. (2000). A multi-scale spatial analysis method for point data. *Landscape Ecology* 15:99-114
- DeFries, R., Townshend, J., Hansen, M. (1999). Continuous fields of vegetation characteristics at the global scale at 1-km resolution. *Journal of Geophysical Research*, 104, 16911-16923
- Diggle, P. J. (1983). *Statistical Analysis of Spatial Point Patterns*. Academic Press Inc., New York.
- Douglass, M. (1995). Global interdependence and urbanization: planning for the Bangkok Mega-urban Region. *The Mega-Urban Regions of Southeast Asia*. Vancouver; UBC Press.
- Entwisle, B., Walsh, S.J., Rindfuss, R.R., Chamrathirong, A. (1998). Landuse/Landcover and Population Dynamics, Nang Rong, Thailand. *People and Pixels*. (D. Liverman, E.F. Moran, R.R. Rindfuss, and P.C. Stern, editors), National Academy Press, National Academy of Sciences, Committee on the Human Dimensions of Global Change, Washington, DC, 121-144.
- Faust, K., Entwisle, B., Rindfuss, R.R., Walsh, S.J., Sawangdee, Y. (2000). Spatial Arrangement of Social and Economic Networks Among Villages in Nang Rong District, Thailand. *Social Networks*, 21: 311-337.

- Foody, G.M. (1996). Relating the land-cover composition of mixed pixels to artificial neural network classification output. *Photogrammetric Engineering and Remote Sensing* 62:491-499.
- Forster, B.C. (1983). Some urban measurements from Landsat data. *Photogrammetric Engineering and Remote Sensing* 49:1693-1707.
- Fuller, T.D. (1990). *Thailand. International Handbook on Internal Migration* (C.B. Nam, W.J. Serow, and D.F. Sly, editors), New York: Greenwood Press.
- Fuller, T.D., Lightfoot, P, Kammnuansilpa, P. (1985). Rural-urban mobility in Thailand: a decision-making approach. *Demography* 22(4).
- Gatrell, A.C., Bailey, T.C., Diggle, P.J., Rowlingson, B.S. (1996). Spatial Pattern Analysis and Its Application in Geographical Epidemiology. *Transactions of the Institute of British Geographers*, NS 21: 256-274.
- Guest, P., Chamrathirong, A., Archanvanikul, K., Piriathamwong, N. Richte, K. (1994). Internal Migration in Thailand. *Asian and Pacific Migration Journal* 3(4):531-544.
- Guest, P. (1996). Assessing the consequences of internal migration: methodological issues and a case study on Thailand based on longitudinal household survey data. *Migration, Urbanization, and Development: New Directions and Issues*. United Nations Population Fund and Kluwer.
- Hirschman, C., Tan, J., Chamrathirong, A., Guest, P. (1994). The path to below replacement-level fertility in Thailand. *International Family Planning Perspectives* 20: 82-87.
- Hugo, G.J. (1981). *Population Mobility in West Java*. Yogyakarta, Indonesia. Gadjah Mada University Press.
- Jensen, J.R., Cowen, D.C. (1999). Remote sensing of urban/suburban infrastructure and socio-economic attributes. *Photogrammetric Engineering and Remote Sensing* 65: 611-622.
- Knodel, J., Chamrathirong, A. Debavalya, N. (1987). *Thailand's Reproductive Revolution: Rapid Fertility Decline in a Third-World Setting*. Madison, Wisconsin: The University of Wisconsin Press.
- Korinek, K., Entwisle, B., Jamplakay, A. (2005). Through thick and thin: layers of social ties and urban settlement among Thai migrants. *American Sociological Review* 70: 779-800.

- Liu, W. (2005). Comparison of non-linear mixture models: sub-pixel classification. *Remote Sensing of Environment* 94: 145-154
- Manly, B.F.J. (1991). *Randomization and Monte Carlo Methods in Biology*. Chapman and Hall, New York.
- Manusphaibool, Ghuta. (1991). *Rural-urban migration trend and employment status: a case study of Bangkok Metropolis*. The international Conference on Migration, National University of Singapore.
- Massey, D.S., (1990). Social structure, household strategies, and the cumulative causation of migration. *Population Index* 56:3-26.
- Massey, D.S., Arango, J., Hugo, G., Kouaouci, A., Pellegrino, A., Taylor, J.E. (1993). Theories of international migration: a review and appraisal. *Population and Development Review* 19: 431-466.
- Mesev, V. (1998). The use of census data in urban image classification. *Photogrammetric Engineering and Remote Sensing* 64: 431-438.
- Paola, J.D., Schowengerdt, R.A. (1995). A Detailed Comparison of Backpropagation Neural Network and Maximum-Likelihood Classifiers for Urban Land Use Classification. *IEEE Transactions on Geoscience and Remote Sensing* 33: 981-996.
- Pejaranonda, C, Sureerat, S, Guest, P. (1995). Rural-Urban Migration in Thailand. Trends, Patterns and Implications of Rural-Urban Migration in India, Nepal and Thailand. *Asian Population Studies Series* 138:171-243.
- Phongpaichit, P. (1993). The Labour Market Aspects of Female Migration to Bangkok. *Internal Migration of Women in Developing Countries*. New York: United Nations, 179-191.
- Rashed, T., Weeks, J.R., Gadalla, M.S., Hill, A.G. (2001). Revealing the anatomy of cities through spectral mixture analysis of multispectral satellite imagery: a case study of the greater Cairo region, Egypt. *Geocarto International* 16: 5-15.
- Ridd, M.K. (1995). Exploring a V-I-S (vegetation-impervious surface-soil) model for urban ecosystem analysis through remote sensing: Comparative anatomy for cities. *International Journal of Remote Sensing* 16: 2165–2185.
- Rindfuss, R.R., Turner, B.L., Entwisle, B., Walsh, S.J. (2004). Land Cover/Use and Population. In Gutman, G, Janetos, T, Justice, C., Moran, E., Mustar, J., Rindfuss, R.R., Skole, D., Turner, B. (editors), *Land Change Science: Observing, Monitoring and Understanding Trajectories of Change on the Earth's Surface*. Boston: Kluwer Academic Publishers. 351-366.

- Romesburg, H. C. (1989). Zorro: A randomization test for spatial pattern. *Computers and Geoscience* 15: 1011-1017.
- Shao, Y., Walsh, S.J., Entwisle, B., Rindfuss, R.R. 2007. Spatial Clustering and Urban Settings of Rural Migrants in Bangkok, Thailand. *GeoCarto International*, in press.
- Small, C. (2001). Estimation of urban vegetation abundance by spectral mixture analysis. *International Journal of Remote Sensing* 22: 1305–1334.
- Stern, R., White, R., Whitney, J. (1992). *Sustainable Cities: Urbanization and the Environment in International Perspective*. Boulder, CO: Westview Press.
- Susangkarn, C, Yongyuth C. (1996). Thailand: Development Strategies and Their Impacts on Labour Markets and Migration. In *Development Strategy, Employment and Migration*, edited by David O'Connor and Leila Farsakh. Paris: Organisation for Economic Co-operation and Development: 91-126.
- United Nations. (2004). Department of Economic and Social Affairs. *World Urbanization Prospects: The 2003 Revision*. New York: United Nations.
- Walsh, S.J., Rindfuss, R.R., Prasartku, P, Entwisle, B., Chamratrithirong, A. (2005). Population Change and Landscape Dynamics: Nang Rong Studies. in Barbara Entwisle and Paul C. Stern (eds.), *Population, Land Use, and Environment: Research Directions*. Washington, DC: National Academy Press.
- Ward, D., Phinn, S.R., Murray, A.T. (2000). Monitoring growth in rapidly urbanizing areas using remotely sensed data. *Professional Geographer* 52: 371-386.
- Weeks, J.R., Larson D.P., Fugate D.L. (2005). Patterns of Urban Land Use as Assessed by Satellite Imagery: An Application to Cairo, Egypt in *Population, Land Use, and Environment: research directions*, The National Academies Press.
- White, M., Montgomery, M.R., Brennan-Galvin, E.M., Visaria, P. (2003). Urban Population Dynamics: Models, Measures and Forecasts. In National Research Council, *Cities Transformed: Demographic Change and Its Implications in the Developing World*. Panel on Urban Population Dynamics, Mark R. Montgomery, Richard Stren, Barney Cohen, and Holly E. Reed (eds.). Washington, DC: The National Academies Press: 108-154
- Wu, C., Murray, A. T. (2003). Estimating impervious surface distribution by spectral mixture analysis. *Remote Sensing of Environment* 84, 493-505
- Xian, G, Crane, M. (2005). Assessments of urban growth in the Tampa Bay watershed using remote sensing data. *Remote Sensing of Environment* 97, 203-215.

CHAPTER 6

CONCLUSIONS

The movement of people towards cities has accelerated over the past 50-years. Currently, about one-half of the world's population live in urban areas, and it is projected that 70-percent of the population will live in urban within the next 20-years (Cohen, 2003; UN, 2004). Accordingly, urban areas have been growing at a striking rate. Most of the fast growing cities are located in developing countries (UN, 1998b). The transformation of natural and agricultural lands to urban land use is typically irreversible and has implications for biodiversity, climate change, green house gas, hydrological change, and quality of life more generally (Mayer and Turner, 1992; Kalnay and Cai, 2003; Landsberg, 1981; Mckinney, 2002; Wear, 1998; Lo and Faber, 1997). Rapid urban growth and the spread of low-density forms of settlement are two of the main concerns for urban planners, decision-makers, and researchers in the social, spatial, and natural sciences. This research examined urban land use/cover characterization, urban growth, urban form, and human settlement pattern using remote sensing, GIS, spatial analysis, and statistical techniques.

The goals of this research were to examine 2-D and 3-D urban land use/cover mapping using remotely-sensed data; assess urban-rural gradients, urban form, and urban function; and understand rural-urban migrants' settlement patterns in Bangkok. Chapter 1 provided an overview of research objectives and significance. Chapter 2 focused on the sub-pixel classification of a Landsat TM/ETM time-series. Chapter 3 used high spatial-

resolution IKONOS images to derive 3-D building height information, with particular emphasis on high-rise buildings. Chapter 4 examined the urban form and urban functions using the results from the sub-pixel classification and 3-D building height estimates. Chapter 5 considered the spatial patterns of migrants' locations in Bangkok, Thailand. Spatial patterns of migrants from origin villages were geo-coded and spatial clustering of migrants were assessed. In addition, migrants' neighborhood environments were characterized and modeled using a number geographical and socio-demographic variables.

This research emphasized the use of remote sensing as a tool for mapping and monitoring urban areas. The mapping of imperviousness was of particular interests. The primary advantage of using imperviousness is that it is a relatively simple land cover type to classify. In an Asian city such as Bangkok, it might be very difficult to characterize urban land use at the Anderson's Level II classification scheme, because there is no clear zoning of urban land use, and most land use types (e.g., residential, commercial, industrial) are inter-mixed together (Kaothien and Webster, 2001). Without detailed ground truth data or aerial photography as reference data, a simple land cover (i.e., imperviousness) classification scheme is probably the most feasible solution for urban landscape characterization. The main challenge of urban land cover classification is the spectral mixture problem. In fact, it has been suggested that the most important technical issue in urban remote sensing is the spatial resolution of image data (Welch, 1982). One of the important contributions of this research is to assess the feasibility of a neural network-based, sub-pixel classifier for mapping a large metropolitan area using a Landsat TM/ETM image time-series. The results from sub-pixel classification provided a

consistent measure (i.e., imperviousness) for characterizing the rates and patterns of urban growth, urban form and function, and migrants' neighborhood environments. Another contribution of this research is 3-D building height estimation using high spatial resolution satellite imagery. The shadows on high spatial resolution images are typically considered “noise” or the loss of information for an image classification task. However, this study used shadow information to derive building height. The results of building height estimation and 3-D urban mapping provide useful information for detailed urban land use classification and urban form/feature analysis. The research suggests that shadows can be automatically detected using advanced image classification and shape analysis techniques. The building heights, especially those from high-rise buildings, can be estimated with a high level of accuracy. The approach has both theoretical and practical implications, because shadows are an important component for high spatial resolution image.

In addition to urban mapping, this research addresses the spatial patterns of impervious cover and the locations of high-rise buildings to provide valuable information for urban form characterization and urban feature identification. Urban form was analyzed using a landscape ecology perspective that considered the interactions between patterns, processes, and scale. It was hypothesized that a meaningful urban-rural gradient can be characterized by analyzing the density and the spatial structure of imperviousness and urban features such as core, inner zone, periphery, and rural landscape, delineated according to the landscape pattern indices. In other words, the delineation of urban features was largely based on the contextual information, rather than land cover types from a single pixel. Furthermore, the concept of spatial neighborhoods and the contextual

information provided a framework for characterizing urban growth models, including infilling, diffusive expansion, and isolated growth. Diffusive expansion and isolated growth was further linked to the concept of urban sprawl (Wilson et al., 2003).

This research also examined the relationship between population and physical characteristics of urban space. The results from 2-D and 3-D urban mapping, and the urban change and urban form analysis were linked to the residence locations of rural-urban migrants. The uniqueness of this study is that it relies on a special socio-spatial dataset of rural-urban migrants from Nang Rong to Bangkok, Thailand. Specially, the location of each migrant was geo-coded using GPS techniques, and the social survey was spatially linked to each GPS location. Therefore, the socio-demographic characteristics of rural-urban migrants were examined from a spatial perspective by integrating remote sensing, GIS, and spatial statistical techniques. This research is useful to understand questions such as: Are migrants choosing to settle in the urban center or urban fringes? Are migrants choosing to settle in newly urbanized areas in the cities, or in pre-existing urban places? What are the migrants' neighborhood environments (i.e., imperviousness)? What are the influential factors for migrants' settlement pattern in urban setting (i.e., job location, housing/rent price, social networks)? A better understanding of migrants' settlement pattern in urban space helps urban planners and decision-makers design more efficient policies in infrastructure/residential development, land use and environmental planning, and quality of life in general.

6.1 Technical Improvements in Remote Sensing and Spatial Analysis

This study used a neural network *classification* approach, instead of the more widely used neural network *regression* approach to characterize the proportional

impervious cover from Landsat TM/ETM image. This approach was taken, because of the limited availability of training data and the generalizability of neural networks. The neural network *regression* approach typically requires the used of high spatial resolution images for network training. However, a metropolitan region such as Bangkok often has a very complex spatial organization of land use/cover types. The number and the type of dominant land cover may differ from the urban core area to the urban edge and rural landscape. This makes it difficult to generalize a trained neural network *regression* classifier across large spatial extents. On the other hand, a neural network *classification* approach may select training pixels in a more relaxed manner for all apparent classes in the image. The approach is similar to a traditional neural network per-pixel classification task. The only difference is that the outputs of the neural network are retained in a fuzzy format. One of the important improvements of this research is its consideration for the Bayesian interpretation of neural network outputs. In theory, MLP neural networks require a large number of training data points to model the posterior probabilities (Richard and Lippmann, 1991). However, most previous studies ignore this fundamental assumption and use a very limited number of training samples. In this study, practical techniques were developed to improve the accuracy level of the neural network classification approach. It was found that a large sample size and spectral heterogeneity in the training set are both important for deriving robust sub-pixel estimations.

Advanced image processing techniques were applied to high spatial resolution image classification and 3-D urban mapping. The OBIA (i.e., object-Based Image Analysis) algorithm was used to generate image objects with homogeneous spectral and texture signatures. This is advantageous to the traditional per-pixel classifiers (i.e.,

ISODATA). However, it was found that there were substantial areas of confusions between shadow and water objects. The size, shape, and spatial neighborhood information were used to separate these objects. A shadow detection system was developed as a rule-based classifier (i.e., Wharton, 1989). For instance, the one-to-one relationship between shadow and its spatial neighborhood of an impervious object is a robust rule that aids shadow identification. The shadow detection system also automatically produced the shadow length and building height estimation. The approach is similar to the commonly used aerial photogrammetry technique, but an automatic detection and estimation is emphasized. This can be advantageous if large study areas and large numbers of buildings are involved in the analysis. Moreover, it is among a new wave of research that uses shadow information from high spatial resolution IKONOS to estimate building height. For most isolated high-rise buildings, the shadow detection method generated excellent results (i.e., less than 4-m error). The algorithm is problematic for the clustered high-rise buildings and the fragmented building shadows, however, this is a common problem for most automatic or semi-automatic shadow/building extraction algorithms.

For spatial pattern analysis of migrants' locations, a nearest neighbor distance and Monte Carlo simulation were combined to perform the spatial point-pattern analyses. The pattern of migrants from source villages was simply characterized using a nearest neighbor distance measures, but Monte Carlo simulation provided a statistical test of significance. This is important because the number of migrants from a specific village may affect the result of nearest neighbor distance measures. Furthermore, simple correlation coefficient analysis was used to examine the relationship between the level of

spatial clustering and socio-demographic characteristics of rural-urban migrants. For instance, it was found that the level of spatial clustering was positively correlated with the occupation variable -- the higher the percentage of migrants in manufacturing, the greater the spatial clustering. The education level is negatively correlated with spatial clustering -- the higher the percentage of migrants who completed 10 or more years' of education, the less the degree of spatial clustering. This finding suggests that migrants with higher education backgrounds may have greater flexibility in the job market, and they may rely less on village networks. The spatial point-pattern analysis of rural-urban migrants' locations is new in the literature. In this study, only a few socio-demographic variables are examined, however, this approach can be easily extended to more detailed social survey data. Adding a spatial aspect to traditional social science may generate additional information that helps us understand socio-demographic processes to a greater extent.

6.2 Implications on Urban Growth, Urban Form and Human Settlement Analysis

For the entire study area, the total area of impervious cover is 560km², 708 km² and 779 km² for 1993, 1999, and 2002, respectively. Simple post-classification change detection was used to examine urban growth rates from 1993 to 1999 and 1999 to 2002. The annual growth rate is 4-percent and 5-percent from 1993 to 1999 and from 1999 to 2002, respectively. The dominant trend of land use/cover change is the conversion from agricultural land to urban development or impervious cover. There is a slight increase of the urban growth rate through time. It should be noted that the urban area of Bangkok has extended well beyond official administrative boundaries. In fact, most urban developments are located outside of Bangkok's city boundary. For instance, the airport

corridor is extended into Pathum Thani province, and heavy industry is extended into Samut Prakarn province. The new Bangkok International Airport is currently developing in the east of Bangkok, thus it is expected to see rapid urban growth along the east corridor. There is no efficient mechanism that coordinates the urban planning of Bangkok with the surrounding provinces. The comprehensive planning of the Bangkok metropolitan area has not been effectively implemented (Kaothien and Webster, 2001). As a result, the urban growth rates and patterns are relatively uncontrolled, largely depending on the impacts from the private sector. In Chapter 4, the urban form and urban structure analysis, it was found that the primary urban form of Bangkok is highly irregular and shaped by several major transport corridors. Population growth and urban development in these areas may quickly outstrip urban services and related infrastructure. The problems of traffic congestion and air pollution will remain and potentially worsen with time. The results from Chapter 4 also show that most newly urbanized pixels can be labeled as diffusive expansion growth and isolated growth (Wilson et al., 2003). This may suggest that Bangkok has increased the level of urban sprawl through time.

The identification of urban features (i.e., urban core) from image analysis varies, depending on the nature of the input dataset (i.e., 2-D or 3-D maps) and indices used in their analysis. For instance, the urban core can be delineated by thresholding the density or the patch size of impervious cover. On the other hand, the 3-D urban map can provide a more meaningful urban core or CBD area. This occurs because most high-rise office buildings and hotels are clustered in the urban core or CBD area in Bangkok. One shortcoming of this research is that only high-rise buildings were identified. Ideally, the urban structure and urban features can be characterized using a combination of 2-D and

3-D information. A 2-D map provides the density and spatial structure of land use/cover types, while a 3-D map provides variations in the building heights. As a result, more meaningful socio-demographic statistics and processes can be inferred from this type of urban structure or urban morphology. With the availability of high spatial resolution imagery (i.e., IKONOS, QuickBird) and advanced digital image processing techniques (i.e., OBIA), there is ample opportunity for urban mapping, urban structure/feature analysis, and urban growth modeling.

Finally, the settlement patterns and neighborhood environments of rural-urban migrants were analyzed. The spatial definition of neighborhood is arbitrary. Simple distance buffers were used in this study. The neighborhood environments were characterized using a measure of the density and spatial organization of impervious cover. This is different from more widely used vegetation indicators in the literature (e.g., Lo and Faber, 1998). The main reason is that there are mixed uses of agricultural land and residential areas in the Bangkok area. A high percentage of vegetation cover (i.e., crops) in a neighborhood does not mean a better quality of life. Impervious cover, on the other hand, may have a direct or indirect implication of urban form and urban function (Ridd, 1995). It was found that both a density index and a spatial structure index can be modeled using a set of geographic and socio-demographic variables. For instance, variation in the density of impervious cover is associated with the distance to the nearest major road, the distance to the city center, age, occupation, and sex. The mean patch size was associated with the distance to the nearest major road, the distance to the city center, and occupation. For socio-demographic factors, the job locations and characteristics may impact the trend of residential segregation for rural-urban migrants. It should be noted

that a large proportion of these rural-urban migrants are seasonal or temporary migrants. Their residential location in urban setting may not be recorded through a census or large-scale social surveys. Without this unique socio-spatial dataset, it is impossible to characterize the spatial patterns of these migrants' locations and their neighborhood environments. This rural-urban migration following-up dataset and the analysis conducted may provide useful information that could not be derived from census-based studies.

This research makes contributions to image processing of remotely-sensed images and urban studies. Both areas benefit from the links established between urban form and function and the capability to derive additional information about urban land use patterns. The goal has been to approach the study of Bangkok from the perspective of a remote sensing and spatial analyst, and then to focus on commonly available satellite data for broad applicability of the methods to cities across the globe. In many ways the study challenges planners and social scientists to engage remote sensing scientists to link talents and perspectives to address customary and new questions about the "peopling" of urban places.

Reference

- Cohen, B., White, M., Montgomery, M.R., McGee, T.G., Yeung, Yue-Man. (2003). Urban Population Change. National Research Council, *Cities Transformed: Demographic Change and Its Implications in the Developing World*. Panel on Urban Population Dynamics, Montgomery, M.R., Stren, R., Cohen, B., and Reed, H.E. (editors). Washington, DC: The National Academies Press, 75-107.
- Kalnay, E, Cai, M. (2003). Impact of urbanization and land-use change on climate. *Nature*, 423:528-31.
- Kaothien, U, Webster, D. (2000). Globalization and Urbanization: The Case of Thailand. In *Local Dynamics in an Era of Globalization*, edited by S. Yusuf, W. Wu and S. Evenett. Washington, DC: Oxford University Press, Inc for The World Bank.
- Landsberg. H.E. (1981). *The Urban Climate*. Academic Press, 275 pp.
- Lo, C. P., Faber, B. J. (1997). Integration of Landsat Thematic Mapper and census data for quality of life assessment. *Remote Sensing of Environment* 62, 143-157.
- Mayer, W.B., Turner, B. L. (1992). Human population growth and global land-use/cover change. *Annu. Rev. Ecol. Syst.* 23:39-61.
- McKinney, M.L. (2002) Influence of settlement time, human population, park shape and age, visitation and roads on the number of alien plant species in protected areas in the USA. *Diversity and Distributions*, 8, 311–318.
- Richard, M.D., Lippmann, R.P. (1991). Neural network classifiers estimate Bayesian a Posteriori probabilities. *Neural Computation*, 3, 461-483.
- United Nations. (2004). Department of Economic and Social Affairs. *World Urbanization Prospects: The 2003 Revision*. New York: United Nations.
- Wear, D.N., Turner, M.G., Naiman, R.J. (1998). Land cover along an urban-rural gradient: implications for water quality. *Ecological Applications* 8, 619–630.
- Welch, R. (1982). Spatial resolution requirements for urban studies. *International Journal of Remote Sensing*, 3, 139-146.
- Wilson, J.S., Clay, M., Martin, E., Struckey, D., Vedder-Risch, K. (2003). Evaluating environmental influences of zoning in urban ecosystems with remote sensing. *Remote Sensing Environment*, 86, 303-321.